Micro- and Nanostructured Immuno-Tip Sensors for Point-of-Care Diagnosis of *Tuberculosis*

Jong-Hoon Kim

A dissertation

submitted in partial fulfillment of the

requirements for the degree of

Doctor of Philosophy

University of Washington

2013

Reading committee:

Jae-Hyun Chung, Chair

Dayong Gao

Kyong-Hoon Lee

Program Authorized to Offer Degree:

Mechanical Engineering

University of Washington

Abstract

Micro- and Nanostructured Immuno-Tip sensors for Point-of-Care Diagnosis of *Tuberculosis*

Jong-Hoon Kim

Chair of the Supervisory Committee:
McMinn Endowed Associate Professor Jae-Hyun Chung
Department of Mechanical Engineering

Point-of-care(POC) diagnosis of *tuberculosis* (TB), one of the most widely spread diseases in the globe today, has been critically demanded over a century. To date, many diagnostic methods have been developed for detection of *Mycobacterium tuberculosis* (MTB); polymerase chain reaction latex agglutination, enzyme-linked immunosorbent assay, radiometric detection, genprobe amplified MTB direct test, TB rapid cultivation detection technique, and flowcytometry. The methods are more sensitive and rapid than the traditional microbial culture-based methods; however, the performance should be further improved. In addition, due to the large volumes and the low analyte concentration of actual sputum samples, a cumbersome concentration step is required. Currently available concentration methods employ centrifugation, microfiltration, or magnetic beads. However, the methods are limited in cumbersome preparation steps, low yield, and low throughput. To address the

challenges, microtip- and nanotip immunosensors are studied for fluorescence- and electrical measurements, respectively.

For a microtip immunofluorescence sensor, concentration mechanisms based on flow circulation and electric field are combined at different scales to concentrate target bacteria in 1 mL sputum samples onto the surfaces of microscale tips. Genus-specific antibodies are immobilized on the microtip surface for specific capturing. Experimentally, the concentration mechanism is studied. Then, the performance of conentration mechanism is validated by using an immunofluorescence. To understand specific capturing mechanism of target bacteria on a microtip surface, the bacterial behavior on the microtip surface during evaporation is investigated as a function of the substrate properties, liquid composition, and environmental conditions. The novel concentration mechanism using a microtip can detect MTB complex cells in sputum within 25 minutes. The detection limit in sputum is 200 CFU/mL with a success rate of 96 %, which is comparable to PCR. The presented microtip based immunosensor shows great potential for POC diagnostic tool.

For simpler POC diagnosis, an electrical detection method using a dendritic nanotip is presented. The dendritic nanotip is composed of SWCNTs and Si nanowires, which is designed to maximize the surface area for high sensitivity. Upon the binding of target cells on to SWCNTs of a nanotip, the gating effect is induced to increase the resistance of the sensor system. The working principles are studied for each binding layer by cyclic voltammetry. A SWCNT-based dendritic nanotip is utilized to concentrate target bacteria by using an electric field and capillary effect. The captured targets on the nanotip are detected by measuring the

resistance change in deionized water. The detection results are verified by fluorescence- and scanning electron microscopes. In the experimental results, *Bacillus Calmette-Guérin* (BCG) cells strain of *Mycobacterium bovis* can be detected within 15 minutes using both electrical and fluorescent detection. The sensitivity is 1,000 CFU/mL for both methods.

As a future plan, the surface phenomena for specific detection of target bacteria will be studied to understand the specific capturing mechanism on microtip surface. The detection mechanism using a nanotip will be studied further to clarify the detection mechanism.

Table of Contents

List of Figures

Page

List of Tables

Page

Acknowledgements

The author wishes to express sincere appreciation to Professor Jae-Hyun Chung for his valuable advice, encouragement and support, to Professor Dayong Gao and Professor Gerard A. Cangelosi for their kind advice and discussion, and to Dr. Kyong-Hoon Lee for his support, encouragement and advice.

This research was funded by the National Science Foundation (NSF) Career award (ECCS-0846454) and NSF STTR PHASE I and II grant (IIP 0740525 and IIP 0956876).

Dedication

This dissertation is dedicated to my lovely wife Jahae, and the wonderful son Junsoo. Their support, encouragement, and constant loves have sustained me throughout my life.

Chapter 1: Introduction: Point-of-Care Diagnosis of *Tuberculosis* (TB)

1.1 Introduction

Tuberculosis (TB) remains a major global health problem. It causes ill-health among millions of people each year and ranks as the second leading cause of death from an infectious disease worldwide. The latest estimates show that there have been almost 9 million new cases in 2011 and 1.4 million TB deaths [1]. In addition, healthcare workers are a population at risk for latent TB infection, with real possibilities of subsequent reactivation. TB cases frequently occur in low-income countries that have poorly resourced public health care sectors [2]. Delayed diagnosis has serious consequences for both the prognosis of the patient and onward transmission to fuel the epidemic [3, 4]. Thus, the rapid diagnosis and follow-up treatment are crucial for the effective control of TB.

A number of methods are available for TB diagnosis but the performance should be further developed to satisfy the demand. Sputum smear microscopy remains a main tool of TB diagnosis in developing countries. The method depends upon the quality and bacterial load of the sputum specimen and the skills of laboratory technicians [5, 6]. It is applicable for developing areas, relatively inexpensive, and field-deployable. Even in the absence of electricity, slides can be examined with a light microscope using reflected sunlight. However, the smear microscopy is insensitive – it detects approximately 50% of all the active cases of TB. Sensitivity can be as low as 20% in children and HIV infected people [7, 8]. Furthermore, the smear microscopy cannot detect drug resistant TB. The smear

microscopy also places a burden on a patient. A person, who is suspected of TB, has to visit a clinic at least twice before a diagnosis can be completed, and then should return again for the results. In terms of transportation costs and wages, this process can be expensive. Some people never complete the testing process, or do not return for their results. It has been estimated that a single-visit diagnostic test offering 100% accuracy could save 625,000 lives per year if widely implemented, and a test with only 85% sensitivity and 97% specificity might save 392,000 lives, or 22.4% of the current annual worldwide deaths attributable to TB [9].

The gold-standard diagnostic method is bacteriological cultivation of *Mycobacterium tuberculosis* (MTB) cells from pulmonary specimens *i.e*. sputum. Traditional microbial culture-based tests are the most common methodologies currently used [10, 11]. Culture of MTB on liquid or solid media is a more sensitive method for TB diagnosis than smear microscopy. Drug resistance can also be detected. However, it requires extensive laboratory infrastructure and up to 1 month to yield results, which makes it impractical for use in most cases. Chest radiography is also used in some countries, but lacks sensitivity and specificity [12]. In one study, experts missed approximately 25% of TB cases in a series of films [13].

To date, many diagnostic methods have been developed for rapid detection of M. tuberculosis; polymerase chain reaction (PCR) [14-17], latex agglutination [18], enzyme-linked immunosorbent assay (ELISA) [19-21], radiometric detection [22], genprobe amplified *M. tuberculosis* direct test [23], TB rapid cultivation detection technique [24], and flowcytometry [25]. The methods are more sensitive

and rapid than the traditional microbial culture-based methods; however, the methods are not capable of offering POC diagnosis of TB. Thus a rapid and low-cost method for MTB detection is strongly demanded to effectively control TB infection [26, 27]. To clearly identify the needs for a TB diagnostic method, this chapter reviews (1) the current concentration methods of MTB out of sputum samples and (2) potential POC test methods.

1.2 Concentration Methods of MTB out of Sputum

Due to the large volume and the low analyte concentration of actual sputum samples, a pre-concentration step is required. Available concentration methods are centrifugation, magnetic beads, and electrokinetic manipulation.

Centrifugation is to concentrate target cells due to larger inertia of target cells in a sample. After centrifugation, the pellets in a sample are used for analysis. The centrifugation process can marginally improve the sensitivity. Two studies have shown a two-fold increase in the sensitivity compared with smear microscopy [28, 29]. Studies using clinical samples have shown more modest benefit. In one study, the overall sensitivity increased from 54.2% to 63.1% while another showed sensitivity in HIV-positive patients increased from 38.5% to 50.0% after centrifugation [30, 31]. This improvement was marginal when compared with the sensitivity of smear microscopy supported by clinicians' judgment in diagnosing pulmonary tuberculosis. In other studies, a noticeable advantage has not been observed for centrifugation over smear microscopy in sputum samples in diagnosis of pulmonary tuberculosis [32, 33]. The evidence supporting the use of sputum concentration is not consistent potentially due to personal skill. Moreover, such techniques require more time and expertise, and the available resources must be considered before recommendation to low-income countries.

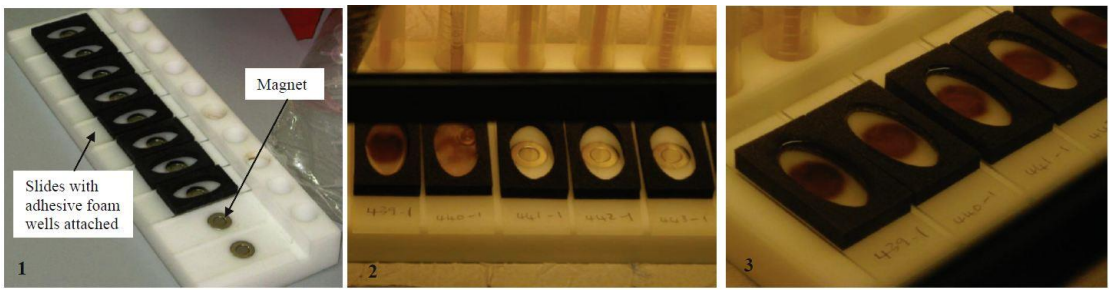

Figure 1. Steps in Magnetic bead procedure. 1. Attachment of adhesive wells onto slides and placement on magnetic workstation. 2. Addition of thinned sputum with TB Beads into adhesive wells on slides. 3. Capture of TB Beads onto magnets below slides on magnetic workstation. Reprinted with permission from [34].

Another method to concentrate MTB from sputum samples is to utilize magnetic beads. The 'TB-Beads' technology concentrates MTB from sputum using ligand-coated magnetic beads prior to detection by LED-based fluorescence microscopy. The approach provides a simple, manual alternative to centrifugation for sputum concentration prior to microscopy [35] (Figure 1). Compared to culture, magnetic beads had higher sensitivity than smear microscopy (65.4% vs. 51.4%), but the specificity of magnetic bead was lower than smear microscopy (88.6% vs. 98.9%) [34]. Although the sensitivity was higher than that of smear microscopy, the specificity was shown decreased. Furthermore, the magnetic bead procedure was as complex as the centrifugation method.

The microfluidic devices combined with other concentration mechanisms also have been tried to concentrate MTB in sputum samples. The three main concepts for microfluidic concentration are physical trapping, functionalized particles, and electrokinetic techniques [36]. Physical traps for bacteria are fabricated by shallow channels or arrays of microbeads [37, 38]. In spite of the simple configuration, viscous samples can be clogged in the channel.

Another method is to use antibody-coated particles which can selectively bind to the target species. These particles are trapped in microchannels by physical barriers [40] or magnetic fields[39, 41-43]. The capture efficiency strongly depends on the quality of the coatings and proper mixing of particles and analytes. To increase the capture efficiency, further advances in bead modification and controllability of the magnetic field should be made with improvement of device integration [44, 45].

Electrokinetic methods can manipulate targets without labeling and be easily integrated into devices [46]. The methods depend on the conductivity and permittivity of targets and liquid medium. Dielectrophoresis (DEP) has been widely used for preconcentration and separation of cells and bacteria [47]. Using DEP, cells could be concentrated to designed positions in a chip [48-52]. A number of DEP traps and separators have been optimized for continuous operation by careful scaling of the device and electrode dimensions, as the dielectrophoretic force depends on the volume of the biological particles [53-57]. However, the high field strengths can strongly affect the viability of bacteria [57]. In addition, the high electric field can easily give rise to stong circulation of flows, such as electrothermal flow and AC electroosmosis, in high ionic medium. It could reduce the capture efficiency [51, 58, 59]. Bacteria exhibit a negative charge at physiological pH values. Therefore, while electrophoretic concentration has the advantage for concentration of various target pathogens, the capture efficiency still needs to be improved especially for sputum samples due to charged particles [60].

Other approaches, such as concentration using bleach-induced

precipitation, have been extensively studied and can yield higher sensitivity than smear, but standardization of the bleach is problematic because the treated samples can be partially lost from the slide [61]. In addition, the time for bleach exposure varies from one hour to tens of hours, which requires a standard protocol [62].

1.3 Potential POC for TB Technologies

1.3.1 Immunochromatography

One of major POC diagnostic tests is the lateral flow immunochromatography, which uses either a membrane or paper strip to indicate the presence of bio-markers [63]. For the past decade, immunochromatographic strip tests have been one of the very few diagnostic technologies successfully used in the developing world. The disposable devices can be operated with little instruction and diagnosis is completed within a few minutes. The cost is less than US $2 to the end user because the sensors, including off-the-shelf components and reagents, are inexpensive and affordable. Immunochromatography can be formatted for detection of antigens or antibodies. A wide range of specimens can be utilized for different applications [64]. The diagnostic sensitivity of such test will depend on both the concentration and accessibility of the target analyte in the test sample (usually urine, saliva or blood), as well as the avidity of the antibody-binding reaction. Similarly, the specificity of such a test is dependent on the availability of disease markers of a high prediction value. Since the sensitivity is limited for detection of multiple targets, a strategy is necessary for accurate diagnosis of TB through more sophisticated microfluidic devices. A further concern is the disposal of the devices after use. The current tests are made from robust plastic, and disposal in countries lacking the appropriate infrastructure can cause environmental issues. One possible approach for mitigating the environmental impact is to use bio-degradable materials [65], and the suitability of the disposable devices as fuel in local energy generation should also be explored

[66].

1.3.2 PCR and other amplification methods

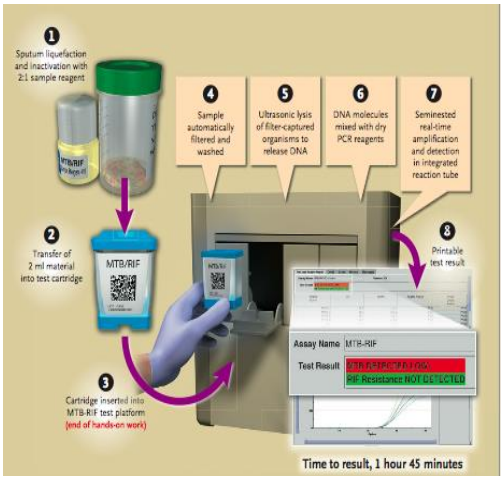

Figure 2. Fully automated PCR device (GeneXpert® System, Cepheid, CA)

Amplification and detection of MTB DNA are one of the most sensitive and rapid ways to detect tuberculosis, and also can detect genetic mutations associated with drug resistance. Unfortunately, conventional DNA amplification methods are cumbersome, require specialized training, and can only be performed on material that has been subjected to processing and DNA extraction. This has limited their use to reference laboratories. Thus, it cannot be directly used at the POC. Recently, a cassette-based ‘one-step’ sample treatment device has been combined with automated real-time PCR to provide a safe, integrated diagnostic platform(Figure 2). The Xpert MTB device is a fully automated system that allows a relatively untrained operator to perform sample processing, DNA amplification, and detection of *M. tuberculosis* and screening for rifampin resistance in less than 2 hours and only minutes of hands-on time [67-70]. Results can be available while patients wait in clinic. The only manual step, adding sample treatment reagent to the specimen cup before loading the cartridge, kills over 99.9% of TB bacilli in the

specimen. Although this assay is rapid and easy to use, the device is not portable and remains a laboratory- or clinic-based tool. In addition, the device that automates the procedure is a computer-driven, sophisticated piece of equipment that will require reliable energy supply, security and maintenance. The technology is to be made available at a discounted price for public-sector and not-for-profit organizations in developing countries. However, despite the discount, the anticipated cost of the instrument (US$17,000, excluding taxes and delivery charges) and individual test cassettes (approximately $16 each) is likely to limit the implementation of this test into those countries where TB is endemic [71].

1.3.3 Optical detection methods

Raman spectroscopy is an optical method, enabling spectroscopic fingerprints to be obtained from biological samples in a few seconds. These fingerprints represent the molecular composition of a sample, and are ideally suited for identification of a microorganism at both the species and the strain level. Raman spectroscopy is an analytical tool that has been exploited in the food industry but has so far had limited application in the medical field [72, 73]. When the method is applied to cultured bacteria, Raman spectroscopy proved to be highly specific, differentiating MTB from other mycobacteria [74]. The test is rapid and requires minimal manipulation of samples. However, it is yet to be shown that the method is available for sputum or other body fluids for the diagnosis of TB. Another optical detection technique, evanescent wave fluorometry, measures changes in fluorescence of molecules, which has been used

in a novel POC device to detect *M. tuberculosis* antigens. The RBS Breathalyzer test (Rapid Biosensor Systems, Cambridge, UK) captures cough condensate and assesses the presence of antigen 85B through displacement of a fluorescence labeled analogue. The test was rapid (<10 minutes) and simple to use for a medical doctor [75]. The approach may have some merit, but further study is needed to assess the sensitivity and specificity of the device.

1.3.4 Nanowire sensor

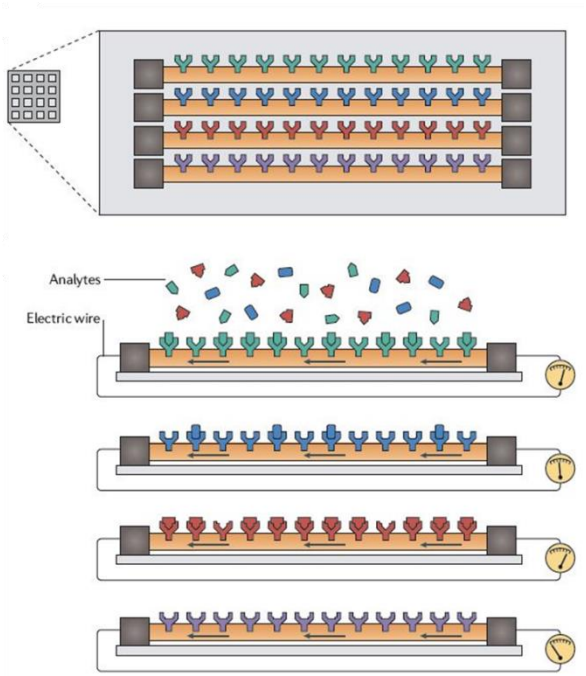

Figure 3. Silicon nanowire field effect transistors. Each wire is coated with molecules that interact with analytes, and these interactions change the electrical properties of the wire, altering its conductance and providing instant detection. Reprinted with permission from [71]. Copyright 2011 Nature Publishing Group.

Nanotechnology is a discipline to handle molecular-size structures; these 'nanoparticles' are measured in millionths or billionths of a meter (10^{-6} to 10^{-9} meters). Working at such a miniscule scale dramatically increases the number of

reactive sites and greatly increases the capacity for the simultaneous detection of multiple markers (Figure 3). The application of nanotechnology to TB diagnosis is in its infancy, although early work has shown that this technology has the capacity to assist detection of MTB through enhancement of fluorescent signals [76]. Nanoparticles have also been used in combination with microfluidic technology and nuclear magnetic resonance both for the detection and molecular analysis of cells[77]. In a miniaturized device, nanoparticles enabled the rapid detection of the *M. tuberculosis*-related organism *M. bovis bacille Calmette–Guérin* (BCG) in sputum [78]. However, in spite of the high potential, further development should be made with scalable manufacturing and at a low cost.

1.4 Summary

Table 1. Summary of potential TB POC test, (+): Meets the test specification, (-): Does not meet the test specification*, NA: Data not available

Minimum specification for TB POC test (Minimum specification)	PCR (GeneXpert)	Microfluidics (μNMR)	Magnetic (TB beads)
Medical decision: (treatment initiation)	+	+	+
Sensitiviy (-95% for SSM and culture positive -60-80% for SSM negative, culture positive)	+	NA	-
Specificity (-95% compared to culture)	+	NA	-
Time to results (<30 minutes)	-	+	+
Power (can work on battery)	-	+	+
Throughput (20 tests/day)	+	+	+
Cost (less than US$3 per test)	-	+	+
Biosafety (level 1)	+	+	+

*The table was reconstructed with the review results of an undergraduate student, Paola Florio.

The current progress for low-cost TB POC tools was summarized in this section and Table 1. A POC diagnostic tool should not require laboratory facilities or specialist training. The major challenge for a new TB POC diagnosis is to build up a rapid, low cost platform without compromising the performance of a laboratory equipment. To date, many new diagnostic tools have been developed, but none of them meet the requirements for the POC test. Limited access to a capable diagnostic tool results in failure to diagnose millions of TB cases each year. Therefore, a new TB POC diagnostic test should be developed to meet the demands satisfying the most urgent medical needs in resource-limited settings.

1.5 Objectives

The main objective of this dissertation is to study the specific contentration and detection mechanisms of MTB in sputum by using microtips and nanotips. Using a microstructured tip, the specific concentration mechanism of MTB in sputum is studied by analyzing streaming flow and electric field induced forces. A specific capturing mechanism of concentraed bacteria is studied by analyzing capillary-induced binding on a functionalized tip surface. For a field-deployable platform, a novel electrical detection method is investigated by using nanostructured tip. The direct detection mechanism due to immunocomplex formation on a nanotip surface is investigated for rapid and low-cost diagnosis. To this end, the novel specific concentration and detection methods render the development of TB POC diagnostic platform for laboratory and field uses, which will have direct impact on infectious disease diagnosis, furthermore, in the field of nanoengineered medicine and biology.

Chapter 2: Microtip Immunosensor for TB Diagnosis

2.1 Introduction

A major technical challenge of TB diagnosis is in detecting low concentration of MTB cells in highly viscous media, sputum samples. Various microfluidic and electrokinetic approaches[63, 79-81] have been tested for detecting bacteria and biomolecules in samples. However, the methods have not been applied to viscous sputum samples.

In our previous work, microtip or nanotip sensors were used to concentrate target bacteria and DNA by using an alternating current (AC) electric field[82-84]. However, the approach was not specific to target analytes, and the small sample volume (<10 μL) limited sensitivity. This chapter describes a microtip-based immunosensor that overcomes these limitations. The diagnostic platform specifically detects *Mycobacterium* cells in combination of electric field, streaming flow, and immuno-affinity binding. The novel concentration mechanism enables rapid detection of target bacteria in sputum samples without requiring bacteriological culture, centrifugation, or nucleic acid amplification. This platform enables rapid and inexpensive diagnosis of infectious diseases potentially with minimal training.

In this chapter, the theory of electrokinetic manipulation is discussed. The concentration mechanism of MTB in a large volume of 1mL is analyzed. The developed assay is tested in sputum samples. The performance and characteristics of the assay is evaluated in comparison with other methods.

2.2 Theoretical Study of Electrokinetic Manipulation

Electric fields can be used to manipulate particles in a solution in the form of electrophoresis, dielectrophoresis, and electroosmosis. Electrophoresis is generated by electrostatic forces among charged particles while dielectrophoresis is induced by the polarization of particles in a medium. The direction and magnitude of the forces depend on the electric properties of particle and medium, and geometry of particles. Electroosmosis is generated by ions that interact with a charged surface. In this section, the details of electric field induced forces are discussed to understand the electrokinetic manipulation of particles, which will envision effective concentration of particles. As experimental validation of the working principles, an electric field is used to manipulate nanowires for convenience of imaging.

2.2.1 Electrophoresis

Electrophoresis is commonly used to arrange charged particles in a liquid. Particles are charged in a suspension solution and moving toward the oppositely charged electrode. Electrophoretic force on a particle can be derived from the Coulomb's law[42]:

$$\vec{F}_{12} = \frac{Q_1 Q_2}{4\pi\varepsilon_0 r^2}\vec{r}_{12} \tag{2.1}$$

,where $\vec{F}_{12}$ is the force acting on the particle of charge 2 (Q_2) by another particle of charge 1 (Q_1), ε_0 is the permittivity of vacuum, r is the distance between the particles, and $\vec{r}_{12}$ is the unit vector from Q_1 to Q_2.

The electric field ($\vec{E}$) created by a point charge (Q) at the distance r is given by:

$$\vec{E} = \frac{Q}{4\pi\varepsilon_0 r^2}\vec{r} \tag{2.2}$$

By combining Equation (2.1) and Equation (2.2), the electrophoretic force ($\vec{F}_{EP}$) acting on a particle that has net charge Q_{net} is:

$$\vec{F}_{EP} = Q_{net}\vec{E} \tag{2.3}$$

In Equation (2.3), the electrophoretic force can be computed by the net charge of a particle under an electric field. To observe the electrophoretic behavior, planar electrodes with a 25 μm gap were prepared. Silicon(Si) nanowires with a length of 15 μm were prepared by using conventional photolithography and deep reactive ion etching. The Si nanowires suspended in dimethylformamide (DMF) solution were placed on the electrodes. When a DC potential of 1.5 V was applied across the electrodes, the nanowires were attracted to the edge and surface of an electrode on the right-hand side in Figure 4. The negatively charged nanowires were attracted to the positive electrodes.

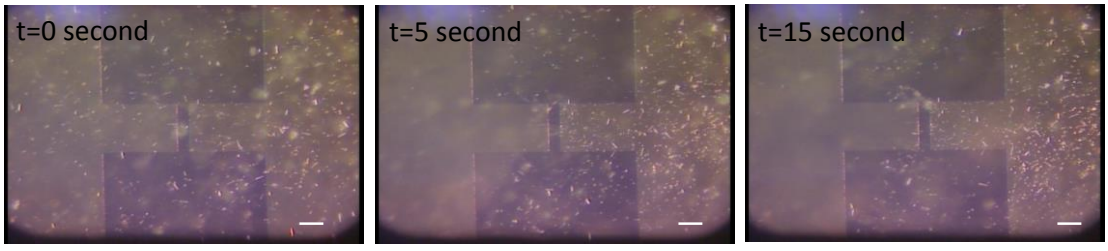

Figure 4. Electrophoretic deposition of Si nanowires; sequential images under a DC potential of 1.5 V. The scale bar is 100 μm.

2.2.2 Dielectrophoresis

Dielectrophoresis is induced by the dipole of a particle under a non-uniform electric field. The net force ($\vec{F}$) acting on the particle can be computed by summing the forces on each pole[42]:

$$\vec{F} = Q\vec{E}(\vec{r} + \vec{d}) - Q\vec{E}(\vec{r}) \tag{2.4}$$

,where is the position vector of negatively charged pole ($-Q$) and is the vector from negative pole ($-Q$) to positive pole (Q). In comparison with the characteristic length of a non-uniform electric field, $\vec{d}$ is small. The first term in the right side of Equation (2.4) can be expressed by using Taylor series expansion:

$$\vec{E}(\vec{r} + \vec{d}) = \vec{E}(\vec{r}) + \vec{d} \cdot \nabla\vec{E}(\vec{r}) \tag{2.5}$$

,where all the higher order terms are neglected by the assumption that the distance between the dipole is so small that their effect can be negligible. By applying Equation (2.5) into Equation (2.4), the force on the dipole ($\vec{F}_{dipole}$) is obtained:

$$\vec{F}_{dipole} = Q\vec{d} \cdot \nabla\vec{E}(\vec{r}) \tag{2.6}$$

For an AC field, the dipole moment ($\vec{p} = Q\vec{d}$) is:

$$\vec{p} = V\alpha\vec{E}e^{i\omega t} \tag{2.7}$$

,where V is the volume of a particle, α is the polarization factor (Clausius-Mossoti factor), and ω is the angular frequency of an input voltage. Time averaged dielectrophoretic force on a particle can be derived by using

Equation (2.6) and Equation (2.7):

$$\left\langle \vec{F}_{DEP} \right\rangle = \frac{1}{4} V \,\mathrm{Re}[\alpha] \nabla \left| \vec{E} \right|^2 \tag{2.8}$$

This analytical expression is called the effective dipole moment (EDM) theory. Using this equation, dielectrophoretic force on a particle can be computed by using a gradient of an electric field at a single point, e.g. particle center. However, EDM is not effective when a particle size is comparable to the characteristic length of an electric field. Because the force is computed at one point, the non-uniformity of electric field around a particle cannot be considered in the computation of the force.

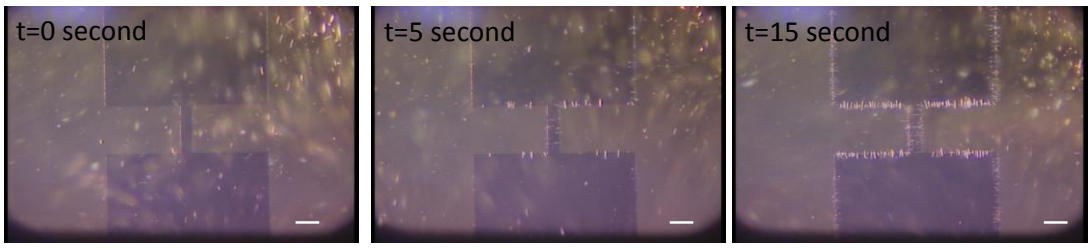

Figure 5. Sequential images of 15 μm-long nanowires deposition on the planar electrode using Dielectrophoresis. Applied voltage is 20 Vpp (peak to peak voltage) at 5 MHz. The scale bar is 100 μm.

Considering the DEP force and torque, particles are attracted to a high electric field region with orientation. More polarizable and longer particles can be more easily attracted, which can be used for the selective deposition of particles. For demonstration of DEP, 10 μL solution containing Si nanowires was placed on planar electrodes. When an electric potential of 20 Vpp at 5 MHz was applied between the electrodes, Si nanowires were attracted and deposited along the edge of the electrodes (Figure 5). The orientation of nanowires was orthogonal to the edge of the electrodes.

2.2.3 Electroosmosis

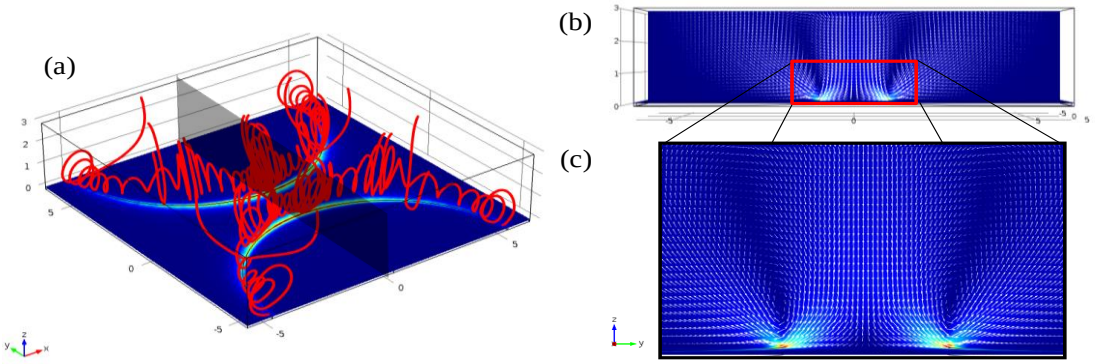

Figure 6. Simulation results of flow generated by the electroosmosis above the planar electrodes (a) Streamlines near the electrode edges. (b) Velocity vectors in the plane that indicated by the gray color in Figure 7 (a). (c) Magnified image of velocity vectors in vicinity of the edge.

When an electric potential is applied to electrodes in a solution, ions are attracted to the charged electrodes due to electrostatic interaction. The ions above an electrical double layer are not firmly anchored to the surface due to the electrical screening effect of the first layer. The ion concentration of this diffuse layer is changed along the variation of an electric field at the edge of electrodes. The decay of an electric field from the edge to the electrode surface is exponential, which induces ionic motion. The electroosmotic flow for a DC electric field can be calculated by[45]:

$$U_{EOF} = -\frac{\varepsilon_m \zeta}{\mu} E_t \tag{2.9}$$

,where ζ is the zeta potential of the layer, μ is the fluid viscosity and E_t is the tangential directional electric field. Figure 6 is the simulation result for electroosmotic flow. Figure 6(a) shows the streamlines. Flow speed at the edge is the highest and decreases drastically far from the edge. Thus the rotational flow is

induced above the electrode edge as shown in Figure 6(b) and (c). For an AC electric field, frequency-dependent terms are added [46].

For the electroosmosis observation, 10 µL solution containing Si nanowires was placed on planar electrodes. The rotation of Si nanowires was observed due to the electroosmotic flow (Figure 7). The electric potential was 4 V_{pp} at 100 Hz. The electroosmotic flow can attract nanowires in the vicinity of electrodes by circulation flows, which is much more effective than DEP. However, the random characteristic of the flow can be challenging to precise assembly of nanowires. The attraction of ions can damage the surface of nanowires and electrodes.

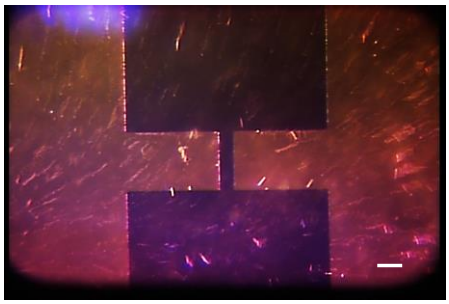

Figure 7. Behavior of 15 µm-long nanowires under electroosmosis. Applied voltage is 4 Vpp at 100 Hz. The scale bar is 100 µm.

2.3 Concentration mechanism of a microtip immunosensor

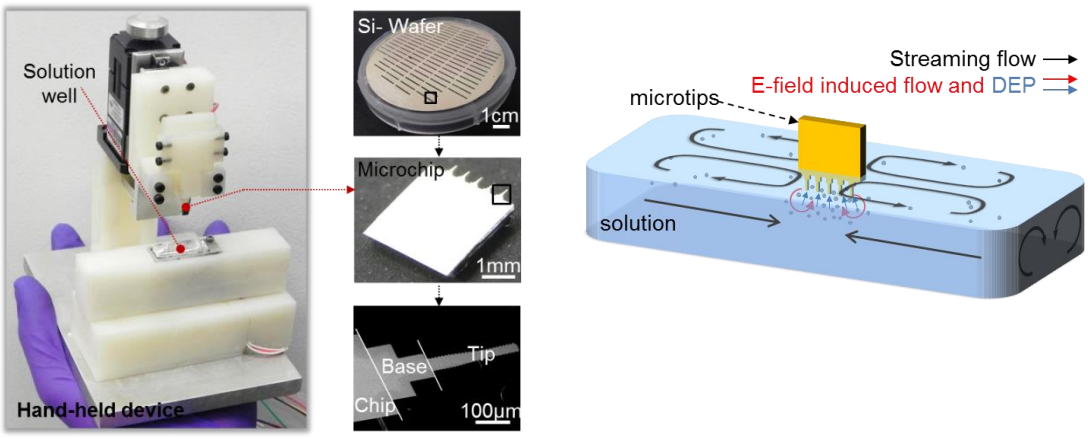

(a) (b)

Figure 8. (a) Prototype device composed of microtips and aluminum well. A silicon chip consists of 5 microtips that are divided into three regions, namely chip, base, and tip. A total of 340 chips are fabricated on a 100 mm-diameter wafer. (b) Concentration mechanism of target bacteria in 1mL sputum samples using streaming flow, Electric field induced flow, and dielectrophoresis.

The microtip immunosensor was develpoed to handle a processed sputum sample of 1 mL, yielding a 'Yes or No' answer. The prototype device (Figure 8a) is composed of a linear motor to control the dipping and withdrawal of microtips and a 1mL aluminum well that is vibrated to generate a streaming flow. A function generator (Agilent 33220A, Santa Clara, CA) was used to apply an AC electric field (20Vpp at 5MHz).

For rapid concentration of target bacteria, streaming flow, electrohydrodynamic (EHD) flow, and dielectrophoresis were combined (Figure 8b). The bacteria in the 1 mL sample well were transported within 1 mm distance from the microtips by streaming flow. The steady streaming flow was induced by the longitudinal vibration of the well with amplitude of 45μm at 31.3 Hz. Within this 1 mm distance, the average flow speed was reduced to 100~200 μm/second

based on our observation. The transported bacterial cells were delivered in the vicinity of microtip surface by electric field induced flow. The electric field-induced flow could be generated by both electroosmotic- and electrothermal flows. The electric field induced flow speed was 900 μm/second at maximum at the microtip end and decreased towards the base- and chip regions of the microtip. The delivered cells were further attracted to the microtip surface by dielectrophoresis. In the following sections, the concentration mechanism is analyzed with the evaluation of the assay performance in sputum.

2.4 Experimental Study

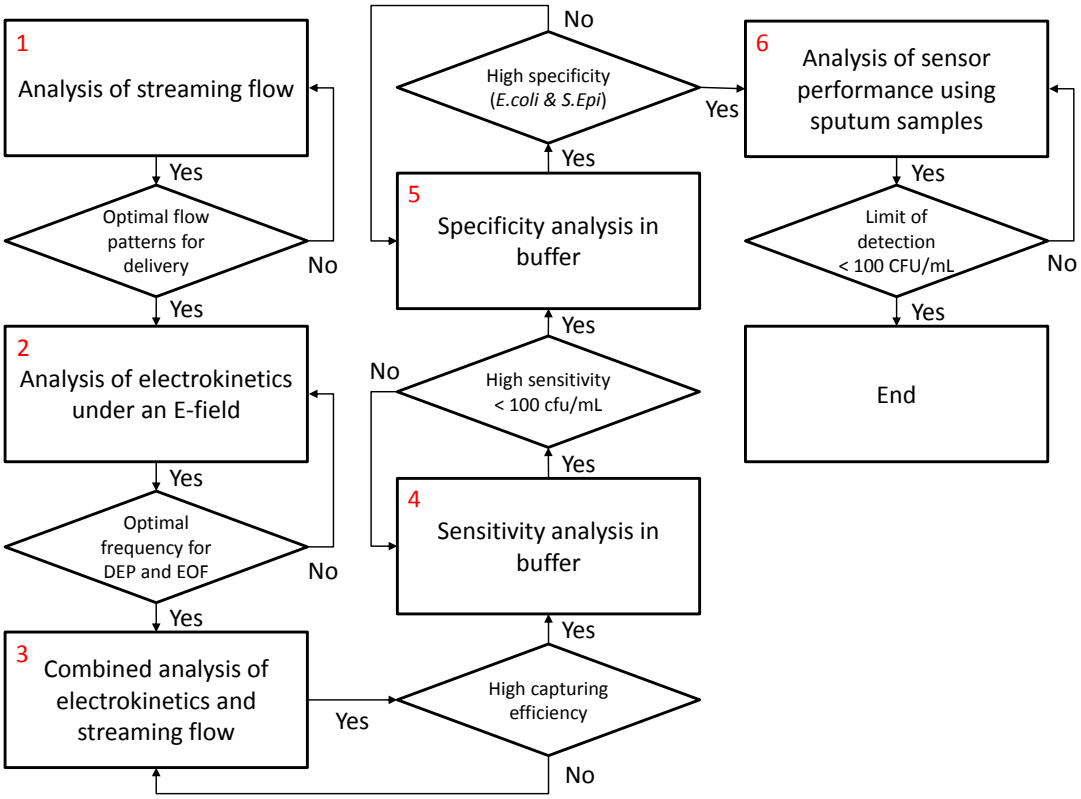

Figure 9. Flow chart of the experimental study to check the performance of the microtip immunosnesor.

For the effective concentration, streaming flow and electric field were optimized through experimental study. The contribution of streaming flow and an electric field to the concentration of target bacteria was then studied using the functionalized microtips. Afterwards, the sensitivity and specificity of the microtip immunosensor was checked with various bacteria cells (BCG, *E.coli*, and *S.Epi*) spiked in 1x PBS buffer. Finally, to decide the lower limit of detection of the microtip immunosensor, various concentration of target bacteria cells (BCG and MTB) spiked in sputum samples was tested. Figure 9 shows the flow chart of the experimental study to check the performance of the microtip immunosensor.

2.4.1 Experimental Method

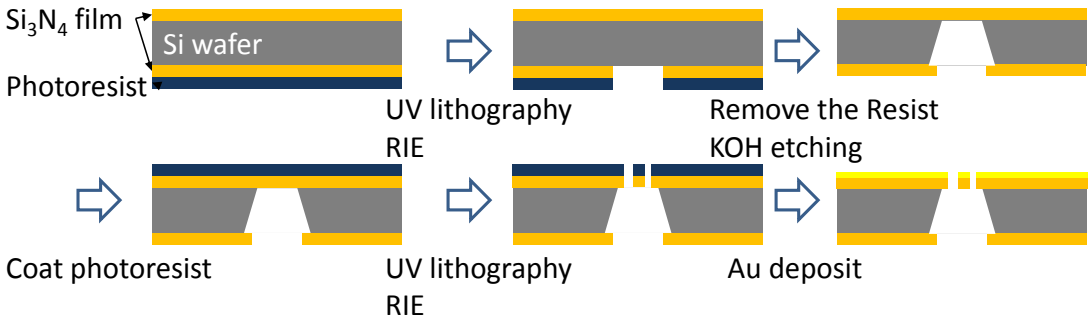

(a)

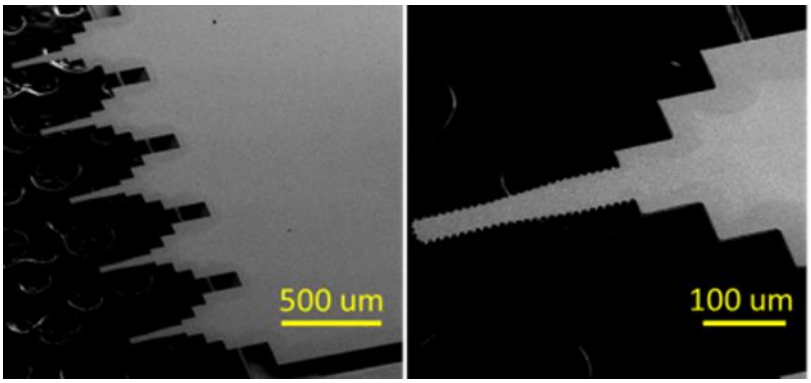

(b)

Figure 10. (a) Microtip fabrication procedure. (b) SEM images of the microtips.

Microtip fabrication: Microtips were fabricated in a microfabrication laboratory (Washington Technology Center, University of Washington) as illustrated in Figure 10(a). The microtips were fabricated from Si wafers having 100mm in diameter. Using low pressure chemical vapor deposition (LPCVD), a 1 µm thick silicon nitride layer was grown on Si wafers (100 mm in diameter). Rectangular areas were patterned on the back side of a Si_3N_4 layer using conventional UV lithography and etched using reactive ion etching (RIE) followed by KOH etching. The wavy-shape of the tip was then patterned on the Si_3N_4 layer and etched by the RIE process to create free-standing microtips. Finally, the tip surface was coated with gold for electrical conductivity. Figure 10(b) shows

microtip images by scanning electron microcopy (SEM, NanoTech User Facility, University of Washington).

Functionalization of microtips: The microtips were functionalized for the specific binding (Figure 11). Polyethyleneimine (1% PEI in DI water, Sigma-Aldrich, St. Louis, MO) was coated as an adhesive layer. The PEI treated tip was then immersed in biotinylated bovine serum albumin (10mg/mL in PBS, Sigma-Aldrich) for 5 minutes. The biotin-BSA coated tip was coupled with streptavidin (1mg/mL in PBS, Sigma-Aldrich) for 1 minute. For the specific binding, the streptavidin-coated tip was immobilized with the biotinylated IgY antibodies (3 mg/ml biotin-Antibody in PBS).

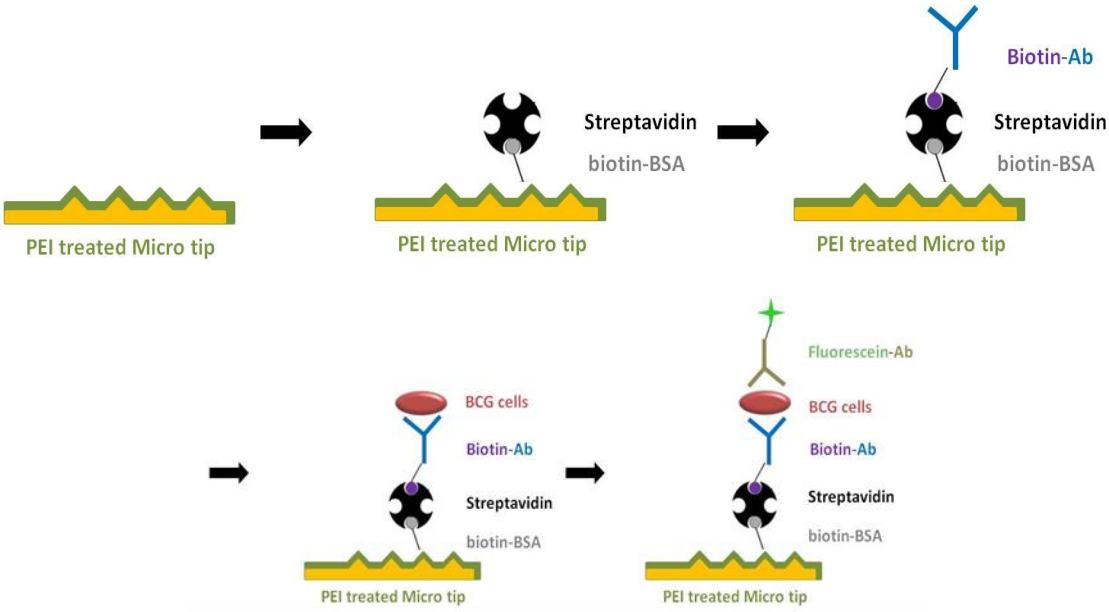

Figure 11. Functionalization process of a microtip

Analysis of electrokinetics under an electric field: To observe the behavior of BCG cells under an electric field, Au-coated microtips without antibodies were utilized. BCG cells at 10^7 CFU/mL in PBS buffer were stained with live-dead staining kits (LIVE/DEAD® BacLight™ Bacterial Viability Kit, Invitrogen,

Carlsbad, CA). With an AC field, circulation flows were generated with attraction of MTB cells on to the microtip surface. The attraction process was video-recorded, which was analyzed by using mPIV (Matlab Particle Image Velocimetry, MATLAB®, The MathWorks, Inc., Natick, MA). The frequencies were also changed from 1 MHz to 20 MHz to check the dependence of frequencies for the EHD flow.

Analysis of streaming flow by vibration: The fluid motion by streaming flow was anlayzed by 19.0 μm-diameter polystyrene spheres in the steady state. The streaming flow is generated by free surface motion of fluid that is induced by the linear excitation of a well with an amplitude of 45μm at 31.3 Hz. The flows were measured along 2 horizontal-, 3 vertical-, and 3 side planes dissecting the well. The measured flows in each plane were integrated into 3 dimensional flows

Combined analysis of electrokinetics and streaming flow: To study the effects of a streaming flow and an electric field to the concentration of target bacteria, the functionalized microtips were used in combination with *M. bovis* BCG cells at a concentration of 10^7 CFU/mL in 1×PBS. For counting individual cells, BCG cells were stained with an intercalating dye (SYTO 9® green fluorescent nucleic acid stain; Molecular Probes L7007, Invitrogen, Carlsbad, CA), visualized by an epi-fluorescence microscope (Olympus BX-41, Olympus America Inc., Melville, NY), and quantified. A 1 mL sample solution containing stained BCG cells was loaded on the aluminum well. For concentration, the microtips were immersed in 1 mL sample for 2 minutes. For comparison, four cases involving on-off combinations of vibration and electric field (20 Vpp at 5

MHz) were tested. After 2 minute-concentration, the number of captured BCG cells was counted on the microtips surface for each case.

Sensitivity analysis: To test the sensitivity of microtips, various concentrations of BCG cells in PBS (10^1~10^6 CFU/mL) were suspended in PBS buffer. A 1 mL solution of prepared bacteria sample was loaded on the aluminum well. The microtips were immersed in 1 mL of a bacteria solution for 2 minutes with a vibration and an applied AC field (20 Vpp at 5 MHz). After 2 minute-immersion, the microtips were withdrawn at a rate of 100 μm/s. Subsequently, the microtips were immersed in a prepared fluorescein conjugated antibody solution (10 μL, 2mg/mL) for 5 minutes and then rinsed with a deionized water (200 μL) for 5 seconds. The rinsed microtips were observed under an epi-fluorescence microscope. The raw fluorescence image was digitized into a black and white image based on a threshold intensity. The threshold value was determined in order to suppress most negative control signals. The experiment was repeated 4 times for each concentration. For the control experiment, 1×PBS buffer (conductivity: σ=1.58 S/m) without bacteria cells was used.

Specificity analysis: Enzyme-linked immunosorbent assay (ELISA) was conducted to check the affinity and avidity of antibodies. Equal concentrations (OD 600 matched) of three different bacteria (BCG, *E. coli* and *S.epidermidis*, approximately 10^5 cells in 100 μl PBS) were assayed for binding to anti-BCG IgY antibody using a 0.45 micron filter plate (Millipore #MAHVN4510). Aliquots of the bacterial suspensions were added to the 96-well filter bottom plate and washed with PBS (4x200 μL). A 100 μl aliquot of 10 μg/ml IgY-BCG antibody in PBS

was then added to the washed cells and incubated for 1hour at 37C. After a PBS wash (4x200 µl) a secondary antibody was added (rabbit anti-IgY-HRP conjugate, Thermo Scientific #31401) and incubated for 1hour at 37C. The sample was then washed with PBS (4x200 µl), followed by addition of 100ul ABTS substrate (Thermo Scientific #37615), incubated for 5 minutes, and filtered into 96-well receiver plate. Aabsorbance was then read at 405 nm. The specificity of the microtip sensor was then tested with various bacteria spiked into 1×PBS buffer. Suspensions of BCG (concentration: 10^2 CFU/mL), *Escherichia coli* (*E. coli*, 10^4 CFU/mL), and *Staphylococcus epidermidis* (S. epi, 10^4 CFU/mL) were prepared in 1×PBS buffer. The experimental procedure was the same as the sensitivity test using BCG. For verification, 3 experimental runs were conducted for each case.

Analysis of sensor performance: The sputum samples varied in terms of viscosity, opacity, and color. The viscosity and conductivity could be key parameters to characterize each sputum sample in terms of effective fluid motion. However, the measurement tools for viscosity and conductivity can be contaminated by sputum samples. In addition, a large volume sample over 10 mL is required for a reliable measurement. Thus the variation of the processed sputum samples was monitored on the basis of the turbidity using UV spectrophotometer. Turbidity was the ratio of the absorbance of the sample solution to a reference at a wavelength of 600nm. 6 sputum samples were randomly chosen and then processed following the liquefaction procedure. The processed sample was transferred to a cuvette, and the absorbance was then measured at 600 nm using a UV spectrophotometer (BioRad SmartSpecTM 3000, Bio-Rad, Hercules, CA). For

the reference measurement, the mixture of PBS, NALC and SDS without sputum was used.

For preliminary test for sputum samples spiked with BCG, the concentrations of sputum samples spiked with BCG were 2×10^2 ~ 2×10^6 CFU/mL by 10 fold increments. The images of individual microtips were digitized and compared at each concentration. In addition, a total of 11 tests were conducted as 6 negative sputum controls and 5 sputum samples spiked with BCG of 2×10^2 CFU/mL. Sputum samples from people known not to have TB were purchased from BioReclamation, Inc. Sputum spiked with BCG (total 600 μL) was mixed with 4 mg/mL N-Acetyl-L-Cysteine (NALC; 300 μL, σ=0.12 S/m) and 3 mm glass beads. The sample was vortexed for 5 minutes. 4% sodium dodecyl sulfate (SDS; 300 μL, σ=0.37 S/m) was added to the mixture. Additional vortexing for 5 minutes was conducted for complete liquefaction. The liquefied degree of sputum was tested by the turbidity. In the process, the final concentration of BCG in the processed sputum was the half of each initial concentration.

2.4.2 Results and Discussion

Analysis of electrokinetics under an electric field: Stained BCG cells were circulated around the microtip due to EHD flow and attracted on the surface of a microtip by DEP as shown in Figure 12(a). When the frequencies were changed from 1 MHz to 20 MHz, the EHD flow velocity was reduced from 456 μm/s to 63 μm/s in Figure 12(b).

Regarding the dielectrophoretic attraction of target cells, BCG bacteria in a

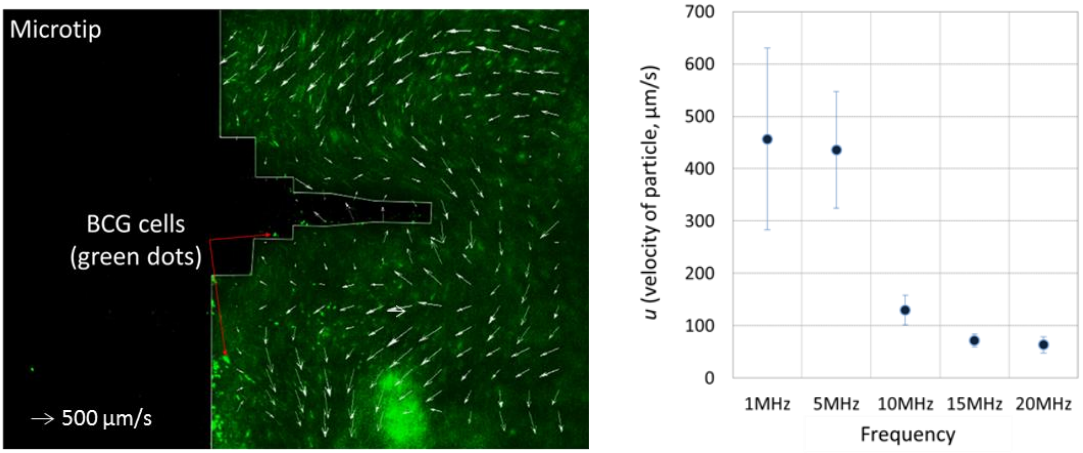

(a) (b)

Figure 12. Motion of BCG cells under an AC e-field (5MHz at 20 Vpp). (a) Stained BCG cells were circulated around the microtip due to EHD flow and attracted on the surface of a microtip by DEP. (b) Average velocities of EHD flow in the vicinity of a microtip according to frequencies.

medium were polarized and attracted to the microtip by induced dipole moment. To estimate the electric field strength and the corresponding DEP force, a finite element software (COMSOL Multiphysics®, COMSOL, Inc., Burlington, MA) was used. Through 3-D simulation studies as shown in Figure 13(a), an optimal tip design was determined to have a wavy shape to generate multiple maximum points of an electric field. The highest gradient of an electric field was generated at the first and fifth microtips among 5 microtips (Figure 13b). Thus more target cells could be captured on both microtips. The Clausius-Mossotti factor was assumed as 1, considering bacteria as a spherical particle having 4 µm in diameter. Dielectric constant used for modeling the media (PBS) was 78. The maximum DEP force was 1.4 nN.

The electrokinetic flow is mainly generated by electroosmosis but can be affected by electrothermal flow. To clarify the generation mechanism of EHD flow

at 5MHz, the flow velocities were measured in response to frequency variation. The change of the flow velocities was also compared with the trend presented by analytical equations for electroosmotic- and electrothermal flows.

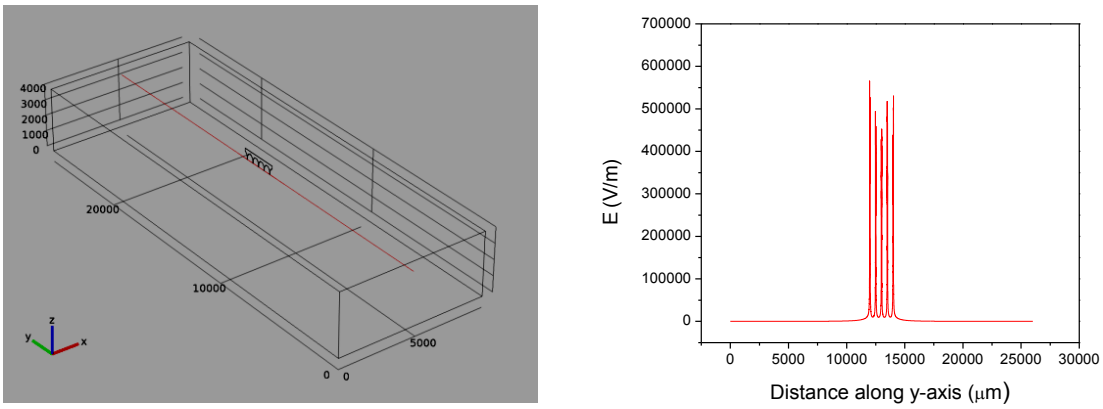

(a) (b)

Figure 13. (a) Geometry of microtips and a well for calculation of an electric field (unit: μm). (b) E-field distribution along the red line shown in Fig. 13(a). Five peaks of an electric field are generated at five microtips.

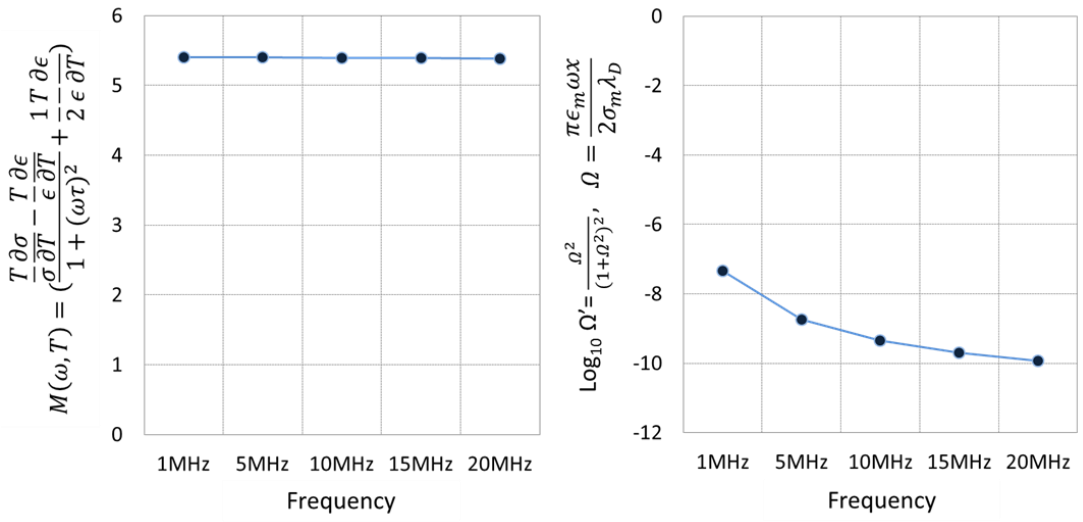

(a) (b)

Figure 14. Factors proportional to velocities of electrothermal- and electroosmotic flows in terms of frequency variation (a) M factor for electrothermal flow (b) $\Omega^2/(1+\Omega^2)^2$ for electroosmotic flow. This parameter is the dominant variable of time-averaged AC electroosmotic velocity.

Electrothermal flow arises from the temperature gradient in a medium generated by joule heating of the fluid. This temperature gradient induces local changes in the conductivity, permittivity, viscosity, and density of the solution. These gradients can generate forces acting on fluid. An electrothermal factor M (Ramos et al.) is given by:

$$M(\omega,T) = \left(\frac{\frac{T\partial\sigma}{\sigma\partial T}-\frac{T\partial\epsilon}{\epsilon\partial T}}{1+(\omega\tau)^2} + \frac{1}{2}\frac{T}{\epsilon}\frac{\partial\epsilon}{\partial T}\right) \quad (2.10)$$

M(ω,T) is a dimensionless factor that shows the variation of the electrothermal force as a function of the frequency. Since the electrothermal force is proportional to the velocity of electrothermal flow, M factor is proportional to the velocity of electrothermal flow. The value of $M(\omega,T)$M(ω, T) is calculated for σ=1.58 S/m$\sigma = 1.5\frac{\mathrm{S}}{\mathrm{m}}$ S/m, T=300K, ε=80$\varepsilon_o\epsilon = 80\varepsilon_0$, V=20V (peak to peak), ω=2πf, and τ=ε/σ. The computed M-values are shown in Figure 14(a). According to this analytical result, the flow velocity for electrothermal flow should be constant in the frequency range of 1~20MHz.

Time-averaged ac electroosmotic velocity is derived from a generalization of the Smoluchowski formula given by:

$$u_{ACEO} = \Lambda\frac{\epsilon_m V_p^2}{8\mu x}\frac{\Omega^2}{(1+\Omega^2)^2} \quad (2.11)$$

Here a nondimensional frequency Ω is:

$$\Omega = \frac{\pi\epsilon_m\omega x}{2\sigma_m\lambda_D} \ . \quad (2.12)$$

The value of Ω is calculated for $\epsilon = 80\varepsilon_0$, $\sigma = 1.5\frac{\mathrm{S}}{\mathrm{m}}$ S/m, λ_D=1nm

(double layer characteristic thickness), and x=1mm (characteristic length in system). Figure 14(b) shows $\Omega' = \Omega^2/(1+\Omega^2)^2 \frac{\Omega^2}{(1+\Omega^2)^2}$ that continuously decreases between 1 and 20 MHz, meaning that the time-averaged AC electroosmotic velocity also decreases in the range.

When the experimental results (Figure 12b) are compared with the analytical results in the frequency range of 1 ~ 20MHz, the drop of the flow velocity is consistent with the trend of Ω´ for electroosmotic flow. If the flow is dominated by electrothermal flow, the flow velocity should be constant in the frequency range of 1MHz ~ 20MHz, following the trend presented in Figure 14(a). Thus the fluid flow at 5 MHz can be dominated by AC electroosmosis. When the frequency is greater than 10MHz, a flow velocity reaches a bottom plateau. This flow can be caused by electrothermal flow. According to the results, electroosmotic flow is dominant at 5 MHz but electrothermal flow also coexists. The transition between electroosmotic- and electrothermal flows for 1.58 S/m buffer at 5 MHz is consistent with the previous analysis[85]. The delivered cells by EHD flow were attached to microtip surfaces by dielectrophoresis.

Analysis of streaming flow by vibration: For the streaming flow, particle image velocimetry revealed 3 dimensional circulation flow that delivered particles to the center of the well. The flows were measured for 2 horizontal-, 3 vertical-, and 3 side planes, which were integrated into 3 dimensional flow as shown in Figure 15. Microtips were immersed in the center of the well where the flow velocity was reduced to 100 μm/second. Thus MTB cells were delivered to microtips by the circulation flows and further concentrated and captured on to

microtip surface by electrokinetic flow and dielectrophoresis.

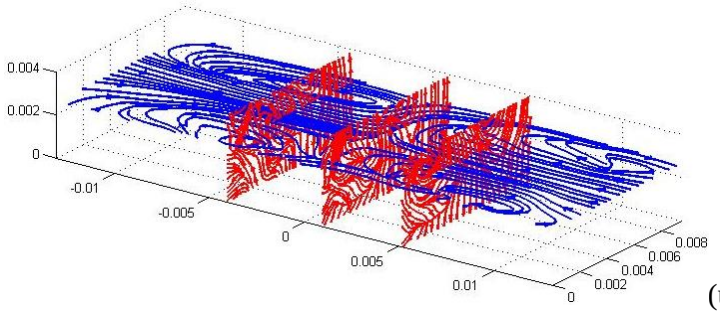

(unit: meter)

Figure 15. 3 dimensional flow that is generated by longitudinal vibration of an aluminum well.

Combined analysis of electrokinetic and streaming flow: To study the relative contributions of vibration-induced flow and electric field to concentration of bacteria, four cases involving on-off combinations of vibration and electric field were tested. When both vibration and electric field were activated, the number of captured cells was greatest (Figure 16a). When either vibration or electric field was applied alone, fewer cells were captured.

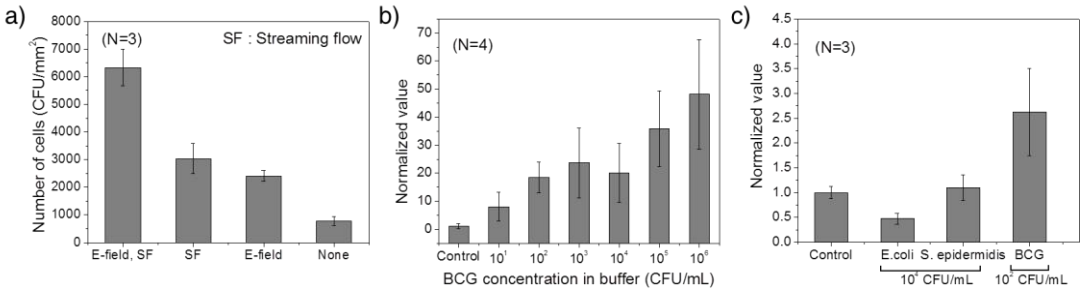

Figure 16. (a) Effect of each concentration mechanism. Each value represents the number of captured cells per microtip. (b) Sensitivity test for BCG cells in PBS buffer by using immunofluorescence microtip sensor. (c) Specificity test for *E. coli*, *S. epidermidis*, and *M. bovis* (BCG) solutions. The concentration of *E. coli* and *S. epidermidis* is 10^4 CFU/mL while that of BCG is 10^2 CFU/mL.

Sensitivity and specificity analysis: When the microtips were tested for capture and detection of various concentrations of BCG cells in a PBS buffer, the

sensitivity was 10 CFU/mL (Figure 16b). Overall, the fluorescence intensity was enhanced with increasing cell concentration but the signal was not quantitative. In repetitive measurements, the signals separated into three regions ranging from the low level of the negative control, to the intermediate level of $10\sim10^4$ CFU/mL, and to the high level of $10^5\sim10^6$ CFU/mL.

The anti-BCG polyclonal IgY is used both for detection as well as capture. Its specificity was evaluated by using an ELISA. Compared with the response for *S. epi* and *E. coli*, the antibodies bound significantly more avidly to BCG (Figure 17). In the specificity test using immunofluorescence microtip sensor, The BCG signal significantly exceeded the signals of *E. coli*, and *S. epi* whose concentrations were greater by two orders of magnitude than that of BCG (Figure 16c).

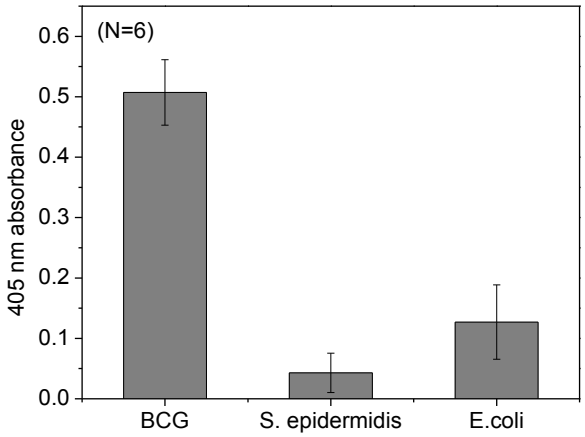

Figure 17. Anti-BCG IgY ELISA results. The experiment was kindly conducted by Scott Soelberg.

Analysis of sensor performance: To characterize the processed sputum samples, the turbidiy was measured. The turbidity of the processed sputum samples was 0.054±0.034 at 600 nm while that of the original sputum was greater

than 1. In addition, the conductivity of each reagent for using sputum liquefaction was measured to study dominant conductivity of a reagent. The conductivities of 1xPBS, 4mg/mL NALC, and 4% SDS were 1.58 S/m, 0.12 S/m, and 0.37 S/m, respectively. The conductivity of the mixture was 0.71 S/m, which was dominated by that of PBS.

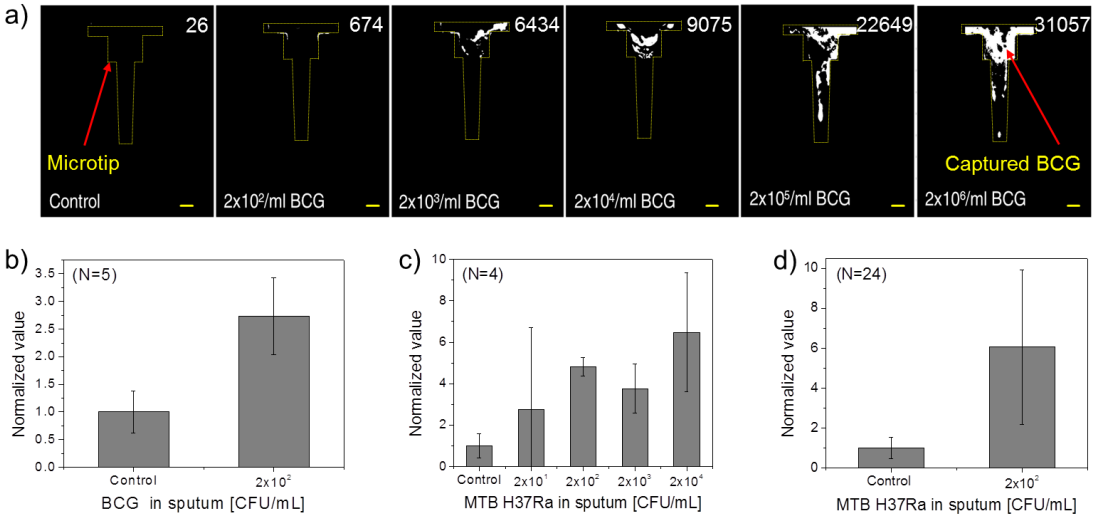

Figure 18. Test results for detection limit of the microtip-immunosensor for sputum. (a) Digitized images from sputum samples spiked with BCG. The concentrations of BCG and the average numbers of white pixels are shown at the bottom and top in the images, respectively. The scale bar is 50 μm. (b) Immunofluorescence detection of BCG at 200 CFU/mL. (c) Dose response for MTB spiked in sputum samples. At an MTB concentration of 20 CFU/mL, 3 positive signals out of 4 samples are higher than the negative controls. (d) Reproducibility test at a MTB concentration of 200 CFU/mL in sputum. Compared with 6 negative controls, 23 out of 24 samples show positive signals. The total success rate is 96%.

For the preliminary test using human sputum spiked with BCG, the white spots indicated captured *M. tuberculosis* complex cells on the microtips (Figure 18a). The bacteria were observed in greater numbers at the base regions of the microtips. Interestingly, the cells were detected at the terminal end of the microtip only when the initial concentration was greater than 10^5 CFU/mL. In this test, the signal was discernable down to 200 CFU/mL. At the concentration, a total of 11

tests were conducted. The signals generated by spiked samples were clearly differentiated from the negative controls (Figure 18b).

In the dose response test using MTB H37Ra in sputum, the detection limit was 200 CFU/mL (Figure 18c). In order to assess the reproducibility of the microtip sensor when challenged with diverse spiked sputum samples, an additional 30 sputum samples (6 negative controls and 24 distinct samples spiked with MTB H37Ra at 200 CFU/mL) were tested. On the basis of 6 negative controls, 23 tests out of 24 positive samples gave correct calls, a 96% success rate. As mentioned above, the samples in Figure 18(d) varied in terms of viscosity, opacity, and color, suggesting that the method is robust and can be applied to diverse sputum samples. The detection limit of 200 CFU/mL is equivalent to PCR amplification-based methods applied to sputum samples following similar protocols[69]. Given that sputum samples are replete with human cells, bacteria, and other microorganisms, these results also demonstrate the specificity of the microtip sensor.

The high specificity of this method is due in part to the polyclonal IgY antibody. The antibody has not yet been tested for cross-reactivity to non-tuberculous *Mycobacterium* (NTM) species that frequently occur in respiratory samples from symptomatic patients. Given the close antigen relatedness between MTB and NTM, cross-reactivity is likely. However, in the resource-limited countries for which the microtip technology is designed, NTM-related disease remains relatively rare. For example, in a recent large study conducted on 1730 suspected TB cases at sites in Peru, Azerbaijan, South Africa, and India, fewer

than 3% of confirmed *Mycobacterium*-positive cases had NTM disease[70].

2.4.3 Comparison with other TB diagnostic methods

Table 2. Comparison microtip immunosensor with other TB diagnostic methods.

Contents	GeneXpert	Magnetic particles based fluorescence	Microtip-fluorescence
Biomarkers	DNA	MTB (whole cells)	MTB/DNA
Limit of detection	130 cfu/mL	10,000 cfu/mL	200 cfu/mL
Power requirement	150W	5W	5W
Assay time	2 hours	45 minutes	25 minutes
Detection of MDR-TB	Yes	No	Yes (next-generation with DNA detection)
Sample number	4	20	1 (extended to 4)
POC diagnosis	No	No	Yes

2.5 Summary

In summary, the immunofluorescence microtip sensor specifically detected *Mycobacterium* cells through the combination of electric field, streaming flow, and immuno-affinity binding. The electrokinetic flow at 5MHz was generated by electroosmosis and the dielectrophoresis attracted target cells on to the microtip surface.

The detection limit was 200 CFU/mL in human sputum, which was comparable to PCR but without requiring bacteriological culture, centrifugation, or nucleic acid amplification. In spite of the complex nature of physical, chemical, and biological mechanisms, the simple operation of “dipping and withdrawal” of tips will allow for screening by minimally trained personnel within 30 minutes. In addition, the minimal power requirement (5 W) combined with the low assay cost is ideal for point-of-care (POC) screening in limited resource settings.

Chapter 3: Study of Contact Angle Reduction due to Immunocomplex Formation

3.1 Introduction

Infectious diseases, such as AIDS, malaria, and tuberculosis, show profound disparities in health outcomes between the advanced and developing economies. Thus, one of the grand challenges in global health is to control infectious diseases accurately and economically in developing countries.[86] Early detection and full treatment of the highly contagious diseases is especially important for patient care and control of disease transmission. For the rapid identification of target biomarkers, immunoassays have been frequently used for the last few decades. Immunoassays rely on the inherent binding ability of antibodies to specific molecules. The interaction between antigen and antibody is one of the fundamental immune responses, which plays an important role to prevent and resolve the infections by foreign objects through highly specific interaction.[87] The interactions are also crucial for biological characterizations and disease diagnosis. When an immunoassay runs, multiple binding and rinsing steps are routinely required. For characterization of an immunoassay, antibodies are immobilized on a substrate. For this step, a liquid drop containing antibodies is dried on a sensing region. To detect a target, a liquid having targets is then applied on the surface for binding followed by rinsing. Through the multiple handling of liquid drops, the detection results can be significantly affected by the immunocomplex formation in conjunction with capillary action as illustrated in Figure 19.

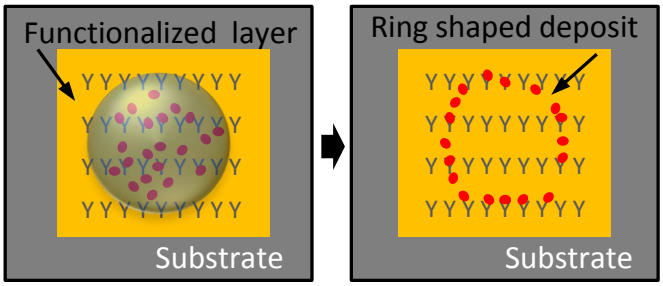

Figure 19. Conventional procedure for immunoassays

When a solution drop containing particles dries on a solid surface, the particles are arranged with a complex pattern on a substrate. The drying pattern also significantly affects the assay performance.[88, 89] Such drying pattern has been used for crystal formation of dispersed molecules.[90-92] The deposit pattern is correlated with the behavior of liquid evaporation.[93] One of the deposits is the 'coffee ring' pattern.[92] Over the past decade, it has been discovered that various physical parameters including pinning criteria[94], particle size[95], particle shape[96], solvent type[97], and surfactant effects[98] affect the coffee ring pattern. The coffee-ring effect can be manipulated for a wide range of microarray deposition[91], ink jet printing[99], and particle separation[100]. Recent studies have also shown that the pattern formation in liquid drops containing bio-entities, such as protein molecules, micro-organisms, and cells can be utilized as a biological indicator[95, 100]. However, the study of the coffee ring formation due to immunocomplex formation is yet to be studied.

In this chapter, the contact angle and the deposit patterns of cell suspension are investigated in the context of binding affinity. To study how the binding affinity affects the contact angle of a solution drop on a functionalized surface, a rectangular gold substrate immobilized with specific antibodies is utilized as a

model system. Two different kinds of cells, BCG and *E. coli* are used with the corresponding antibodies.

3.2 Theoretical Study

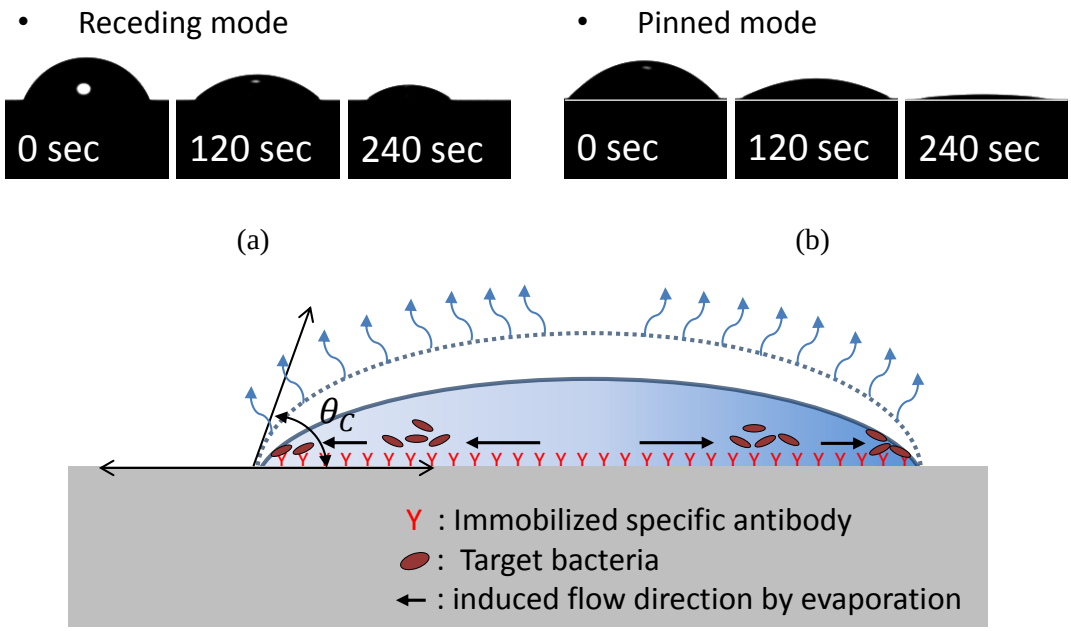

Figure 20. (a) Side view of an evaporating droplet over time, Receding mode on bare gold surface (top): the diameter of the wetting area decreases, Pinned mode with antibody-coated surface (bottom): the contact angle decreases while the wetting area remains constant. (b) Young's equation combined with binding forces at a steady state and during evaporation.

The evaporation of water droplets is categorized into two main modes. One is the receding mode where the contact area between droplet and substrate continuosly decreases (Figure 20a). In this mode, the contact angle can be either changed or maintained. The other is the constant contact-area (pinned) mode where the contact angle decreases with constant contact area. In this mode, the contact angle is gradually decreased (Figure 20b). Evaporation, which is a complex, hard-to-control, and nonequilibrium system, occurs over the entire drop surface. During the receding mode, the drop profile would be preserved. Thus, Marangoni flow induced by a suface tension gradient due to temperature differences is dominant and results in a recirculatory flow. However, for the

pinned mode, the contact angle decreases. Thus, a capillary flow outward from the drop's center to its edges is induced to replenish evaporating liquid at the contact line and brings suspended particles to the edge as evaporation proceeds.

When a liquid drop containing bateria is placed on the substrate, the contact angle of a liquid drop can be changed due to the binding affinity of the bateria on the substrate. Without bateria, the contact angle of the liquid drop on the surface immobilized with antibodies is governed by the Young-Laplace equation (Figure 20c).

$$\gamma_{SG} - \gamma_{SL} - \gamma_{LG}\cos\theta_0 = 0 \tag{3.1}$$

where γ_{SG} is the solid–vapor interfacial energy, γ_{SL} is solid–liquid interfacial energy, and γ_{LG} is the liquid–vapor interfacial energy.

When bateria are introduced in the liquid drop, the binding forces at the steady state (f_b) and during evaporation [$f'(t)$] can be added in the Young's equation as illustrated in Figure 20(c). The total solid-liquid interfacial energy (γ'_{SL}) modified by the binding affinity is:

$$\gamma'_{SL} = \gamma_{SL} - f_b - f'(t) \tag{3.2}$$

Due to the modified γ'_{SL}, the contact angle is changed into θ_b as below:

$$\gamma_{SG} - \gamma'_{SL} - \gamma_{LG}\cos\theta_b = 0 \tag{3.3}$$

By combining equations (3.2) and (3.3), the contact angle (θ_b) is given by:

$$\cos\theta_b = \left(\frac{\gamma_{SG} - \gamma_{SL} + f_b}{\gamma_{LG}}\right) + \frac{f'(t)}{\gamma_{LG}} \tag{3.4}$$

In equation (3.4), the contact angle (θ_b) of the solution can be changed according to the binding forces between cells and antibodies.

For the immunocomplex formation, specific bindings between cells and antibodies show higher binding force than nonspecific biniding [101]. In case of specific binding, the cells are more strongly pinned at contact line of a liquid drop, which increases the evaporation flux and reduces contact angle (θ_{bs}). With the nonspecific binding, the weakly pinned contact line causes smaller evaporation flux and higher contact angle (θ_{bn}) compared to the specific binding. In the case of a pinned contact line, the projected area of the droplet should be maintained. Through the outward flow, more cells are transported to the contact line and thus form the thick perimeter of the cells. [97] Therefore, the larger binding forces can hold the contact line during the evaporation, which induces the outward flow in the solution droplet. The resulting outward flow concentrates target pathogens at the edge of the meniscus. In summary, the specific binding between cells and antibodies induces the pinning of cells at the edge of a solution drop, which increases the evaporation flux and reduces the contact angle. In case of nonspecific bindings, the contact angle can be reduced but with lower degree in comparison with specific binding. Thus the contact angles should be reduced from the pure liquid (θ_0), to the nonspsecific binding (θ_{bn}), to the specifici binding (θ_{bs}), which is validated by experiment.

3.3 Experimental Study

3.3.1 Experimental Method

In experiment, BCG and *E. coli* were chosen as a model system. Both cells have similar size and shape, but antigenicity of both cells is different. Both BCG and *E. Coli* cells are typically rod-shaped, and are about 2 μm in length and 0.5 μm in diameter. The anti-BCG polyclonal IgY antibodies were raised against *M. tuberculosis* complex (*M. bovis* BCG) cells and the anti-*E. coli* polyclonal IgG antibodies were purchased from ProSci Inc (Poway, CA).

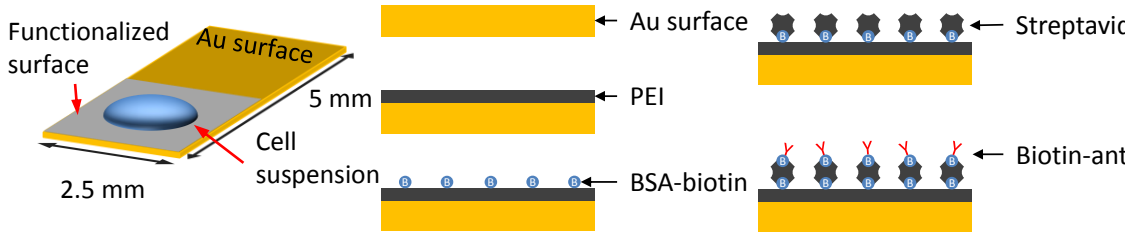

Figure 21. (a) Experimental setup (b) surface modification method

To investigate how the binding affinity affects the contact angle of a liquid drop including bacteria cells, a rectangular gold-coated Si substrates having 2.5 mm in width and 5 mm in length were coated wtih antibodies (Figure 21a). On Si wafer, a 1μm-thick oxide layer was thermally grown. A 20 nm-thick gold layer was evaporated on the oxide layer by electron-beam evaporator. For immobilization of antibodies (Figure 21b), the gold layer was coated with polyethyleneimine (PEI, Sigma-Aldrich) by dipping a rectangular strip into PEI solution. PEI was water-soluble polymer and had the strong hydrogen bond interaction with proton donors. Since PEI was cationic, the negatively charged protein was attracted to the gold surface. The coated surface was dried at room temperature for 2 minutes. Subsequently, the PEI-coated substrate was dipped in

biotinylated bovine serum albumin (biotin-BSA, Sigma-Aldrich) for 5 minutes. The surface was dried in air after withdrwal. Subsequently, streptavidin (Sigma-Aldrich) was coated by dipping and withdrawal of the substrate on the biotin-BSA coated substrate. Finally, the surface was functionalized with the biotinylated antibodies. For the antibodies, either anti-BCG IgY (2mg/mL) or anti-E.oli IgG antibodies (2mg/mL) was coated on the substrate.

To analyze the specific binding of bacteria cells on the functionalized surface, both BCG and *E. coli* cells at 10^7 cfu/mL in 1xPBS buffer were stained with an intercalating dye (SYTO 9® green fluorescent nucleic acid stain; Molecular Probes L7007, Invitrogen, Carlsbad, CA). To eliminate unbound staining dyes, the solution was centrifuged to collect the pellet in a tube. The collected pellets were resuspended in PBS.

To study the contact angle, both stained BCG and *E. coli* cells were used. Considering the two kinds of antibodies, the initial contact angles using liquid without bacteria are measured on the subtrates. For the analysis of the specific- and nonspecific binding cases, four combinations were tested as summarized in Table 3. A 0.5μL-droplet of stained BCG cells (or *E. coli* cells) was placed on the functionalized substrates. Subsequently, both the contact angle at the initial state and the contact angle at evaporation were measured by goniometer (rame-hart, model 500 Adv G/T). Each case was repeated three times (n=3). The dried pattern was then observed under an an epi-fluorescence microscope (Olympus BX-41, Olympus America Inc., Melville, NY). To evaluate the distribution of bacteria, the fluorescence images were digitized based on the threshold value using a Matlab.

The threshold value was chosen to eliminate most background signals.

Table 3. Summary for experimental combinations and contact angles

	Antibodies on substrate	
	BCG IgY antibodies	*E. coli* IgG antibodies
PBS	Buffer-BCG IgY: $(\theta_0)_{\text{BCG-IgY}}$	Buffer-*E. coli* IgG: $(\theta_0)_{\textit{E. coli}\ \text{IgG}}$
BCG	Specific-BCG IgY: $(\theta_{bs})_{\text{BCG-IgY}}$	Nonspecific-*E. coli* IgG: $(\theta_{bn})_{\textit{E. coli}\ \text{IgG}}$
E. coli	Nonspecific-BCG IgY: $(\theta_{bn})_{\text{BCG-IgY}}$	Specific-*E. coli* IgG: $(\theta_{bs})_{\textit{E. coli}\ \text{IgG}}$

As a reference, the binding affinity of anti-BCG IgY and anti-*E. coli* IgG was also evaluated by ELISA. Equal concentrations of two bacterial strains (BCG and *E. coli*, approximately 10^5 cells in 100 µL PBS) were assayed for binding anti-BCG IgY antibody using a 0.45 micron filter plate (Millipore Billerica, MA, #MAHVN4510). Aliquots of the bacterial suspensions were added to the 96-well filter bottom plate and washed with PBS. Subsequently, a 100 µL aliquot of 10 µg/mL IgY-BCG antibody in PBS was added to the washed cells and incubated for 1hour at 37°C. After the PBS wash, a secondary antibody was added (rabbit anti-IgY-HRP conjugate, Thermo Scientific #31401) and incubated for 1 hour at 37°C. The sample was then washed with PBS, followed by addition of 100uL ABTS substrate (Thermo Scientific #37615), incubated for 5 minutes, and filtered into a 96-well receiver plate. Absorbance was then recorded at 405 nm.

3.3.2 Results and Discussion

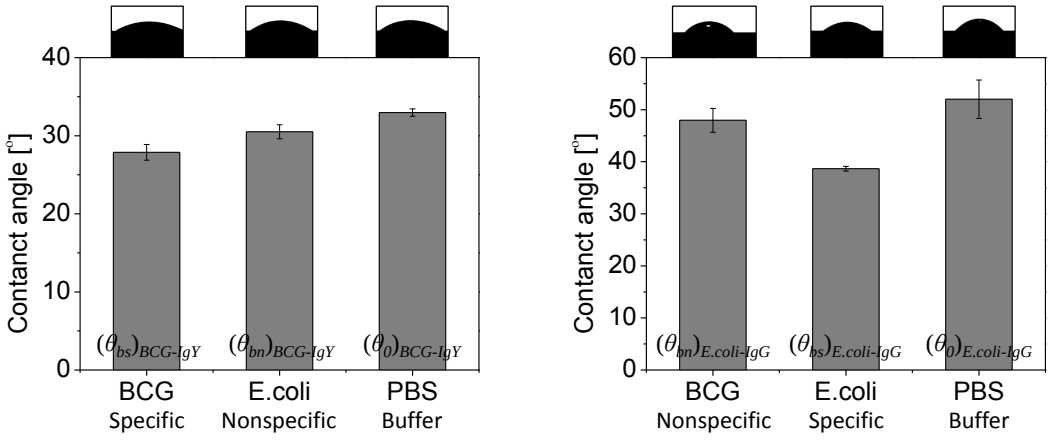

(a) (b)

Figure 22. Initial contact angle measurement results for both BCG and *E. coli* on a surface functionalized with (a) anti-BCG IgY and (b) anti-*E. coli* IgG

When the contact angle was measured for specific- and nonspecific bindings, the contact angle at specific bindings was reduced in comparison to the case of the nonspecific binding. When a liquid drop of PBS buffer was placed on substrate immobilized with antibodies, the contact angles without cells were 33 and 52 degrees for anti-BCG IgY- and anti-*E. coli* IgG substrates. The contact angles of pure liquid drop could vary with the electric charge of antibodies. Subsequently, when the drops containing *E. Coli* and BCG cells were placed on the anti-BCG IgY substrate, the contact angles were reduced to 31 and 27, respectively (Figure 22a). When the substrate was changed into the anti-*E. coli* IgG substrate, the contact angle was sequencially reduced from the pure liquid to the nonspecific and to the specific cases (Figure 22b).

The contact angle was gradually reduced as the evaporation continued. The difference of the contact angles was maintained and the smaller contact angles

showed faster evaporation. Due to the pinning effect, the solution was evaporated more quickly in the specific binding case (Figure 23).

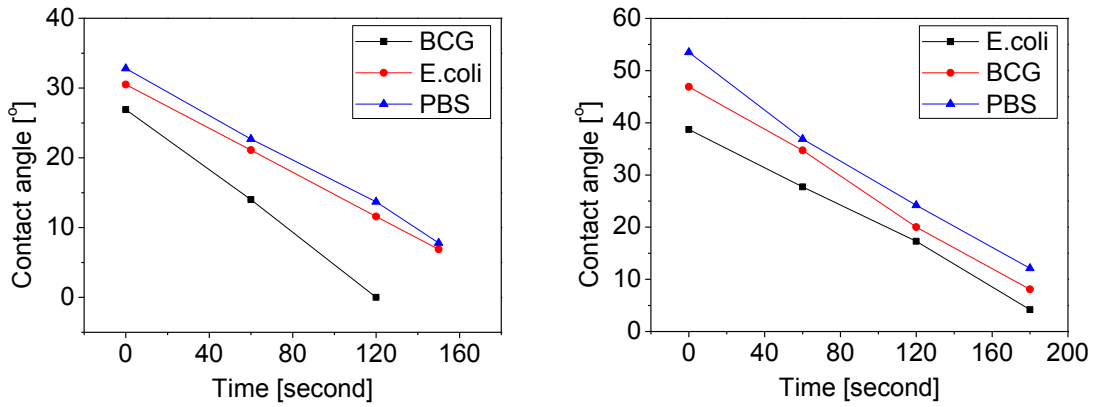

(a) (b)

Figure 23. Contact angle measurement during the evaporation for both BCG and *E. coli* cells on a surface functionalized with (a) anti-BCG IgY and (b) anti-*E. coli* IgG

When the liquid containing target bacteria was evaporated on the substrate, the bacteria were transported to the edge of the liquid drop due to the pinning and the evaporation. The larger binding force for specific case held the contact line of the liquid drop, which formed a coffee ring of bateria. When the patterns of the cells were also compared for both specific and nonspecific cases, the specific cases showed a clearer coffee ring composed of cells. A coffee ring effect was enhanced due to specific binding, which could align more target bacteria cells to the contact line as shown in Figure 24(a). For the nonspecific cases, the majority of cells were located in the middle of droplet for (Figure 24b).

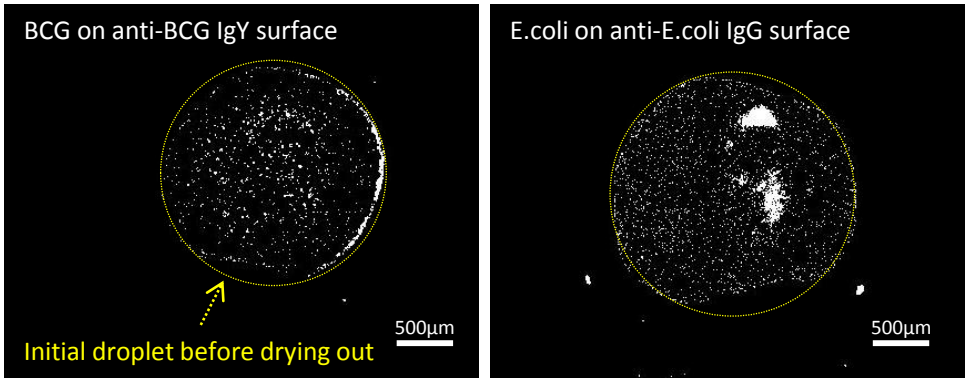

(a)

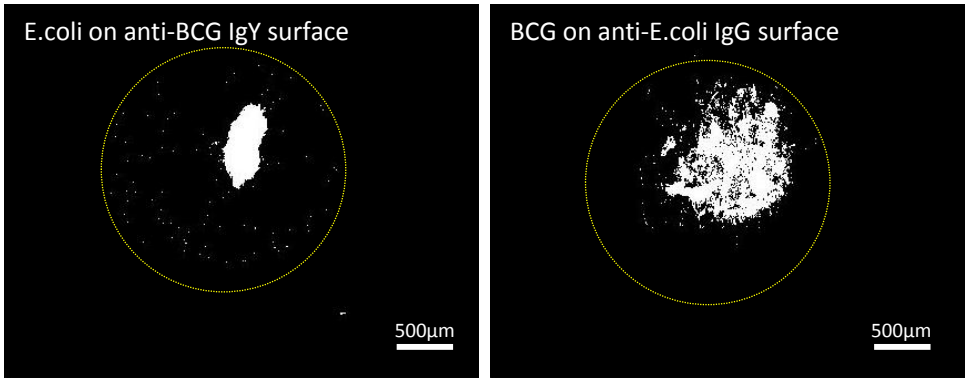

(b)

Figure 24. Drying patterns for four different cases a) specific case: target bacteria cells on the corresponding antibody-coated surface b) nonspecific case: bacteria cells on the nonspecific antibody-coated surface.

3.4 Summary

The change of a contact angle due to immunocomplex formation was studied in this chapter. The analytical model was derived from Young-Laplace equation in consideration of the binding forces. The model was then experimentally validated by anlyzing the contact angle, evaporation rate, and drying patters. At equilibrium, the contact angle for specific binding was smaller than that for nonspecific binding due to the binding forces of immunocomplex formation. With evaporation, the higher binding force of specific binding reduced the contact angle and the evaporation time in comparison to the nonspecific binding case. The lower contact angle for specific binding cases induced a strong outward flow to the edge of the liquid. Thus, the coffee-ring effect was enhanced in the presence of target cells, which aligned the target in a circular-ring pattern. On the contrary, the contact angle increased for nonspecific binding cases with less formation of a coffee ring. Therefore, the coffee-ring effect due to the specific binding can align the target bacteria cells at the contact line of droplet, which can amplify the signal of the immunosensor due to the concentration at the contact line.

Chapter 4: Study of Specific Capturing Mechanism of Target Bacteria on a Microtip Surface

4.1 Introduction

Pulmonary TB, one of the world's most significant infectious diseases, claims over 1 million lives each year worldwide [102]. A rapid, low-cost tool is crucial for POC diagnosis of TB. However, such a tool is not present at this moment due to various technological barriers [8, 102]. To diagnose pulmonary TB, MTB cells are identified in sputum samples[103-116]. The gold standard diagnostic method is bacteriological culture of the bacterial species[108, 109, 115, 116], which requires more than two weeks and is challenging to TB-stricken countries with limited infrastructures[108, 115]. For this reason, direct microscopy of a Ziehl–Neelsen (ZN) smear using sputum is regarded as effective[117, 118] and has traditionally been preferred in resource-limited environments. For effective TB detection, it is essential to assure the quality of smear microscopy[117, 118]. In a global effort to control the disease, WHO has attempted to increase the rate of detecting new TB patients diagnosed with the ZN smear (smear positive) and reached 61% in 2006 (target 70%)[119]. However, the ZN smear method is labor-intensive, poses a large source of potential errors, has a limited sample throughput, and is not sufficiently sensitive. Consequently, the main challenge in TB diagnosis is to develop a simple, inexpensive, and rapid test to replace the smear method.

For rapid and sensitive detection of TB, two major approaches are available without bacterial culture[108, 114, 120-122]. One is to use nucleic acid probes

with amplification strategies such as the Cepheid GeneXpert PCR system [122], and the other is to employ an immunoassay[103-107, 110-114, 123, 124]. However, none of the methods can satisfy all the requirements associated with the simplicity, cost, sensitivity, and turnaround time.

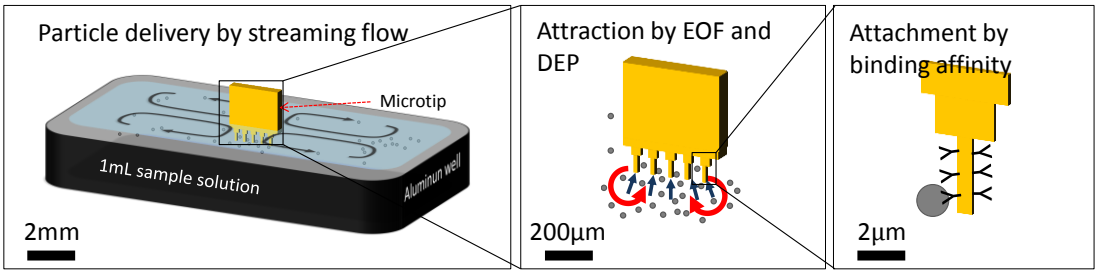

Figure 25. Illustration of the working principle of a tip sensor; Concentration of target bacterial cells in a large volume using streaming flow, electroosmosis, dielectrophoresis, and binding affinity.

To address this critical challenge of POC diagnosis, a microtip immunosensor has been demonstrated to detect low-concentration bacteria in sample mixtures. For the concentration principle of a microtip sensor (Figure 25), a microtip captures target particles contained in an aluminum vessel, working also as the counter electrode. The microtip is made of a Si_3N_4 film coated with a 30nm-thick gold layer, which is immobilized with capture antibodies. A multiscale concentration mechanism works in three different scales; (1) streaming flow induced by vibration of a solution well (10 mm-scale), (2) electroosmotic flow (EOF) and dielectrophoresis (DEP) from an electric field (1 ~ 1,000 µm-scale), (3) antibody-antigen binding due to binding affinity (sub-µm-scale). Target pathogens in a 1 mL well are delivered by the streaming flow (mm-scale) to a microtip within a 1 mm distance. In this range, an EOF generated by an AC field (applied between the microtips and the aluminum well) becomes dominant to concentrate the

delivered bacteria in the vicinity of the microtip. The concentrated bacteria are further attracted to the microtip surface by DEP. The attracted bacteria are then strongly bound to the tip surface by immunocapture. A selective capture is conferred by capillary force through withdrawal of the tip out of the solution. When the tip is one-dimensional, the capillary force removes unbound particles, especially whose diameters are greater than the that of the microtip [82, 83]. When the tip is two dimensional, the captured cells are rearranged in the solution drop that is captured on the tip surface. If the microtip is immobilized with antibodies, the tip sensor can specifically concentrate target cells in samples, which can facilitate highly sensitive detection of the target. The novel concentration mechanism demonstrated detection of 200 CFU/mL in sputum. Since it has the simple and rapid action, point-of-care diagnosis can be achieved by using the microtip immunosensor.

To achieve a more uniform performance of a microtip sensor, the understanding of the specific capturing mechanism is crucial. In particular, the role of capillary action on the microtip surface immobilized with antibodies should be understood for reproducible detection of low-concentrations of bacteria in sample matrices. In this chapter, the capturing mechanism of target bacteria on the microtip surface is experimentally validated with and without immobilization of antibodies. To study the role of capillary action, a microtip coated with a gold layer is used to nonspecifically capture *E. coli* and BCG. For study of specific capture, a gold-coated microtip functionalized with BCG-antibodies is used to capture both cells. On the basis of the capturing mechanism, the fluorescence

signals on the microtip surface are analyzed to estimate the concentration of target bacteria spiked in sputum samples.

4.2 Experimental Study

4.2.1 Experimental Method

To study the specific and nonspecific capturing mechanism on the microtip surface, both BCG and *E. coli* cells at 10^6 CFU/mL in PBS buffer were stained with an intercalating dye (SYTO 9® green fluorescent nucleic acid stain; Molecular Probes L7007, Life Techologies). The SYTO 9 generally labeled most bacteria in suspension – those that with intact membranes and those with damaged membranes. To evaluate the expression of SYTO 9 stain, high concentration of stained BCG cells (10^8 CFU/mL) were captured on Au-coated microtips. The fluorescence images were then compared with those by scanning electron microscope (FEI Sirion SEM, FEI, Hillsboro, Oregon).

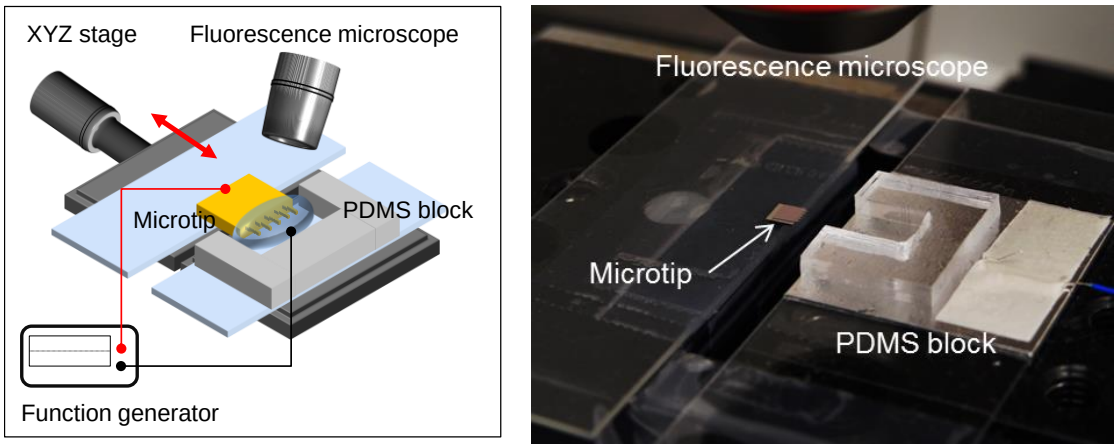

(a) (b)

Figure 26. a) Experiment setup for imaging the concentration, withdrawal, and capturing process of cells. b) Picture for the experimental setup.

To study the cell behavior, the experimental setup was designed as illustrated in Figure 26(b). A Si chip composed of 5 microtips was positioned on a glass slide. The glass slide was installed on an x-y-z stage to control the microtips

in the longitudinal direction. Under the glass slide, an aluminum well was positioned for electrical connection. A 30 µL Cell suspension was contained in the well. When the Si chip was immersed in the 30 µL cell solution, an AC electric potential of 20 Vpeak-to-peak at 5MHz was applied between the microtips and the aluminum foil well through a signal generator (Agilent 33220A, Santa Clara, CA). Without an electric field, the microtips were not so wet as those with an electric field due to electrowetting. Thus an experiment without an electric field was not conducted. The concentration and withdrawal process in solution was monitored by a fluorescence microscope (Nikon Eclipse 55i, Nikon Instruments Inc., Melville, NY). After the withdrawal, the captured cells on the microtip surface were also imaged to compare the concentration and capturing process.

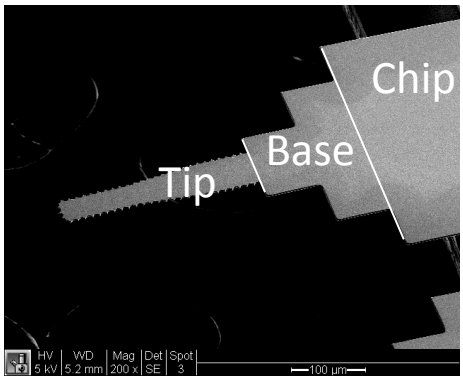

Figure 27. SEM image and defined three regions of a microtip.

The 5 microtips were made of a 1 µm-thick Si_3N_4 film on a silicon chip. For convenience of description, the microtips were divided into three regions as tip, base, and chip (Figure 27). The width of the tip area was changed from 50 to 60 µm. The base area was composed of two areas having the widths of 100 and 160 µm. Compared with the tip and base areas, the chip area had an infinite width. For functionalization with antibodies, the microtips were coated with reagents by

dipping and withdrawal of the microtips. First, polyethyleneimine (PEI, Sigma-Aldrich) was coated to form an adhesive layer. PEI was water-soluble polymer and had the strong hydrogen bond interaction with proton donors. Since PEI is cationic, the negatively charged protein molecules are attracted to the microtip surface. The coated microtip was left to dry at room temperature for 2 minutes. Subsequently, the PEI-coated tips were immersed in biotinylated bovine serum albumin (biotin-BSA, Sigma-Aldrich) for 5 minutes. The biotin-BSA was bound with streptavidin (Sigma-Aldrich) for 1 minute. Finally, the microtip surface was functionalized with the biotinylated IgY antibodies for 5 minutes.

Both BCG and *E. coli* cells were used for both gold-coated and functionalized microtips. Thus four combinations of the experimental runs were tested as summarized in Table 4. The motion of bacteria stained with fluorescence was recorded with three experimental runs (n=3). The number of cells was averaged in order to study the statistics of the process. In particular, the images for the functionalized microtips were blurred due to unbound fluorescence particles. The averaging process could yield more consistent experimental study.

Table 4. Experimental parameters capturing BCG and *E. coli* on microtips

	Nonspecific capture; microtips coated with a gold layer	Specific capture; Functionalized microtips with IgY antibodies on a gold-coated microtips
BCG	BCG on gold coated microtips	BCG on Functionalized microtips
E. coli	*E. coli* on gold coated microtips	*E. coli* on Functionalized microtips

4.2.2 Results and Discussion

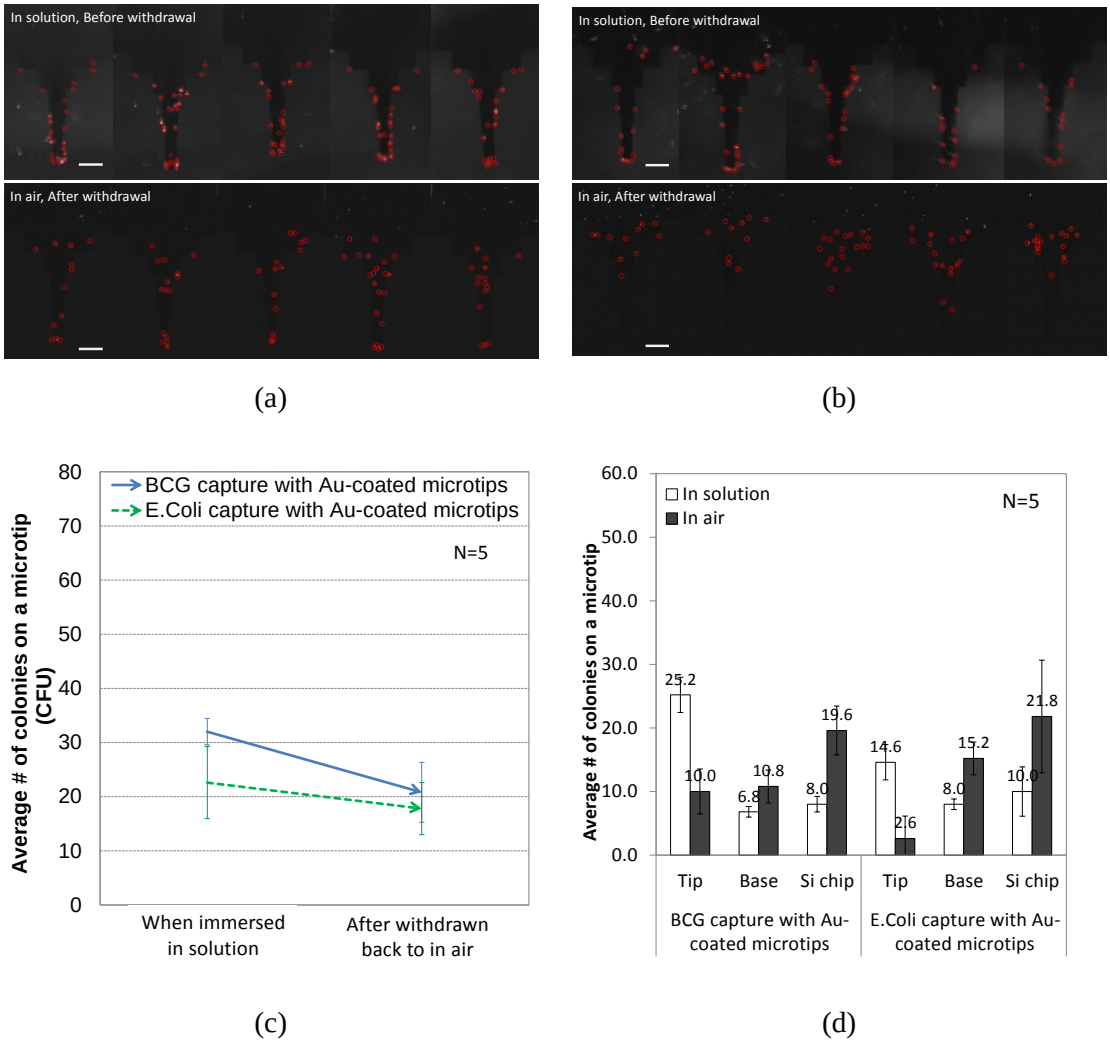

Figure 28. (a) Fluorescence images for nonspecific capture of BCG cells on a gold coated Si substrate. The scale bar is 100 µm. (b) Fluorescence images for nonspecific capture of *E. coli* cells on a gold coated. (c) The total numbers of concentrated and captured cells are similar for both BCG and *E. coli* cells. (d) The number of concentrated and captured cells for each region of microtips as shown in Fig. 26.

The microtips without antibodies were tested to evaluate the number of captured BCG and *E. coli* cells (Figure 28a, b). When the microtips were immersed in BCG and *E. coli* suspensions, both bacteria were concentrated in the vicinity of gold-coated microtips by dielectrophoresis. The numbers of the attracted bacteria in the solution were 32±2.4 and 22.6±6.6 for BCG and *E. coli*,

respectively. When the microtips were withdrawn from the solutions, the numbers were decreased to 20.8±5.5 and 17.8±4.8 for BCG and *E. coli* cells, respectively (Figure 28c). Thus a similar number of BCG and *E. coli* cells were captured on microtip surface without antibodies, which is consistent with the results using a Si substrate.

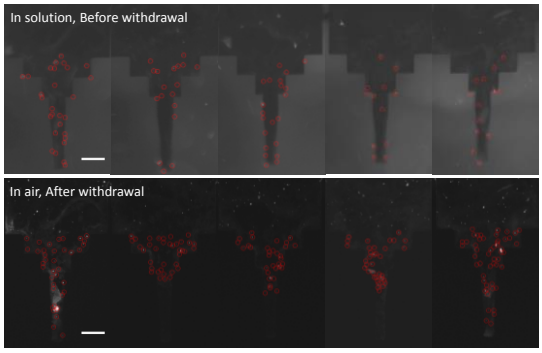

(a)

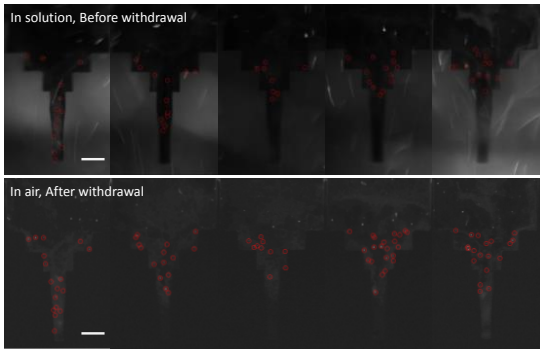

(b)

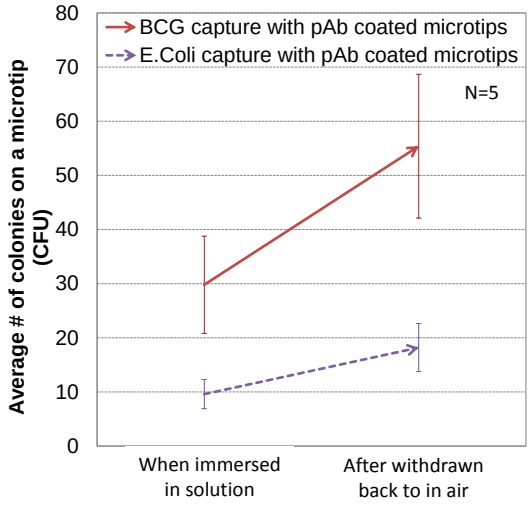

(c)

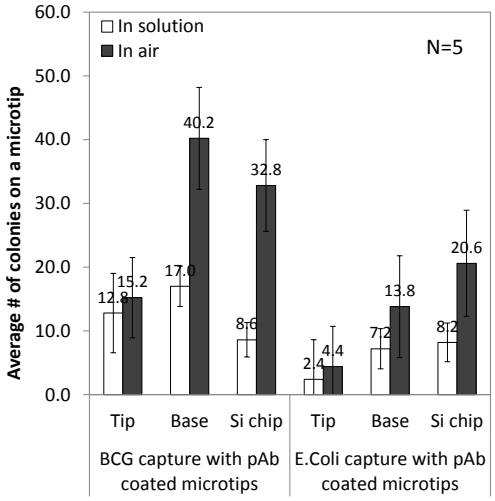

(d)

Figure 29. (a) Fluorescence images for specific capture of BCG cells on an anti-BCG polyclonal-antibody (pAb) coated microtip. The scale bar is 100 μm. (b) Fluorescence images for captured *E. coli* cells on an anti-BCG pAb coated microtip. (c) The total number of concentrated and captured BCG cells is 3.1 times greater than that of *E. coli* cells. (d) The number of concentrated and captured cells for each region of microtips as shown in Fig. 26.

The results indicated that both cells were concentrated and captured to a similar degree for nonspecific bindings. As shown in Figure 28(d), most cells were concentrated at the terminal end of microtips in solution due to dielectrophoresis for both cases. When the microtips were withdrawn, the capillary induced forces removed the cells from the terminal end. The cells on the base and chip area remained as attracted. In addition, since small amount of solution with cells was also captured on the wide areas, the number of cells was increased. For the nonspecific capturing, the similar number of bacteria was attracted and captured at the same, initial concentration of cells.

When the functionalized microtips with anti-BCG IgY were immersed in BCG and *E. coli* suspensions, both bacteria were concentrated in the vicinity of microtips by dielectrophoresis. The numbers of the attracted bacteria in the solution were 29.8±8.9 and 9.6±2.7 for BCG and *E. coli*, respectively. When the microtips were withdrawn from the solutions, the numbers were decreased to 55.4±13.2 and 18.2±4.4 for BCG and *E. coli* cells, respectively. When the microtips with anti-BCG IgY were used, the average number of the concentrated BCG in solution was 3.1 times that of the concentrated *E. coli* cells. After the withdrawal of the microtips, the average number of captured BCG in air was 3.04 times that of the captured *E. coli* (Figure 29c).

According to the results of the Si substrate and the microtips, the specific capture of BCG was conducted by the binding affinity in conjunctions with the capillary action. Figure 30 shows the specific binding mechanism on microtip surface. With functionalized microtips, the average number of the concentrated

and captured BCG in solution was about 3.1 times that of the concentrated and captured *E. coli* cells(Figure 29c). According to this observation, the antibodies held more target cells in solution that were concentrated by an electric field. Unlike the nonspecific capturing, the cells were uniformly distributed on the microtip surface in solution after the functionalization. This is because DEP force at the terminal end of microtips is decreased due to the several layers on gold surface.

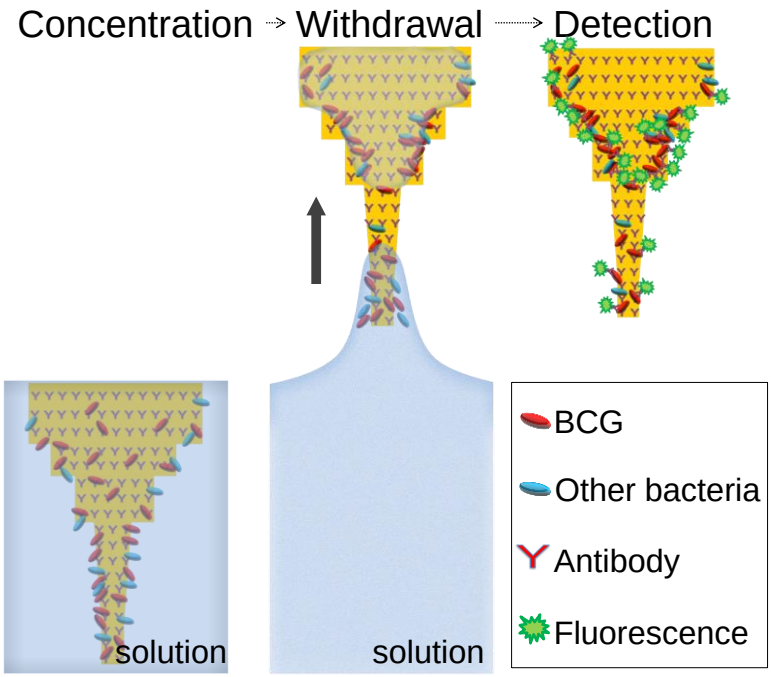

Figure 30. Illustration of the specific capturing mechanism on microtip surface. The capillary action and the binding affinity yield the specific capture of target cells.

With withdrawal of the microtips, the capillary action removed most cells in the tip area while the cells retained in the solution drop were redistributed by the capillary action and the coffee ring effect [92]. In other words, the cells were aligned through the edge of the solution drop that was held on the base- and chip areas by the capillary action. The capillary-induced force, higher than the force by

the binding affinity, pulled the concentrated cells through the solution meniscus in the withdrawal step. Once the meniscus was pinned in the vicinity of the microtip's edges, the cells were finally captured at the meniscus with the coffee ring effect. The redistribution process of *E. coli* and BCG cells is shown in Figure 29(a) and (b). Through the combined effect of the binding affinity and the capillary action, the highest density of target cells was found in the base area of the microtips where the solution drop was held and dried earlier than the chip area (Figure 29d). The cell density of the tip area was smaller than that of the base area because a solution drop could not be held by capillary action due to the small width of the tip. Thus, the capillary action and the affinity binding yielded the specific capture of target cells, which correlated with the width of the microtip as illustrated in Figure 30.

4.3 Discussion

The specific capturing mechanism on the surface of the microtip is described. Note that the microtip is composed of 1-dimensional structure and 2-dimensional surface. The 1D structure generates the higher electric field strength while the 2D surface can align the captured bacteria on the surface. In the 1D structure, target bacteria are concentrated with the generation of electrososmotic flow. However, when the microtip is withdrawn from the liquid, the concentrated bateria are partially removed. The removed bacteria are captured on the 2D surface, which has shown the highest sensitivity. Regarding the specificity, 1-dimensional structure was controlled by capillary action, and 2-dimensional structure by coffee-ring effect induced by immunocomplex formaion. As illustrated in Figure 31, the tip part was required to generate higher electric field strength, which could enhance the concentration for various sizes of target particles by DEP and electroomosis (Figure 31a). After the withdrawal of the microtip, the concentrated particles were captured and aligned on both tip and base part according to their size (Figure 31b). Therefore, the sizes and shapes of a microtip should be designed to capture a specific size of particles to achieve a high sensitivity and specificity(Figure 31c).

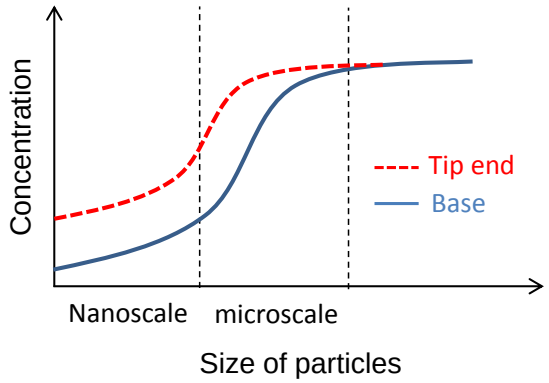

(a)

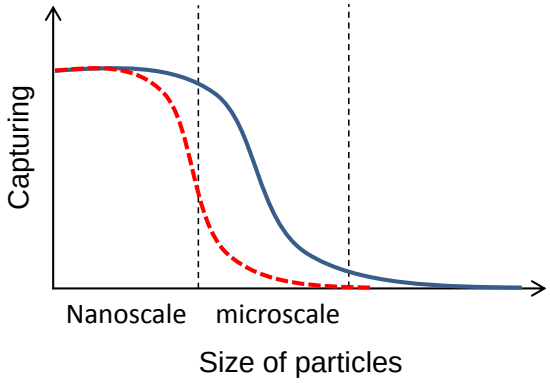

(b)

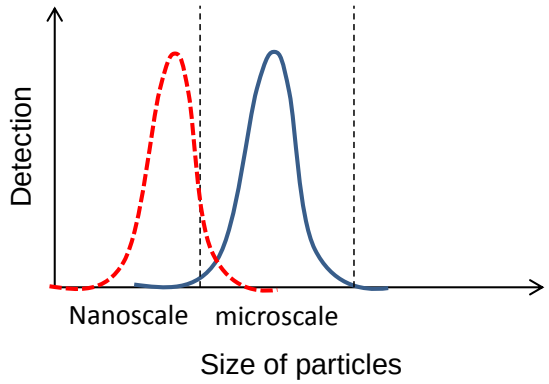

(c)

Figure 31. The specific capturing mechanism on the surface of the microtip: (a) concentration, (b) capturing, and (c) detection for various sizes of particles

4.4 Summary

In this chapter, the capturing mechanism of target bacteria on microtips was studied by using microtips. In the previous chaptre, the capillary-induced coffee ring effect could concentrate target cells on the Si substrate coated with the corresponding antibodies. Without the binding affinity, the coffee ring effect was significantly reduced. When a microtip coated with antibodies against BCG cells, the coffee ring effect could increase the number of captured cells by 3.1 times in comparison with *E. coli* cells. Therefore, the capillary-induced coffee ring effect on antibody-functionalized microtips could offer specific capture of target cells.

Chapter 5: Amperometric Immunosensor using Dendritic Nanotips

5.1 Introduction

Over the past decade, various tools for point-of-care (POC) diagnosis have been developed to achieve rapid and sensitive detection of a target biomarker [71]. Potential POC diagnostic methods can be nucleic acid amplification[69], magnetic materials based methods[34, 77], microfluidic based approaches[63, 125, 126], and nanotechnology based techniques[127, 128]. However, the DNA amplification methods are cumbersome, slow, and expensive with requirement of stable electric power. Magnetic-based approaches are cumbersome in preparation with a limited sensitivity. A microfluidic device handles a limited small volume, and viscous samples are clogged in the channel. Nanotechnology-based devices can be sensitive, but scale-up manufacturing is still challenging. In addition, most methods require sophisticated instruments in stationary laboratories with demand for an optics and skilled personnel. Therefore, a simple and portable detection method that functions independently of laboratory infrastructure without compromising sensor performance would greatly facilitate rapid diagnosis in non-traditional, POC setting[26, 27].

As a detection element in rapid diagnostic tools, nanomaterials have been evaluated for their potentially rapid response and high sensitivity. Among nanomaterials, single walled carbon nanotubes (SWCNTs) could be useful due to their sensitive response upon binding of targets[129]. To detect a target in a liquid phase, an electric current is measured through SWCNTs. A nanostructured tip is

advantageous for electrical detection because the capacitance due to an electrical double layer can be minimized by the confined geometry[82, 84, 130-134]. To reduce the capacitance with electric insulation, the nanotip area except for the terminal end has been sealed with polymer- or other dielectric layers[71, 134]. However, insulated nanotips have proved challenging for fabrication in a reproducible fashion. Moreover, the concentration of target analytes onto the exposed terminal area of a nanotip remains a daunting task.

In our previous work, microtips and nanotips were fabricated to concentrate target analytes[82-84, 135-137]. Nanoparticles and DNA were effectively concentrated onto a dendritic naontip by an electric field, which were detected by a fluorescence microscope[83, 135-137]. Previously, dendritic nanostructures have been studied to enlarge the surface area for increasing adsorption sites of molecules. However, most dendritic nanostructures are not a device but materials[138, 139]. In our previous study, a dendritic nanotip concentrated as few as 10 copies in a sample volume of 2 μL due to a large surface area with a high intensity electric field. However, precise measurement with a fluorescence microscope was required for identification of DNA. In this chapter, an alternative dendritic nanotip strategy was studied for electric detection of target bacteria. A dendritic nanotip coated with probe molecules was used for concentration of target bacteria, which were detected by electrical measurement. Immunocomplex formation between surface antigens of bacteria and fluoresceinlabeled antibodies was measured by the change of electric current between a nanotip and a ring-shaped electrode.

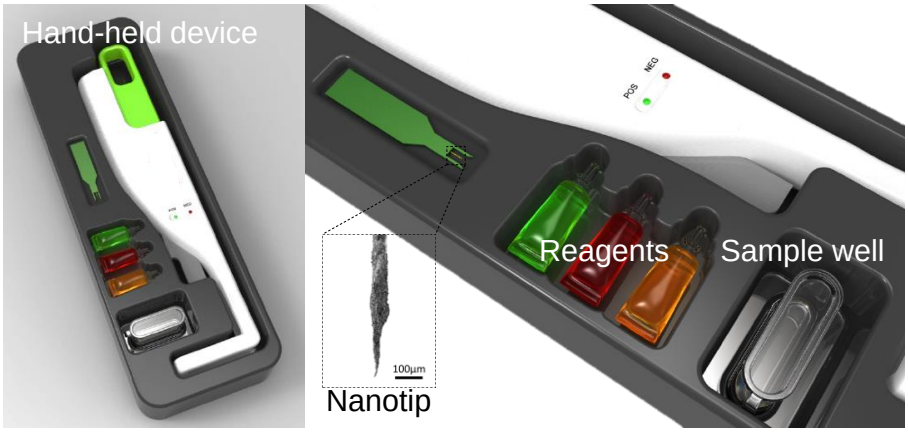

(a)

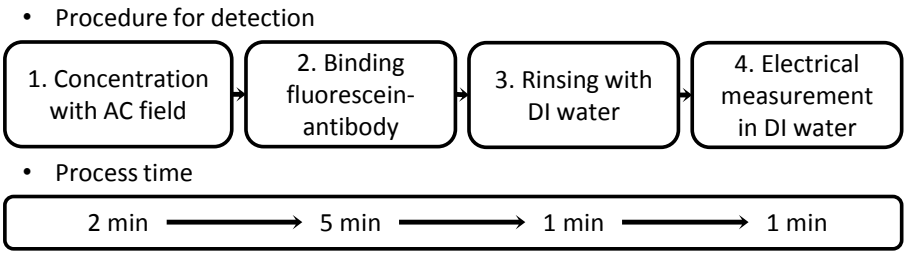

(b)

Figure 32. (a) Conceptual design; a point-of-care (POC) diagnostic tool for infectious diseases. (b) Flow chart of the diagnostic step using a dendritic nanotip with the process time.

The electric measurement was conducted within a medium of deionized (DI) water in order to reduce chemical reactions and an electrical double layer effect, which enabled a reference-free detection. The electrical detection results were validated by fluorescence- and scanning electron microscopy (SEM). Ultimately, the platform is aimed to develop a POC diagnostic tool for infectious diseases. A nanotip sensor is integrated into a handheld devce as illustrated in Figure 32. With the simple detection step, the assay can be completed within 10 minutes at low cost.

5.2 Theoretical Study

5.2.1 Gating effects for SWCNTs upon biomolecular binding

The unique electronic and optical properties[140-142] make carbon nanotubes ideal for next-generation biosensing platforms[128]. In addition, CNTs have the potential to enhance numerous applications where nanosized metallic and semiconducting components are required to outstanding physical strength [143, 144], high flexibility[145] and exceptional chemical stability[146, 147]. In particular, SWCNTs can be an ultimate element for biosensors as following: SWCNTs have the diameter of 1 nm, directly comparable to the size of single biomolecules. The diameter is also similar to the electrostatic screening length in physiological solutions[129]. Furthermore, the low charge carrier density of SWCNTs[148] is comparable to the surface charge density of proteins, which intuitively makes SWCNTs well suited for electronic detection for target biomolecules. Finally, every single carbon atom of SWCNTs is in direct contact with environment, which allows for maximum interaction with adjacent biomolecules.

The structure of CNTs can be visualized as the cylindrical roll-up of one or more flat graphene sheets containing carbon atoms in a honeycomb structure[149] (Figure 33a, b). Graphene is a single molecular sheet of carbon in graphite structure. The band structure of graphene and CNTs can be explained using a simple tight binding model[150] for electronic structure as below:

$$\mathrm{E}(k) = \mathrm{E}_0 \pm \frac{\sqrt{3}}{2}|t|a_{c-c}\left|\Delta\vec{k}\right|, \text{ at } \vec{k} = (\Delta k_x, \frac{4\pi}{3a_{c-c}} + \Delta k_y) \qquad (5.1)$$

Here, E_0 is the energy corresponding to the chosen atomic orbital, $|t|$ is the interaction energy of atom with nearest neighbor, a_{c-c} is the distance between the atoms, and $\vec{k}$ is the wave vector.

Thus, the tight binding model for the band structure of graphene yields conduction and valence bands. These energy bands are proportional to $|\Delta\vec{k}|$, rather than $E(\vec{k}) \sim |\Delta\vec{k}|^2$ near a band minimum or maximum. Furthermore, the Fermi level is typically $E_F = E_0$, thus graphene behaves as a zero band gap semiconductor, or semimetal. CNT electronic band structure can be derived from the graphene sheet, imposing periodic boundary conditions in the circumferential direction. The density of states (DOS) is strongly dependent on the nanotube diameter, the chirality, and the type (metallic versus semiconducting), as shown in Figure 33(c). In addition, because of the low DOS on a SWCNTs as compared to a typical metal, the liquid acts as a highly effective gate that easily changes the Fermi level for SWCNTs [151].

The SWCNT properties can also be modulated by binding biomolecules. Instead of a solid state and liquid gate, biomolecules adsorbed on SWCNTs are used to modulate the conductance. The gate effect of protein adsorption has been validated experimentally. The I(source drain current)–V_{lg}(liquid gate potential) curves can be used as a tool to identify the electronic modulation. Figure 34(a) shows the change of the I-V_{lg} curve due to an electrostatic gating effect. When charged protein molecules are adsorbed on a SWCNT, the doping effect can shift the I-V_{lg} curve along the voltage axis due to partial charge transfer. Note that adsorption of a positively charged species induces additional negative charge in a

SWCNT. The n-doping of the SWCNT shifts the I-V_{lg} to more negative gate voltages.

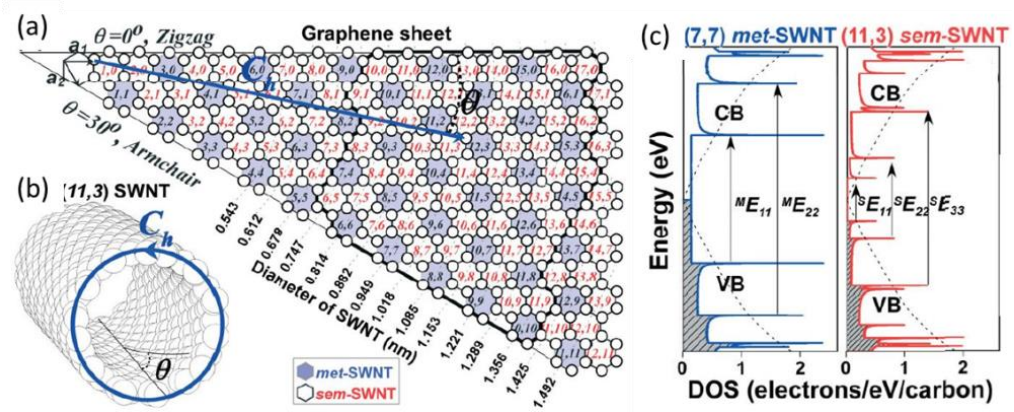

Figure 33. (a) Chirality (θ) and diameter (dt) map of SWCNTs as derived by rolling the Hamada vector (C_h=na_1+ma_2) into a circle. a_1 and a_2 are unit vectors of the graphene sheet constructed by carbon atoms (white circles) in sp2 configuration (n and m: integers). White and light-shaded cells indicate semiconducting and metallic SWCNTs, respectively. (b) Representative structure of carbon nanotube. (c) DOS versus energy for (7, 7) metallic and (11, 3) semiconducting SWCNTs. Shaded and white areas indicate the valence- and conduction bands of SWCNTs, respectively. Dotted curves indicate the valence band and conduction band of the planar 2D graphene lattice. The arrows indicate the allowed electronic transitions. Reprinted with permission from [152]. Copyright (2007) Wiley-VCH.

In case of the Schottky barrier (Figure 34b), adsorbed biomolecules on a SWCNT modulate the local work function and thus the band alignment. Because the Schottky barrier height changes in the opposite directions to hole (p) and electron (n) transport (see insets), an asymmetric conductance change for p- and n-branches of I-V_{lg} is observed. Therefore, SWCNTs are modulated by a combination of electrostatic gating and Schottky barrier effects [127, 153-155], which is the main mechanism for detection of target bacteria.

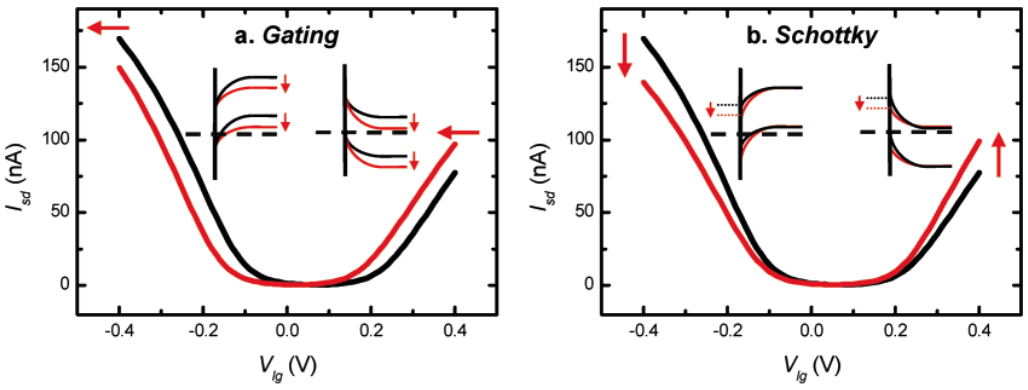

(a) (b)

Figure 34. Computed I-V_{lg}-curves before (black solid line) and after (red solid line) protein adsorption for gating and Schottky barrier effects. Reprinted with permission from [155]. Copyright (2008) American Chemical Society.

5.2.2 Electrical detection mechanism using dendritic nanotips

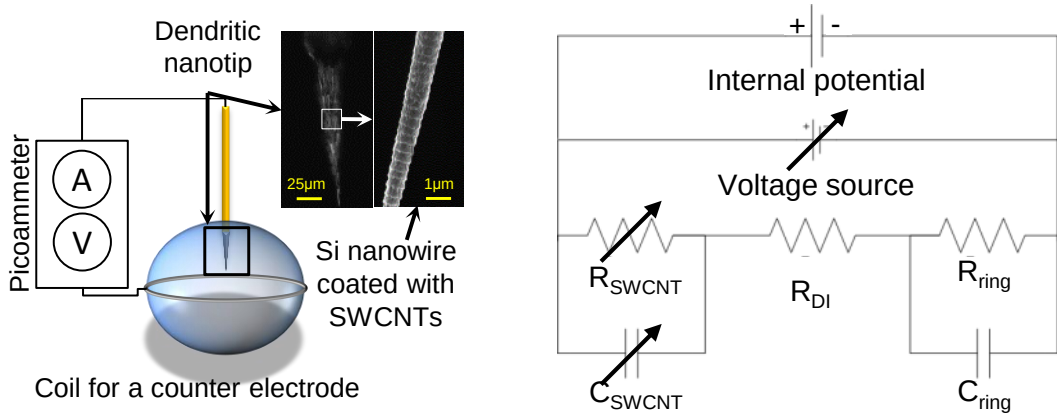

(a) (b)

Figure 35. (a) Configuration for electrical measurement using a dendritic nanotip. The nanotip is composed of Si nanowires wrapped with SWCNTs. (b) Equivalent circuit for the electrical measurement. R_{SWCNT}, R_{DI}, and R_{ring} are the resistances of SWCNTs on a nanotip, DI water, and a ring-shaped electrode, respectively. C_{SWCNT} and C_{ring} are the double layer capacitances on SWCNTs of a nanotip and a ring-shaped electrode, respectively. A DC potential is applied for current measurement. An internal potential is generated due to oxidation of a ring-shaped electrode made of aluminum (Al).

Figure 35(a) shows an experimental configuration of a dendritic nanotip for electric measurement. The nanotip is composed of Si nanowires coated with SWCNTs. The Si nanowires are interconnected with SWCNTs for electric conduction. When a target analyte binds to the nanotip, the electric current between the nanotip and a ring-shaped electrode is changed due to changes in the resistance of SWCNTs and the contact resistance at the SWCNTs-liquid interface. The magnitude of the change depends on the charge carrier density of SWCNTs, which is comparable to the surface charge density of molecules[148]. When bulk SWCNTs are utilized, the charge transport through SWCNTs is averaged over metallic and semiconducting tubes[156]. The electron transfer characteristics through the radial direction of SWCNTs are similar for metallic and semiconducting tubes[157], which is advantageous for reproducible measurement regardless of chirality of SWCNTs.

When a target analyte binds onto a dendritic nanotip wrapped with SWCNTs, the equivalent circuit for the measurement is illustrated in Figure 35(b). For the electric potentials in the circuit, an external DC voltage (0~1V) is applied for current measurement between a nanotip and a counter electrode. Upon introduction of liquid, a redox potential is generated between the electrodes. When the counter electrode is made of aluminum (Al), the Al electrode is oxidized with generation of electrons. To reduce the redox potential (i.e. internal potential) due to the oxidation, DI water is used as the medium. The reactions in DI water are:

$$2Al + 2H_2O \rightarrow 2Al(OH)^{+2} + 2H^+ + 6e^- \text{ (Anode)}$$

$$2H^+ + O_2 + 2H_2O + 6e^- \rightarrow H_2 + 4OH^- \text{ (Cathode)}$$

The electric current due to the redox potential is measured at 0V to observe the dominancy in the measured current. The limitation of ions in DI water significantly decreases the capacitances (C_{SWCNT} and C_{ring}) on the electrodes. As a result, the change of the electric current is dominated by the resistance at the interface between SWCNTs (R_{SWCNT}) and DI water. To study the geometrical dependence of a dendritic nanotip on the electric current, the current density of a dendritic nanotip was compared with those of single nanotips with and without an insulation layer. In previous works, when a single nanotip was insulated by a polymer layer except at the terminal end, the electrical double layer effect could be suppressed for sensitive measurement[130, 132]. Using a numerical model, the current densities for a single-, an insulated-, and a dendritic nanotip were compared to study the path of electric current. A finite element method software (COMSOL Multiphysics®, COMSOL, Inc., Palo Alto, CA) was used to calculate the electric field and the current density near the nanotip.

Figure 36(a) shows a 3-dimensional computational model with boundary conditions. The model consisted of a coil (outside diameter: 2.1 mm and inside diameter: 1.9 mm), a spherical droplet (diameter: 2.0 mm) and a nanotip (the terminal end diameter: 1 μm and length: 250 μm). The nanotip was connected to a microwire (diameter: 50 μm and length: 350 μm). In Figure 36(a), the ground condition (V=0V) and the electric potential (V_0=1V) were applied to the coil and the microwire, respectively. Electric insulation condition ($-\mathbf{n}\cdot\mathbf{J}=0$, $\mathbf{J}$ is current density) is given at the surface of the droplet. In the model, three kinds of nanotips were made as a single-, an insulated- and a dendritic nanotip. The single nanotip

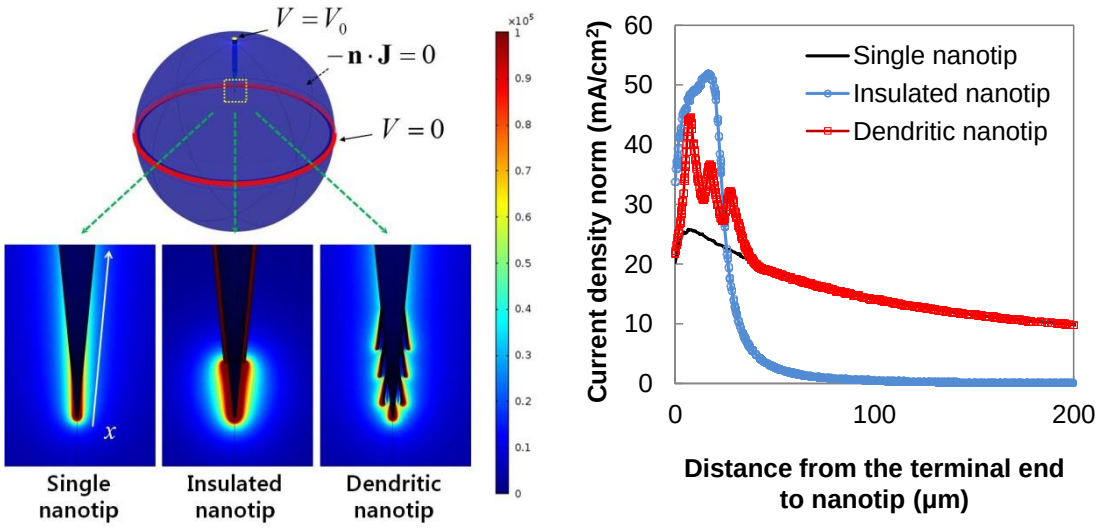

(a) (b)

Figure 36 (a) Numerical model showing two electrodes composed of a nanotip and a ring-shaped electrode (top). The distribution of an electric field is shown for a single-, an insulated-, and a dendritic nanotip (bottom images). See the main text for the specification of each tip. (b) Comparison of electric current densities on a single-, an insulated-, and a dendritic nanotip.

was modeled as conical in shape with a terminal end diameter of 1 μm. The insulated nanotip had the same geometry but was covered with 2 μm-thick dielectric layer except at the terminal end. The dendritic nanotip was modeled to be composed of 1 nanotip and 6 nanowires. Each nanowire was 1 μm in diameter and 10 μm in length. Each model was composed of tetrahedron elements (1,824,875~2,718,187 elements). An 8-core processor (clock speed: 2.67GHz) was used for computation. According to the numerical results (Figure 36b), the current density is highest at the insulated nanotip followed by the dendritic nanotip. The single nanotip showed the lowest current density at the terminal end. Since the electric current flows throughout the nanotip surface, the background noise of a single nanotip should be greater than those of insulated- and a dendritic nanotips.

Although the dendritic nanotip is computed to be a little bit less sensitive than the insulated nanotip, the sensitivity of the actual dendritic nanotip in Figure 36(a) can approach that of the insulated nanotip because the actual dendritic nanotip has a much larger number of nanowires than that of the numerical model. To validate the possible improvement of the sensitivity with a larger number of nanowires, additional simulation was conducted. On a nanotip, the number of nanowires was changed to 2, 4, and 6 as shown in Figure 37(a). As shown in Figure 37(b), the difference of the current density on the nanotip surface increases with increase of the number of nanowires. The simulation results predict that a higher packing density of nanowires and a larger number of nanowires should increase the sensitivity of a nanotip sensor due to the enlarged current density. In addition, the fabrication of a dendritic nanotip is much more straightforward than the insulated nanotip. The larger surface area of the dendritic nanotip can concentrate targets more efficiently than an insulated nanotip[135].

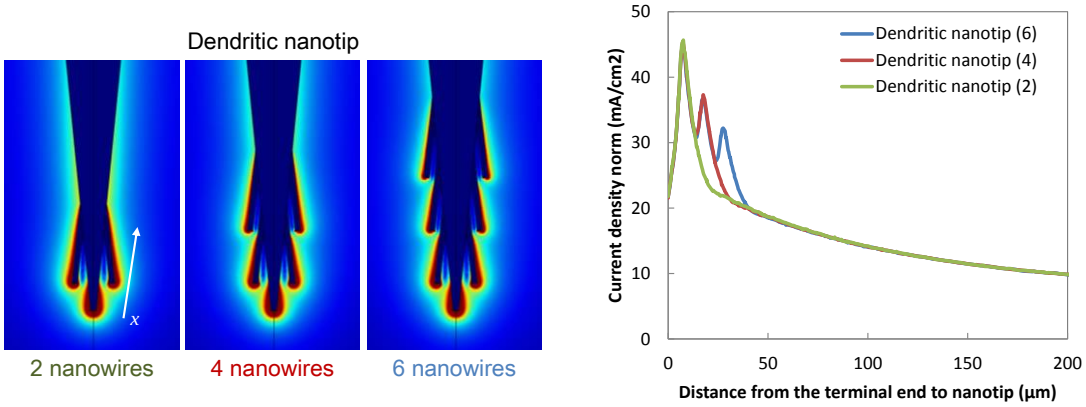

(a) (b)

Figure 37 (a) Electric field distribution of the dendritic nanotips having 2, 4, and 6 nanowires (b) Current densities of the dendritic nanotips having 2, 4, and 6 nanowires

5.3 Experimental Study

5.3.1 Experimental and Imaging Methods

Material preparation (Si micro- and nanowires): Si micro- and nanowires were fabricated on 4 inch wafer by using conventional photolithography and deep reactive ion etching (DRIE) technique. A 100mm-Si wafer was spin-coated with photoresist(AZ1512) at 3000rpm for 30 seconds and baked at 110 ℃ for 1 minute. To fabricate island structres, 4 μm picth lines were exposed and sequentially patterned again with perpendicular directions. The patterned structures were then etched by using DRIE to make nanowires (Figure 38a). Si nanowires were collected by scribing the surface using a flat polydimethylsiloxane (PDMS) piece. The collected Si nanowires were dispersed in dimethyl-formamide (DMF). SWCNTs (Hipco) were also dispersed in DMF by sonication for 10 hours. The concentration of the SWCNT solution was 125 mg/L while the concentration of Si nanowire solution was 1000 mg/L. Then, 4 mL of a pure SWCNT solution and 1 mL of a pure Si nanowire solution were mixed and sonicated in a vial.

Dendritic nanotip fabrication: A dendritic nanotip was made of a mixture of Si nanowires and SWCNTs. A procedure to fabricate a dendritic nanotip made of SiC nanowires and SWCNTs was previously developed [158]. To achieve more uniform performance, randomly grown SiC nanowires were replaced with the fabricated Si nanowires. A gold plated tungsten (W)-tip having 50 μm in diameter (Sylvania, Towanda, PA) was positioned on an xyz stage to control the tip while a metal ring (OK industries, Tuckahoe, NY) was attached on a rotational platform. An AC field (20 Vpp, peak-to-peak voltage) at 5 MHz was applied to the W-tip

and the ring that held a 2 µL solution drop. The W-tip was positioned perpendicular to the metal ring and immersed into the drop. After 1 minute of immersion time, the W-tip was gently withdrawn from the drop. The fabricated nanotip had dendritic structure composed of Si nanowires (Figure 38c). The nanowires were wrapped with SWCNTs to make electrical connection (Figure 38d). The average diameter of the terminal end of a nanotip was 0.7~1.2 µm. (Figure 38a).

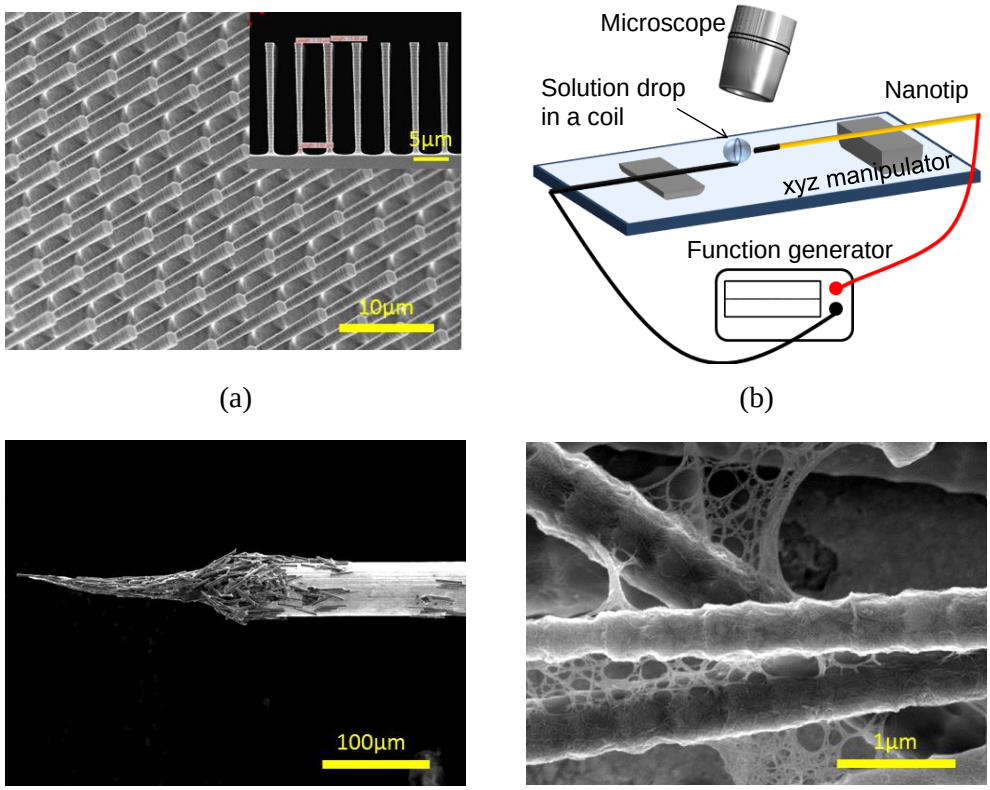

(a) (b)

(c) (d)

Figure 38. (a) SEM image for fabricated Si nanowires on a wafer (b) Experimental setup for the concentration of bacteria cells (c) SEM images for fabricated dendritic nanotip (d) SEM image for Si nanowire wrapped with SWCNTs.

Characterization of dendritic nanotip: Cyclic voltammetry (CV) was used to characterize the dendritic nanotip. 10µL DI water was loaded on an aluminum

coil, and a dendritic nanotip was immersed in the solution. When the cyclic voltage was swept from -1V to 1V with a ramp function (Agilent 33220A, Santa Clara, CA), the current was measured using picoammeter (Keithley, 6487). The sweeping rates were 100, 200, 500, and 1,000 mV/s.

For electric measurement, DI water was used as the medium throughout this chapter, instead of a conventional electrochemical buffer[132]. The electrochemical buffers are convenient media for electric measurement because electrochemical reactions are well-characterized with the assistance of a third, reference electrode. However, precise control of the gap size among three nanoelectrodes including two electrodes plus a reference electrode is challenging in nanofabrication. In addition, ionic concentration can continuously change due to temperature and humidity, which requires calibration by a reference electrode. In fact, excessive ionic concentrations of a medium in electric measurement can interfere the electrochemical measurement of analytes due to unwanted reactions.[159] Therefore, this study evaluated the use of DI water as a medium to detect targets without a reference electrode.

For specific binding, the dendiritic nanotip was functionalized with streptavidin and anitbodies. Streptavidin (1mg/mL in 1xPBS, Sigma) was nonspecifically immobilized on the surface followed by the binding of biotinylated polyclonal IgY antibodies (5 mg/ml biotin-Antibody in PBS). The antibodies were raised against acetone-fixed *M. bovis* BCG cells as described previously. To study the electric response of the functionalized layers, electrical measurement was conducted for both streptavidin and antibody layers. After the coating, the

dendritic nanotip was immersed into 10 μL DI water which was hung on the aluminum ring for the electric measurement (Figure 35a). Both the dendritic nanotip and the Al coil were then connected for current measurement. A picoammeter (Keithley, 6487) was used for voltage input (0~1V) and current measurement. To study the electric response of the functionalized layers, electrical measurement was conducted individually for each layer.

Concentration and detection methods: The experimental setup for concentration of bacterial cells was composed of a dendritic nanotip, a solution drop in a metal coil, and a signal generator (Figure 38b). The fabricated nanotip was placed on an xyz stage, and the axial motion of the nanotip was controlled to maintain the same distance from the terminal end of a nanotip to the metal coil for all the experiments. A liquid drop (10 μL) containing target bacteria was placed on an aluminum coil. All the experiments were conducted on the xyz stage under an optical microscope with an illuminator (MI-150, Dolan-Jenner, Lawrence, MA). A function generator (Agilent 33220A, Santa Clara, CA) was used to apply an AC electric potential (100 kHz, 18 V_{pp}). To study the sensitivity of a dendritic nanotip, various concentrations of BCG cells (10^3~10^5 cfu/mL) were suspended in PBS buffer. Note that the concentrations of BCG were chosen on the basis of the clinical significance.[69, 70] A 10 μL solution of prepared bacteria sample was loaded onto the metal coil. The functionalized nanotip was immersed in the 10 μL droplet for 2 minutes with an applied AC field (18 Vpp at 100 kHz). The nanotip was withdrawn from the solution and then immersed in a prepared fluorescein-conjugated antibody solution (2 μL, 125μg/mL) for 5 minutes. The nanotip was

then rinsed with DI water (300 μL) for 10 seconds. Due to the mass of the droplet, 10 μL was the largest volume which could be held on the coil by surface tension. For detection, the small sample volume (2μL) was chosen because the volume was large enough to measure electric signals for 5 minutes. To control the sample volume precisely, a pipette (Eppendorf Reference® adjustable 2~20μL) was utilized to transfer the exact volume of the solution to the metal coil for all the experiments. The experiment was repeated 3 times for each concentration. For the control experiment, 1×PBS buffer without bacterial cells was used.

Both electrical and fluorescence measurement methods were used to detect concentrated target bacteria on the dendritic nanotip. For fluorescence measurement, the rinsed nanotip was observed under an epi-fluorescence microscope (Olympus BX-41, OlympusAmerica, Melville, NY, USA). The fluorescence intensity was measured by using software, ImageJ (NIH). After fluorescence measurement, the same nanotip was immersed into 10 μL DI water which was hung on the Al coil for electrical measurement. A picoammeter (Keithley, 6487) was used to measure the electric current between a nanotip and a ring-shaped Al coil. The current was measured at 1V.

5.3.2 Results and Discussion

Figure 39a shows the CV characteristics measured for a dendritic nanotip composed of SWCNTs and Si nanowires. The sweeping rates were 100, 200, 500, and 1,000 mV/s for current measurement. In the graph, the capacitance is the accumulated charge on tip surface, which is concealed within the inner region of

CV for one cycle. With the increase of a sweeping rate, both the capacitance and the current increased along with the noise. According to the measurement, the sweeping rates of 100 and 200 mV/s showed reproducible signals with low noise. Thus 200 mV/s was chosen for the rest of the measurement.

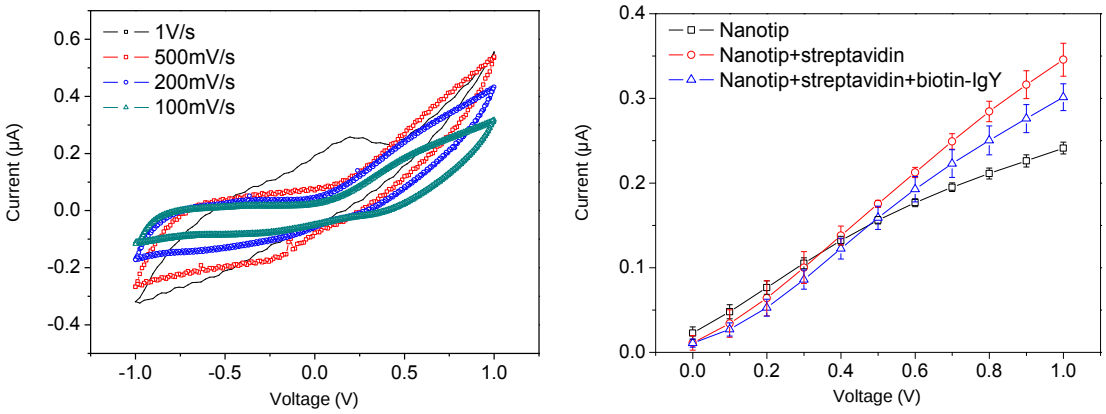

(a) (b)

Figure 39. (a) Cyclic voltammetry for a dendritic nanotip made of Si nanowires and SWCNTs. The sweeping rates vary from 100 mV/sec to 1 V/sec (b) *I-V* response for a dendritic nanotip without coating, with coating of streptavidin, and streptavidin + biotinylated IgY at a sweeping rate of 200 mV/sec (N=3).

When the dendritic nanotips were used to measure the electric current for the functionalized layers of streptavidin and antibodies, the average currents at 1V (scan rate: 200mV/second) were 0.24, 0.35, and 0.3 µA for nanotips without coating, streptavidin-coated nanotip, and additional antibody-coated nanotip, respectively (Figure 39b). Either increase or decrease of the electric current depended on the protein layers on SWCNTs. When streptavidin was coated on SWCNTs, the electric current at 1V increased. However, the current was reduced when the biotinylated IgY antibody was bound onto the streptavidin layer. The measurement results showed a potential as a reference-free amperometry sensor.

In comparison to the CV measurement, the electric current of the dendritic

nanotip at 1V of the *I-V* measurement was reduced because of a different measurement setup. The CV was measured using a function generator and a current meter while the *I-V* was measured using a current meter with its own voltage source. To investigate the effect of the redox potential in the current measurement, the redox potential in DI water was measured as 0.22 V in an open circuit. The electric current due to the redox potential in DI water was smaller than 0.03 µA in the closed circuit at the external voltage of 0V (Figure 39b). The current was also smaller than the current at 1 V by an order of magnitude. Thus effect of the redox potential could be neglected in the measurement at 1 V.

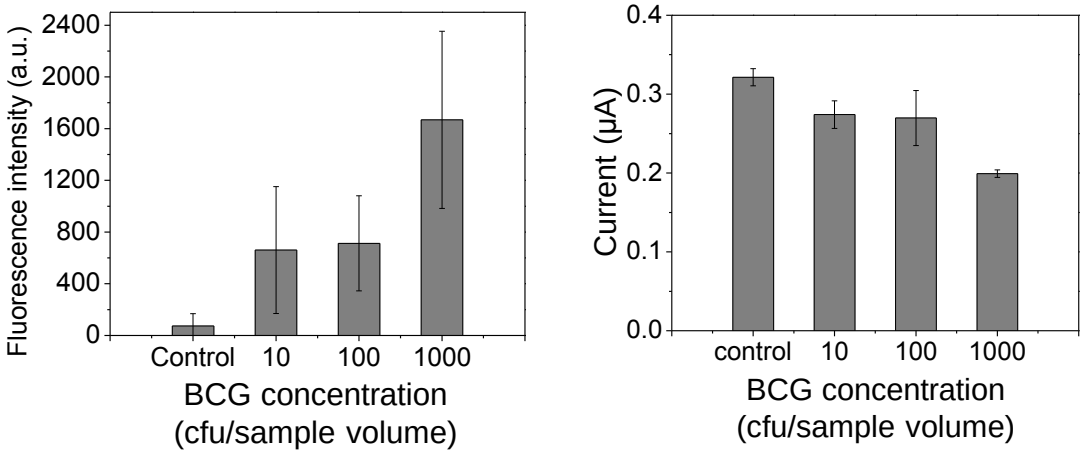

(a) (b)

Figure 40. Sensitivity test for BCG cells in PBS buffer by using (a) fluorescence measurement (b) corresponding electrical measurement (error bars are the standard deviation; N=3).

For the sensitivity test, various concentrations of BCG cells were captured and detected. The sensitivity was 10 cfu in 10 µL buffer solution for both fluorescence (Figure 40a) and electrical measurement (Figure 40b). Thus, the sensitivity of electric measurement using the dendridic nanotip approached that of the more laborious fluorescence measurement method. As the cell concentration increased, the fluorescence intensity increased because of more binding events of

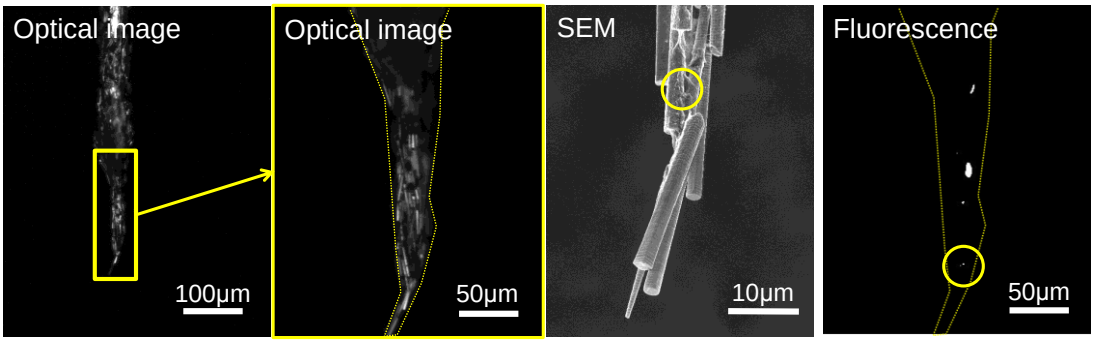

(a) (b) (c) (d)

Figure 41. Dendritic nanotip for capturing BCG (a) optical image of a dendritic nanotip, (b) optical image of a magnified nanotip, (c) SEM image of a dendritic nanotip (d) corresponding fluorescence image. Bright spots are BCG cells stained by fluorescent antibodies. The circles in (c) and (d) are the same spots indicating BCG cells.

fluorescence antibodies. In the electrical measurement, the electric current was reduced with increase of the cell concentration. The charge transfer on SWCNT surface was decreased with the binding of cells and antibodies, which was detected by the measurement of electric current. The captured cells on the nanotip were also visible by SEM and fluorescence microscopy (Figure 41).

For comparison, the current ratio ($-\Delta I/I_o$) was compared with the fluorescence intensity at each concentration of BCG (Figure 42). The current ratio increased proportionally with fluorescence intensity. The deviation of both signals might be caused by different characteristics of fluorescence- and electrical measurement. The fluorescence measurement was strongly dependent on the size of the captured cell clumps because more binding spots were generated by the surface antigen on cell surface. The electrical measurement was strongly dependent on the location and size of bound cell clumps because a higher current density was created toward the terminal end of a dendritic nanotip as computed in

Figure 36(b).

To improve the sensitivity of the device, the required sample volume should be increased over 100 µL. Considering the DEP force effective within 1 mm range, the combination with a circulation flow can enhance the concentration efficiency for a large volume sample. Therefore, with a larger sample volume, a higher sensitivity can be achieved by combining of circulation flow with an electric field for concentration. The electrolyte-free and reference-free configuration potentially offers a rapid and simple platform for rapid disease diagnosis.

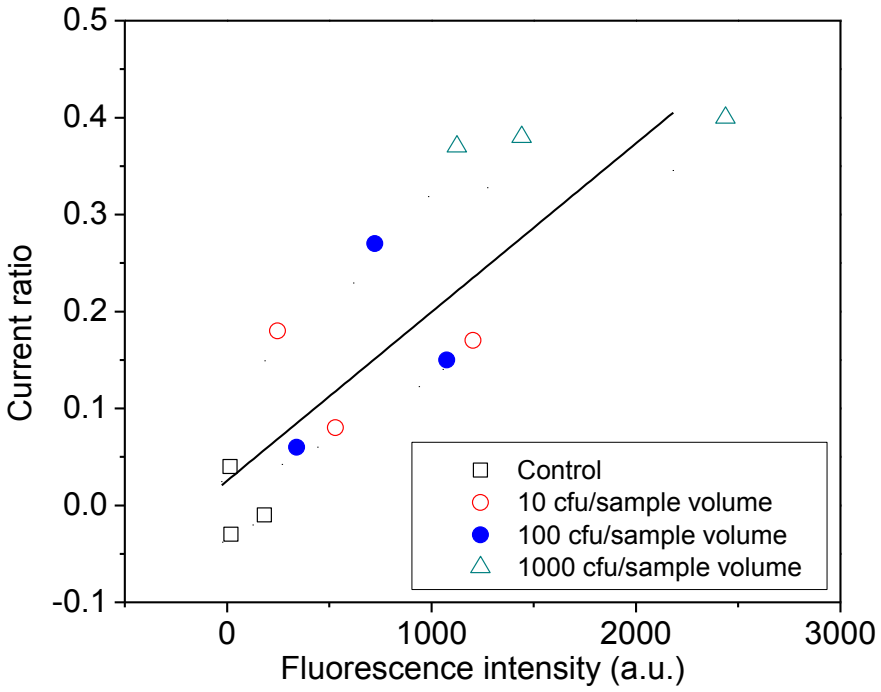

Figure 42. Comparison between the current ratio and fluorescence intensity at various concentrations of BCG in PBS buffer

5.4 Summary

In summary, a rapid and simple amperometric immunosensor was developed by using a dendritic nanotip composed of Si nanowires coated with SWCNTs. Due to the confined current paths of the dendritic nanotip, a capacitance effect by an electrical double layer could be suppressed while the current change on the SWCNT surface could be sensitively measured upon binding of target cells bound with fluorescence-antibodies. The electric measurement was conducted through a medium of DI water, which reduced the double-layer capacitance effect and chemical reactions. The electric measurement could be conducted without a reference electrode. The detection results were validated by fluorescence and SEM studies. Using the electrical measurement setup, the sensitivity was 10 cfu/sample volume (i.e. 10 μL), comparable to a more laborious fluorescence staining method and among the most sensitive amperometric methods reported to date. The simple measurement configuration will offer a rapid diagnostic platform for diseases.

Table 5 summarizes the performance of the immunofluorescence microtip sensor and the amperometry nanotip sensor in comparsion with that of a GeneXpert PCR system. When fully developed, the microtips and the nanotips will offer a unique platform for TB POC diagnosis due to rapid and reliable process. The ulitmate performance of the tip sensor should be validated with further optimization and clinical testing. If successful, the tip sensor will save millions of precious lives in a year.

Table 5. Comparison for the performance of GeneXpert system, microtip-immunofluorescence, and nanotip-amperometry.

Contents	GeneXpert	Microtip-fluorescence	Nanotip –amperometry
Biomarkers	DNA	MTB/DNA	MTB
Limit of detection	130 cfu/mL	200 cfu/mL	1000 cfu/mL
Power requirement	150W	5W	1 W
Assay time	2 hours	25 minutes	25 minutes
Detection of MDR-TB	Yes	Yes (next-generation with DNA detection)	No
Sample number	4	1 (extended to 4)	1
POC diagnosis	No	Yes	Yes

Chapter 6: Summary and Remaining Study

A novel concentration mechanism of target bacteria using a micro- and nano-structured tip was studied through numerical approach and experiment.

The immunofluorescence microtip sensor specifically detected *Mycobacterium* cells by the combination of electric field, streaming flow, and immuno-affinity binding. To elucidate the concentration mechanism, the electric field-induced forces were numerically computed and compared with exeperimental results. The detection limit was 200 CFU/mL in human sputum, which was comparable to PCR but did not require bacteriological culture, centrifugation, or nucleic acid amplification.

The specific capturing mechanism of target bacteria was then studied by using gold-coated Si substrate and microtips. On gold-coated Si substrate, the contact angle of the cell suspension was decreased when the substrate was modified with the corresponding antibodies. Without the binding affinity, the contact angle was larger than that with binding affiinty. When a microtip was coated with antibodies against BCG cells, the coffee ring effect could increase the number of captured cells by 3.1 times in comparison with *E. coli* cells. Therefore, the capillary-induced coffee ring effect on antibody-functionalized microtips could offer specific capture of target cells.

Finally, A dendritic nanotip was characterized for electrical detection of target bacteria. A dendritic nanotip was composed of SWCNTs and Si nanowires for measurement of captured cells due to the resistance change of SWCNTs. The

dendritic nanostructure allowed the direct measurement of the resistance change because the ionic-layer capacitance on the nanotip surface surface was suppressed due to the confined paths of electric current. The reference-free measurement could offer an extremely simple platform for TB diagnosis.

In spite of the complex nature of physical, chemical, and biological mechanisms, the simple operation of “dipping and withdrawal” of tips allows for screening by minimally trained personnel within 30 minutes. In addition, the minimal power requirement (5 W) combined with low assay cost is ideal for point-of-care (POC) screening in limited resource settings. When fully developed, the microtips and the nanotip will offer a unique solution for TB POC diagnosis without compromising the performance of laboratory equipment.

Future research will focus on the further optimization of tip sensors. The ulitmate performance of the tip sensor should be validated with further optimization and clinical testing. If successful, the tip sensor will save millions of precious lives in a year. In particular, future research will study the multiplexing of target bacteria in complex samples. The micro- and nano-stuctured tips can be functionalized with target-specific capturing probes, which can be used for detecting multiple targets. Therefore, the main advantage of the presented approach is a low-cost, high-throughput disease diagnosis with simple device action.

List of References

[1] WHO, "Global tuberculosis control: WHO Report 2010 " WHO, Geneva 2010.

[2] WHO, "Global tuberculosis control: surveillance, planning, financing " WHO, Geneva 2009.

[3] C. Lienhardt, J. Rowley, K. Manneh, G. Lahai, D. Needham, P. Milligan, *et al.*, "Factors affecting time delay to treatment in a tuberculosis control programme in a sub-Saharan African country: the experience of The Gambia," *International Journal of Tuberculosis and Lung Disease,* vol. 5, pp. 233-239, Mar 2001.

[4] J. E. Golub, S. Bur, W. A. Cronin, S. Gange, N. Baruch, G. W. Comstock, *et al.*, "Delayed tuberculosis diagnosis and tuberculosis transmission," *International Journal of Tuberculosis and Lung Disease,* vol. 10, pp. 24-30, Jan 2006.

[5] V. R. Aber, B. W. Allen, D. A. Mitchison, P. Ayuma, E. A. Edwards, and A. B. Keyes, "Quality-Control in Tuberculosis Bacteriology .1. Laboratory Studies on Isolated Positive Cultures and the Efficiency of Direct Smear Examination," *Tubercle,* vol. 61, pp. 123-133, 1980.

[6] J. C. Boyd and J. J. Marr, "Decreasing Reliability of Acid-Fast Smear Techniques for Detection of Tuberculosis," *Annals of Internal Medicine,* vol. 82, pp. 489-492, 1975.

[7] K. R. Steingart, A. Ramsay, and M. Pai, "Optimizing sputum smear microscopy for the diagnosis of pulmonary tuberculosis," *Expert Review of Anti-Infective Therapy,* vol. 5, pp. 327-331, Jul 2007.

[8] M. D. Perkins and P. M. Small, "Partnering for better microbial diagnostics," *Nature Biotechnology,* vol. 24, pp. 919-921, Aug 2006.

[9] E. Keeler, M. D. Perkins, P. Small, C. Hanson, S. Reed, J. Cunningham, *et al.*, "Reducing the global burden of tuberculosis: the contribution of improved diagnostics," *Nature,* vol. 444 Suppl 1, pp. 49-57, Nov 23 2006.

[10] O. Lazcka, F. J. Del Campo, and F. X. Munoz, "Pathogen detection: A perspective of traditional methods and biosensors," *Biosensors & Bioelectronics,* vol. 22, pp. 1205-1217, Feb 15 2007.

[11] E. Torres-Chavolla and E. C. Alocilja, "Aptasensors for detection of microbial and viral pathogens," *Biosensors & Bioelectronics*, vol. 24, pp. 3175-3182, Jul 15 2009.

[12] A. M. Elliott, N. Luo, G. Tembo, B. Halwiindi, G. Steenbergen, L. Machiels, *et al.*, "Impact of Hiv on Tuberculosis in Zambia - a Cross-Sectional Study," *British Medical Journal*, vol. 301, pp. 412-415, Sep 1 1990.

[13] L. H. Garland, "Studies on the Accuracy of Diagnostic Procedures," *American Journal of Roentgenology Radium Therapy and Nuclear Medicine*, vol. 82, pp. 25-38, 1959.

[14] D. Rodriguez-Lazaro, M. D'Agostino, A. Herrewegh, M. Pla, N. Cook, and J. Ikonomopoulos, "Real-time PCR-based methods for detection of Mycobacterium avium Subsp paratuberculosis in water and milk," *International Journal of Food Microbiology*, vol. 101, pp. 93-104, May 1 2005.

[15] L. M. Thomson, H. Traore, H. Yesilkaya, C. Doig, H. Steingrimsdottir, L. Garcia, *et al.*, "An extremely rapid and simple DNA-release method for detection of M. tuberculosis from clinical specimens," *Journal of Microbiological Methods*, vol. 63, pp. 95-98, Oct 2005.

[16] Y. J. Choi, Y. Hu, and A. Mahmood, "Clinical significance of a polymerase chain reaction assay for the detection of Mycobacterium tuberculosis," *American Journal of Clinical Pathology*, vol. 105, pp. 200-204, Feb 1996.

[17] R. Durmaz, A. Aydin, B. Durmaz, N. E. Aydin, B. S. Akbasak, and S. Gunal, "Sensitivity of two-stage PCR amplification for detection of Mycobacterium tuberculosis in paraffin-embedded tissues," *Journal of Microbiological Methods*, vol. 29, pp. 69-75, May 1997.

[18] E. Krambovitis, P. E. Lock, M. B. Mcillmurray, W. Hendrickse, and H. Holzel, "Rapid Diagnosis of Tuberculous Meningitis by Latex Particle Agglutination," *Lancet*, vol. 2, pp. 1229-1231, 1984.

[19] M. Tamminen, T. Joutsjoki, M. Sjoblom, M. Joutsen, A. Palva, E. L. Ryhanen, *et al.*, "Screening of lactic acid bacteria from fermented vegetables by carbohydrate profiling and PCR-ELISA," *Letters in Applied Microbiology*, vol. 39, pp. 439-444, 2004.

[20] E. Nassau, E. R. Parsons, and G. D. Johnson, "The detection of antibodies to Mycobacterium tuberculosis by microplate enzyme-linked immunosorbent assay (ELISA)," *Tubercle*, vol. 57, pp. 67-70, Mar 1976.

[21] C. Delacourt, J. Gobin, J. L. Gaillard, J. Deblic, M. Veron, and P. Scheinmann, "Value of Elisa Using Antigen-60 for the Diagnosis of Tuberculosis in Children," *Chest*, vol. 104, pp. 393-398, Aug 1993.

[22] G. Middlebrook, Z. Reggiardo, and W. D. Tigertt, "Automatable Radiometric Detection of Growth of Mycobacterium-Tuberculosis in Selective Media," *American Review of Respiratory Disease*, vol. 115, pp. 1066-1069, 1977.

[23] F. Gamboa, J. M. Manterola, J. Lonca, L. Matas, B. Vinado, M. Gimenez, *et al.*, "Detection and identification of mycobacteria by amplification of RNA and DNA in pretreated blood and bone marrow aspirates by a simple lysis method," *Journal of Clinical Microbiology*, vol. 35, pp. 2124-2128, Aug 1997.

[24] E. Cambau, C. Wichlacz, C. Truffot-Pernot, and V. Jarlier, "Evaluation of the new MB Redox system for detection of growth of mycobacteria," *Journal of Clinical Microbiology*, vol. 37, pp. 2013-2015, Jun 1999.

[25] D. L. Qin, X. X. He, K. M. Wang, and W. H. Tan, "Using fluorescent nanoparticles and SYBR Green I based two-color flow cytometry to determine Mycobacterium tuberculosis avoiding false positives," *Biosensors & Bioelectronics*, vol. 24, pp. 626-631, Dec 1 2008.

[26] D. Griffiths and G. Hall, "Biosensors - What Real Progress Is Being Made," *Trends in Biotechnology*, vol. 11, pp. 122-130, Apr 1993.

[27] V. M. Owen, "Market requirements for advanced biosensors in healthcare," *Biosensors & Bioelectronics*, vol. 9, pp. xxix-xxxv, 1994.

[28] C. Habeenzu, D. Lubasi, and A. F. Fleming, "Improved sensitivity of direct microscopy for detection of acid-fast bacilli in sputum in developing countries," *Transactions of the Royal Society of Tropical Medicine and Hygiene*, vol. 92, pp. 415-416, Jul-Aug 1998.

[29] N. Gebre, U. Karlsson, G. Jonsson, R. Macaden, A. Wolde, A. Assefa, *et al.*, "Improved microscopical diagnosis of pulmonary tuberculosis in developing countries," *Trans R Soc Trop Med Hyg*, vol. 89, pp. 191-3, Mar-Apr 1995.

[30] J. Bruchfeld, G. Aderaye, I. B. Palme, B. Bjorvatn, G. Kallenius, and L. Lindquist, "Sputum concentration improves diagnosis of tuberculosis in a setting with a high prevalence of HIV," *Transactions of the Royal Society of Tropical Medicine and Hygiene*, vol. 94, pp. 677-680, Nov-Dec 2000.

[31] L. F. Sherman, P. I. Fujiwara, S. V. Cook, L. B. Bazerman, and T. R. Frieden, "Patient and health care system delays in the diagnosis and treatment of

tuberculosis," *International Journal of Tuberculosis and Lung Disease,* vol. 3, pp. 1088-1095, Dec 1999.

[32] K. A. K. Angeby, S. E. Hoffner, and V. K. Diwan, "Should the 'bleach microscopy method' be recommended for improved case detection of tuberculosis? Literature review and key person analysis," *International Journal of Tuberculosis and Lung Disease,* vol. 8, pp. 806-815, Jul 2004.

[33] D. Wilkinson and A. W. Sturm, "Diagnosing tuberculosis in a resource-poor setting: the value of sputum concentration," *Transactions of the Royal Society of Tropical Medicine and Hygiene,* vol. 91, pp. 420-421, Jul-Aug 1997.

[34] H. Albert, P. J. Ademun, G. Lukyamuzi, B. Nyesiga, Y. Manabe, M. Joloba, *et al.*, "Feasibility of magnetic bead technology for concentration of mycobacteria in sputum prior to fluorescence microscopy," *Bmc Infectious Diseases,* vol. 11, May 13 2011.

[35] S. Wilson, A. Lane, R. Rosedale, and C. Stanley, "Concentration of Mycobacterium tuberculosis from sputum using ligand-coated magnetic beads," *International Journal of Tuberculosis and Lung Disease,* vol. 14, pp. 1164-1168, Sep 2010.

[36] C. Lui, N. C. Cady, and C. A. Batt, "Nucleic Acid-based Detection of Bacterial Pathogens Using Integrated Microfluidic Platform Systems," *Sensors,* vol. 9, pp. 3713-3744, May 2009.

[37] L. Zhu, Q. Zhang, H. H. Feng, S. Ang, F. S. Chauc, and W. T. Liu, "Filter-based microfluidic device as a platform for immunofluorescent assay of microbial cells," *Lab on a Chip,* vol. 4, pp. 337-341, 2004.

[38] N. Bao and C. Lu, "A microfluidic device for physical trapping and electrical lysis of bacterial cells," *Applied Physics Letters,* vol. 92, May 26 2008.

[39] H. L. Shao, C. Min, D. Issadore, M. Liong, T. J. Yoon, R. Weissleder, *et al.*, "Magnetic Nanoparticles and microNMR for Diagnostic Applications," *Theranostics,* vol. 2, pp. 55-65, 2012.

[40] X. A. Guan, H. J. Zhang, Y. N. Bi, L. Zhang, and D. L. Hao, "Rapid detection of pathogens using antibody-coated microbeads with bioluminescence in microfluidic chips," *Biomedical Microdevices,* vol. 12, pp. 683-691, Aug 2010.

[41] K. Y. Lien, W. C. Lee, H. Y. Lei, and G. B. Lee, "Integrated reverse transcription polymerase chain reaction systems for virus detection," *Biosensors & Bioelectronics,* vol. 22, pp. 1739-1748, Mar 15 2007.

[42] N. Beyor, T. S. Seo, P. Liu, and R. A. Mathies, "Immunomagnetic bead-based cell concentration microdevice for dilute pathogen detection," *Biomedical Microdevices,* vol. 10, pp. 909-917, Dec 2008.

[43] P. Grodzinski, J. Yang, R. H. Liu, and M. D. Ward, "A modular microfluidic system for cell pre-concentration and genetic sample preparation," *Biomedical Microdevices,* vol. 5, pp. 303-310, Dec 2003.

[44] C. Q. Yi, C. W. Li, S. L. Ji, and M. S. Yang, "Microfluidics technology for manipulation and analysis of biological cells," *Analytica Chimica Acta,* vol. 560, pp. 1-23, Feb 23 2006.

[45] S. Derveaux, B. G. Stubbe, K. Braeckmans, C. Roelant, K. Sato, J. Demeester, *et al.*, "Synergism between particle-based multiplexing and microfluidics technologies may bring diagnostics closer to the patient," *Analytical and Bioanalytical Chemistry,* vol. 391, pp. 2453-2467, Aug 2008.

[46] S. Haeberle and R. Zengerle, "Microfluidic platforms for lab-on-a-chip applications," *Lab on a Chip,* vol. 7, pp. 1094-1110, 2007.

[47] R. Pethig, "Dielectrophoresis: Status of the theory, technology, and applications (vol 4, 022811, 2010)," *Biomicrofluidics,* vol. 4, Sep 2010.

[48] C. P. Jen and H. H. Chang, "A handheld preconcentrator for the rapid collection of cancerous cells using dielectrophoresis generated by circular microelectrodes in stepping electric fields," *Biomicrofluidics,* vol. 5, Sep 2011.

[49] C. Church, J. J. Zhu, G. H. Huang, T. R. Tzeng, and X. C. Xuan, "Integrated electrical concentration and lysis of cells in a microfluidic chip," *Biomicrofluidics,* vol. 4, Dec 2010.

[50] D. Hou, S. Maheshwari, and H. C. Chang, "Rapid bioparticle concentration and detection by combining a discharge driven vortex with surface enhanced Raman scattering," *Biomicrofluidics,* vol. 1, Mar 2007.

[51] M. Koklu, S. Park, S. D. Pillai, and A. Beskok, "Negative dielectrophoretic capture of bacterial spores in food matrices," *Biomicrofluidics,* vol. 4, Sep 2010.

[52] B. H. Lapizco-Encinas, R. V. Davalos, B. A. Simmons, E. B. Cummings, and Y. Fintschenko, "An insulator-based (electrodeless) dielectrophoretic concentrator for microbes in water," *Journal of Microbiological Methods,* vol. 62, pp. 317-326, Sep 2005.

[53] E. T. Lagally, S. H. Lee, and H. T. Soh, "Integrated microsystem for dielectrophoretic cell concentration and genetic detection," *Lab on a Chip,* vol. 5, pp. 1053-1058, 2005.

[54] I. F. Cheng, H. C. Chang, D. Hou, and H. C. Chang, "An integrated dielectrophoretic chip for continuous bioparticle filtering, focusing, sorting, trapping, and detecting," *Biomicrofluidics,* vol. 1, Apr-Jun 2007.

[55] R. S. W. Thomas, P. D. Mitchell, R. O. C. Oreffo, and H. Morgan, "Trapping single human osteoblast-like cells from a heterogeneous population using a dielectrophoretic microfluidic device," *Biomicrofluidics,* vol. 4, Jun 2010.

[56] K. Zhu, A. S. Kaprelyants, E. G. Salina, and G. H. Markx, "Separation by dielectrophoresis of dormant and nondormant bacterial cells of Mycobacterium smegmatis," *Biomicrofluidics,* vol. 4, Jun 2010.

[57] R. S. Kuczenski, H. C. Chang, and A. Revzin, "Dielectrophoretic microfluidic device for the continuous sorting of Escherichia coli from blood cells," *Biomicrofluidics,* vol. 5, Sep 2011.

[58] A. Castellanos, A. Ramos, A. Gonzalez, N. G. Green, and H. Morgan, "Electrohydrodynamics and dielectrophoresis in microsystems: scaling laws," *Journal of Physics D-Applied Physics,* vol. 36, pp. 2584-2597, Oct 21 2003.

[59] J. Oh, R. Hart, J. Capurro, and H. Noh, "Comprehensive analysis of particle motion under non-uniform AC electric fields in a microchannel," *Lab on a Chip,* vol. 9, pp. 62-78, 2009.

[60] S. Podszun, P. Vulto, H. Heinz, S. Hakenberg, C. Hermann, T. Hankemeier, *et al.*, "Enrichment of viable bacteria in a micro-volume by free-flow electrophoresis," *Lab on a Chip,* vol. 12, pp. 451-457, 2012.

[61] M. Bonnet, A. Ramsay, W. Githui, L. Gagnidze, F. Varaine, and P. J. Guerin, "Bleach sedimentation: An opportunity to optimize smear microscopy for tuberculosis diagnosis in settings of high prevalence of HIV," *Clinical Infectious Diseases,* vol. 46, pp. 1710-1716, Jun 1 2008.

[62] L. E. Mohamed A A, Cuevas L E, et al. , "Improving the diagnosis of tuberculosis by the optimization of sputum microscopy. Expert consultation," *Geneva, Switzerland,* vol. WHO, 2005, 2005.

[63] B. Weigl, G. Domingo, P. LaBarre, and J. Gerlach, "Towards non- and minimally instrumented, microfluidics-based diagnostic devices," *Lab on a Chip,* vol. 8, pp. 1999-2014, 2008.

[64] K. Glynou, P. C. Ioannou, T. K. Christopoulos, and V. Syriopoulou, "Oligonucleotide-functionalized gold nanoparticles as probes in a dry-reagent strip biosensor for DNA analysis by hybridization," *Analytical Chemistry,* vol. 75, pp. 4155-4160, Aug 15 2003.

[65] Y. Ikada and H. Tsuji, "Biodegradable polyesters for medical and ecological applications," *Macromolecular Rapid Communications,* vol. 21, pp. 117-132, Feb 2000.

[66] R. C. Poller, "Reclamation of Waste Plastics and Rubber - Recovery of Materials and Energy," *Journal of Chemical Technology and Biotechnology,* vol. 30, pp. 152-160, 1980.

[67] D. Helb, M. Jones, E. Story, C. Boehme, E. Wallace, K. Ho, *et al.*, "Rapid Detection of Mycobacterium tuberculosis and Rifampin Resistance by Use of On-Demand, Near-Patient Technology," *Journal of Clinical Microbiology,* vol. 48, pp. 229-237, Jan 2010.

[68] P. P. Banada, S. K. Sivasubramani, R. Blakemore, C. Boehme, M. D. Perkins, K. Fennelly, *et al.*, "Containment of Bioaerosol Infection Risk by the Xpert MTB/RIF Assay and Its Applicability to Point-of-Care Settings," *Journal of Clinical Microbiology,* vol. 48, pp. 3551-3557, Oct 2010.

[69] R. Blakemore, E. Story, D. Helb, J. Kop, P. Banada, M. R. Owens, *et al.*, "Evaluation of the Analytical Performance of the Xpert MTB/RIF Assay," *Journal of Clinical Microbiology,* vol. 48, pp. 2495-2501, Jul 2010.

[70] C. C. Boehme, P. Nabeta, D. Hillemann, M. P. Nicol, S. Shenai, F. Krapp, *et al.*, "Rapid Molecular Detection of Tuberculosis and Rifampin Resistance," *New England Journal of Medicine,* vol. 363, pp. 1005-1015, Sep 2010.

[71] R. McNerney and P. Daley, "Towards a point-of-care test for active tuberculosis: obstacles and opportunities," *Nature Reviews Microbiology,* vol. 9, pp. 204-213, Mar 2011.

[72] E. B. Hanlon, R. Manoharan, T. W. Koo, K. E. Shafer, J. T. Motz, M. Fitzmaurice, *et al.*, "Prospects for in vivo Raman spectroscopy," *Physics in Medicine and Biology,* vol. 45, pp. R1-R59, Feb 2000.

[73] Y. Ozaki, R. Cho, K. Ikegaya, S. Muraishi, and K. Kawauchi, "Potential of near-Infrared Fourier-Transform Raman-Spectroscopy in Food Analysis," *Applied Spectroscopy,* vol. 46, pp. 1503-1507, Oct 1992.

[74] P. C. A. M. Buijtels, H. F. M. Willemse-Erix, P. L. C. Petit, H. P. Endtz, G. J. Puppels, H. A. Verbrugh, *et al.*, "Rapid identification of mycobacteria by

Raman spectroscopy," *Journal of Clinical Microbiology*, vol. 46, pp. 961-965, Mar 2008.

[75] R. McNerney, B. A. Wondafrash, K. Amena, A. Tesfaye, E. M. McCash, and N. J. Murray, "Field test of a novel detection device for Mycobacterium tuberculosis antigen in cough," *Bmc Infectious Diseases*, vol. 10, Jun 8 2010.

[76] D. L. Qin, X. X. He, K. M. Wang, X. J. J. Zhao, W. H. Tan, and J. Y. Chen, "Fluorescent nanoparticle-based indirect immunofluorescence microscopy for detection of Mycobacterium tuberculosis," *Journal of Biomedicine and Biotechnology*, 2007.

[77] H. Lee, E. Sun, D. Ham, and R. Weissleder, "Chip-NMR biosensor for detection and molecular analysis of cells," *Nature Medicine*, vol. 14, pp. 869-874, Aug 2008.

[78] A. L. Chun, "Nanoparticles offer hope for TB detection," *Nature Nanotechnology*, vol. 4, pp. 698-699, Nov 2009.

[79] H. O. Fatoyinbo, K. F. Hoettges, S. M. Reddy, and M. P. Hughes, "An integrated dielectrophoretic quartz crystal microbalance (DEP-QCM) device for rapid biosensing applications," *Biosensors & Bioelectronics*, vol. 23, pp. 225-232, Sep 30 2007.

[80] J. Gao, M. L. Y. Sin, T. T. Liu, V. Gau, J. C. Liao, and P. K. Wong, "Hybrid electrokinetic manipulation in high-conductivity media," *Lab on a Chip*, vol. 11, pp. 1770-1775, 2011.

[81] J. Wu, Y. X. Ben, and H. C. Chang, "Particle detection by electrical impedance spectroscopy with asymmetric-polarization AC electroosmotic trapping," *Microfluidics and Nanofluidics*, vol. 1, pp. 161-167, May 2005.

[82] W. H. Yeo, F. L. Chou, G. Fotouhi, K. Oh, B. T. Stevens, H. Y. Tseng, *et al.*, "Size-selective immunofluorescence of Mycobacterium tuberculosis cells by capillary- and viscous forces," *Lab on a Chip*, vol. 10, pp. 3178-3181, 2010.

[83] W. H. Yeo, J. H. Chung, Y. L. Liu, and K. H. Lee, "Size-Specific Concentration of DNA to a Nanostructured Tip Using Dielectrophoresis and Capillary Action," *Journal of Physical Chemistry B*, vol. 113, pp. 10849-10858, Aug 6 2009.

[84] W. H. Yeo, S. Liu, J. H. Chung, Y. L. Liu, and K. H. Lee, "Rapid detection of Mycobacterium tuberculosis cells by using microtip-based immunoassay," *Analytical and Bioanalytical Chemistry*, vol. 393, pp. 1593-1600, Mar 2009.

[85] S. Park, M. Koklu, and A. Beskok, "Particle Trapping in High-Conductivity Media with Electrothermally Enhanced Negative Dielectrophoresis," *Analytical Chemistry,* vol. 81, pp. 2303-2310, Mar 15 2009.

[86] H. Varmus, R. Klausner, E. Zerhouni, T. Acharya, A. S. Daar, and P. A. Singer, "Grand challenges in global health," *Science,* vol. 302, pp. 398-399, Oct 2003.

[87] K. Lee, J. Lee, E. J. Jeong, A. Kronk, K. S. J. Elenitoba-Johnson, M. S. Lim, *et al.*, "Conjugated Polyelectrolyte-Antibody Hybrid Materials for Highly Fluorescent Live Cell-Imaging," *Advanced Materials,* vol. 24, pp. 2479-2484, May 2012.

[88] J. W. Hong, K. H. Chung, and H. C. Yoon, "Fluorescence affinity sensing by using a self-contained fluid manoeuvring microfluidic chip," *Analyst,* vol. 133, pp. 499-504, 2008.

[89] Y. S. Gong, L. Chang, K. L. Viola, P. N. Lacor, M. P. Lambert, C. E. Finch, *et al.*, "Alzheimer's disease-affected brain: Presence of oligomeric A beta ligands (ADDLs) suggests a molecular basis for reversible memory loss," *Proceedings of the National Academy of Sciences of the United States of America,* vol. 100, pp. 10417-10422, Sep 2003.

[90] E. Rabani, D. R. Reichman, P. L. Geissler, and L. E. Brus, "Drying-mediated self-assembly of nanoparticles," *Nature,* vol. 426, pp. 271-274, Nov 2003.

[91] S. Choi, S. Stassi, A. P. Pisano, and T. I. Zohdi, "Coffee-Ring Effect-Based Three Dimensional Patterning of Micro/Nanoparticle Assembly with a Single Droplet," *Langmuir,* vol. 26, pp. 11690-11698, Jul 2010.

[92] R. D. Deegan, O. Bakajin, T. F. Dupont, G. Huber, S. R. Nagel, and T. A. Witten, "Capillary flow as the cause of ring stains from dried liquid drops," *Nature,* vol. 389, pp. 827-829, Oct 23 1997.

[93] R. Bhardwaj, X. H. Fang, P. Somasundaran, and D. Attinger, "Self-Assembly of Colloidal Particles from Evaporating Droplets: Role of DLVO Interactions and Proposition of a Phase Diagram," *Langmuir,* vol. 26, pp. 7833-7842, Jun 2010.

[94] A. S. Sangani, C. H. Lu, K. H. Su, and J. A. Schwarz, "Capillary force on particles near a drop edge resting on a substrate and a criterion for contact line pinning," *Physical Review E,* vol. 80, Jul 2009.

[95] J. R. Trantum, D. W. Wright, and F. R. Haselton, "Biomarker-Mediated Disruption of Coffee-Ring Formation as a Low Resource Diagnostic Indicator," *Langmuir,* vol. 28, pp. 2187-2193, Jan 2012.

[96] P. J. Yunker, T. Still, M. A. Lohr, and A. G. Yodh, "Suppression of the coffee-ring effect by shape-dependent capillary interactions," *Nature,* vol. 476, pp. 308-311, Aug 18 2011.

[97] R. D. Deegan, O. Bakajin, T. F. Dupont, G. Huber, S. R. Nagel, and T. A. Witten, "Contact line deposits in an evaporating drop," *Physical Review E,* vol. 62, pp. 756-765, Jul 2000.

[98] H. Hu and R. G. Larson, "Analysis of the effects of Marangoni stresses on the microflow in an evaporating sessile droplet," *Langmuir,* vol. 21, pp. 3972-3980, Apr 2005.

[99] D. Soltman and V. Subramanian, "Inkjet-printed line morphologies and temperature control of the coffee ring effect," *Langmuir,* vol. 24, pp. 2224-2231, Mar 2008.

[100] T. S. Wong, T. H. Chen, X. Y. Shen, and C. M. Ho, "Nanochromatography Driven by the Coffee Ring Effect," *Analytical Chemistry,* vol. 83, pp. 1871-1873, Mar 2011.

[101] M.-P. Larvor, L. Djavadi-Ohaniance, B. Nall, and M. E. Goldberg, "Measurement of the dissociation rate constant of antigen/antibody complexes in solution by enzyme-linked immunosorbent assay," *Journal of Immunological Methods,* vol. 170, pp. 167-175, 1994.

[102] E. Marris, "From TB tests, just a 'yes or no' answer, please," *Nature Medicine,* vol. 13, pp. 267-267, Mar 2007.

[103] G. F. Araj, B. H. Fahmawi, T. D. Chugh, and M. Abusalim, "Improved Detection of Mycobacterial Antigens in Clinical Specimens by Combined Enzyme-Linked Immunosorbent Assays," *Diagnostic Microbiology and Infectious Disease,* vol. 17, pp. 119-127, Aug-Sep 1993.

[104] L. M. P. Arias-Bouda, S. Kuijper, H. van Deutekom, R. van Gijlswijk, I. Pekel, H. M. Jansen, *et al.*, "Enzyme-linked immunosorbent assays using immune complexes for the diagnosis of tuberculosis," *Journal of Immunological Methods,* vol. 283, pp. 115-124, Dec 2003.

[105] L. M. P. Arias-Bouda, L. N. Nguyen, L. M. Ho, S. Kuijper, H. M. Jansen, and A. H. J. Kolk, "Development of antigen detection assay for diagnosis of

tuberculosis-using sputum samples," *Journal of Clinical Microbiology,* vol. 38, pp. 2278-2283, Jun 2000.

[106] A. M. Attallah, C. A. A. Malak, H. Ismail, A. H. El-Saggan, M. M. Omran, and A. A. Tabll, "Rapid and simple detection of a Mycobacterium tuberculosis circulating antigen in serum using Dot-ELISA for field diagnosis of pulmonary tuberculosis," *Journal of Immunoassay & Immunochemistry,* vol. 24, pp. 73-87, Feb 2003.

[107] E. D. Chan, R. Reves, J. T. Belisle, P. J. Brennan, and W. E. Hahn, "Diagnosis of tuberculosis by a visually detectable immunoassay for lipoarabinomannan," *American Journal of Respiratory and Critical Care Medicine,* vol. 161, pp. 1713-1719, May 2000.

[108] V. C. C. Cheng, W. W. Yew, and K. Y. Yuen, "Molecular diagnostics in tuberculosis," *European Journal of Clinical Microbiology & Infectious Diseases,* vol. 24, pp. 711-720, Nov 2005.

[109] J. L. Dahl, "Electron microscopy analysis of Mycobacterium tuberculosis cell division," *Fems Microbiology Letters,* vol. 240, pp. 15-20, Nov 2004.

[110] M. Diaz-Gonzalez, M. B. Gonzalez-Garcia, and A. Costa-Garcia, "Immunosensor for Mycobacterium tuberculosis on screen-printed carbon electrodes," *Biosensors & Bioelectronics,* vol. 20, pp. 2035-2043, Apr 2005.

[111] A. GlatmanFreedman, J. M. Martin, P. F. Riska, B. R. Bloom, and A. Casadevall, "Monoclonal antibodies to surface antigens of Mycobacterium tuberculosis and their use in a modified enzyme-linked immunosorbent spot assay for detection of mycobacteria," *Journal of Clinical Microbiology,* vol. 34, pp. 2795-2802, Nov 1996.

[112] K. P. Lyashchenko, M. Singh, R. Colangeli, and M. L. Gennaro, "A multi-antigen print immunoassay for the development of serological diagnosis of infectious diseases," *Journal of Immunological Methods,* vol. 242, pp. 91-100, Aug 2000.

[113] S. Pottumarthy, V. C. Wells, and A. J. Morris, "A comparison of seven tests for serological diagnosis of tuberculosis," *Journal of Clinical Microbiology,* vol. 38, pp. 2227-2231, Jun 2000.

[114] E. Sada, D. Aguilar, M. Torres, and T. Herrera, "Detection of Lipoarabinomannan as a Diagnostic-Test for Tuberculosis," *Journal of Clinical Microbiology,* vol. 30, pp. 2415-2418, Sep 1992.

[115] A. Van Deun and F. Portaels, "Limitations and requirements for quality control of sputum smear microscopy for acid-fast bacilli," *International Journal of Tuberculosis and Lung Disease,* vol. 2, pp. 756-765, Sep 1998.

[116] WHO, "Tuberculosis Fact Sheet," *http://www.who.int/mediacentre/factsheets/fs104/en/index.html*, March 2006.

[117] H. Yamada, S. Mitarai, L. Aguiman, H. Matsumoto, and A. Fujiki, "Preparation of mycobacteria-containing artificial sputum for TB panel testing and microscopy of sputum smears," *International Journal of Tuberculosis and Lung Disease,* vol. 10, pp. 899-905, Aug 2006.

[118] K. Steingart, M. Henry, V. Ng, P. C. Hopewell, A. Ramsay, J. Cunningham, *et al.*, "Fluorescence versus conventional sputum smear microscopy for tuberculosis: a systematic review," *Lancet Infectious Diseases,* vol. 6, pp. 570-581, Sep 2006.

[119] WHO, "Global Tuberculosis Control Report," *http://www.who.int/tb/publications/global_report/2008/pdf/summary.pdf*, March 2008.

[120] W. C. Yam, V. C. C. Cheng, W. T. Hui, L. N. Wang, W. H. Seto, and K. Y. Yuen, "Direct detection of Mycobacterium tuberculosis in clinical specimens using single-tube biotinylated nested polymerase chain reaction-enzyme linked immunoassay (PCR-ELISA)," *Diagnostic Microbiology and Infectious Disease,* vol. 48, pp. 271-275, Apr 2004.

[121] Y. P. Liu, M. A. Behr, P. M. Small, and N. Kurn, "Genotypic determination of Mycobacterium tuberculosis antibiotic resistance using a novel mutation detection method, the branch migration inhibition M-tuberculosis antibiotic resistance test," *Journal of Clinical Microbiology,* vol. 38, pp. 3656-3662, Oct 2000.

[122] C. C. Boehme, P. Nabeta, D. Hillemann, M. P. Nicol, S. Shenai, F. Krapp, *et al.*, "Rapid Molecular Detection of Tuberculosis and Rifampin Resistance," *New England Journal of Medicine,* vol. 363, pp. 1005-1015, Sep.

[123] N. ISTRATE, "AGGLUTINATION TEST FOR MYCOBACTERIAL ANTIGENS IN BIOLOGICAL SAMPLES," 1992.

[124] G. V. Kanaujia, P. K. Lam, S. Perry, P. N. Brusasca, A. Catanzaro, and M. L. Gennaro, "Integration of microscopy and serodiagnostic tests to screen for active tuberculosis," *International Journal of Tuberculosis and Lung Disease,* vol. 9, pp. 1120-1126, Oct 2005.

[125] C. D. Chin, T. Laksanasopin, Y. K. Cheung, D. Steinmiller, V. Linder, H. Parsa, *et al.*, "Microfluidics-based diagnostics of infectious diseases in the developing world," *Nature Medicine*, vol. 17, pp. 1015-U138, Aug 2011.

[126] P. Yager, T. Edwards, E. Fu, K. Helton, K. Nelson, M. R. Tam, *et al.*, "Microfluidic diagnostic technologies for global public health," *Nature*, vol. 442, pp. 412-418, Jul 27 2006.

[127] B. L. Allen, P. D. Kichambare, and A. Star, "Carbon nanotube field-effect-transistor-based biosensors," *Advanced Materials*, vol. 19, pp. 1439-1451, Jun 4 2007.

[128] G. Gruner, "Carbon nanotube transistors for biosensing applications," *Analytical and Bioanalytical Chemistry*, vol. 384, pp. 322-335, Jan 2006.

[129] A. Maroto, K. Balasubramanian, M. Burghard, and K. Kern, "Functionalized metallic carbon nanotube devices for pH sensing," *Chemphyschem*, vol. 8, pp. 220-223, Feb 2 2007.

[130] H. Boo, R. A. Jeong, S. Park, K. S. Kim, K. H. An, Y. H. Lee, *et al.*, "Electrochemical nanoneedle biosensor based on multiwall carbon nanotube," *Analytical Chemistry*, vol. 78, pp. 617-620, Jan 15 2006.

[131] M. Jouzi, M. B. Kerby, A. Tripathi, and J. Xu, "Nanoneedle method for high-sensitivity low-background monitoring of protein activity," *Langmuir*, vol. 24, pp. 10786-10790, Oct 7 2008.

[132] D. Krapf, M. Y. Wu, R. M. M. Smeets, H. W. Zandbergen, C. Dekker, and S. G. Lemay, "Fabrication and characterization of nanopore-based electrodes with radii down to 2 nm," *Nano Letters*, vol. 6, pp. 105-109, Jan 2006.

[133] Y. H. Lin, F. Lu, Y. Tu, and Z. F. Ren, "Glucose biosensors based on carbon nanotube nanoelectrode ensembles," *Nano Letters*, vol. 4, pp. 191-195, Feb 2004.

[134] K. Yum, N. Wang, and M. F. Yu, "Nanoneedle: A multifunctional tool for biological studies in living cells," *Nanoscale*, vol. 2, pp. 363-372, 2010.

[135] A. M. Kopacz, W. H. Yeo, J. H. Chung, and W. K. Liu, "Nanoscale sensor analysis using the immersed molecular electrokinetic finite element method," *Nanoscale*, vol. 4, pp. 5189-5194, 2012.

[136] D. Kalyanasundaram, S. Inoue, J. H. Kim, H. B. Lee, Z. Kawabata, W. H. Yeo, *et al.*, "Electric field-induced concentration and capture of DNA onto microtips," *Microfluidics and Nanofluidics*, pp. 1-9, 2012.

[137] W. H. Yeo, A. M. Kopacz, J. H. Kim, X. Chen, J. Wu, D. Y. Gao, *et al.*, "Dielectrophoretic concentration of low-abundance nanoparticles using a nanostructured tip," *Nanotechnology*, 2012.

[138] F. Li, X. P. Han, and S. F. Liu, "Development of an electrochemical DNA biosensor with a high sensitivity of fM by dendritic gold nanostructure modified electrode," *Biosensors & Bioelectronics*, vol. 26, pp. 2619-2625, Jan 2011.

[139] W. S. Lu, L. Lin, and L. Jiang, "Nanogold hollow balls with dendritic surface for hybridization of DNA," *Biosensors & Bioelectronics*, vol. 22, pp. 1101-1105, Jan 2007.

[140] P. W. Barone, S. Baik, D. A. Heller, and M. S. Strano, "Near-infrared optical sensors based on single-walled carbon nanotubes," *Nature Materials*, vol. 4, pp. 86-U16, Jan 2005.

[141] P. Cherukuri, S. M. Bachilo, S. H. Litovsky, and R. B. Weisman, "Near-infrared fluorescence microscopy of single-walled carbon nanotubes in phagocytic cells," *Journal of the American Chemical Society*, vol. 126, pp. 15638-15639, Dec 8 2004.

[142] R. J. Chen, S. Bangsaruntip, K. A. Drouvalakis, N. W. S. Kam, M. Shim, Y. M. Li, *et al.*, "Noncovalent functionalization of carbon nanotubes for highly specific electronic biosensors," *Proceedings of the National Academy of Sciences of the United States of America*, vol. 100, pp. 4984-4989, Apr 29 2003.

[143] T. Cagin, A. Jaramillo-Botero, G. Gao, and W. A. Goddard, "Molecular mechanics and molecular dynamics analysis of Drexler-Merkle gears and neon pump," *Nanotechnology*, vol. 9, pp. 143-152, Sep 1998.

[144] M. F. Yu, B. S. Files, S. Arepalli, and R. S. Ruoff, "Tensile loading of ropes of single wall carbon nanotubes and their mechanical properties," *Physical Review Letters*, vol. 84, pp. 5552-5555, Jun 12 2000.

[145] M. Zhang, K. R. Atkinson, and R. H. Baughman, "Multifunctional carbon nanotube yarns by downsizing an ancient technology," *Science*, vol. 306, pp. 1358-1361, Nov 19 2004.

[146] S. Sotiropoulou and N. A. Chaniotakis, "Carbon nanotube array-based biosensor," *Analytical and Bioanalytical Chemistry*, vol. 375, pp. 103-105, Jan 2003.

[147] W. Zhou, J. Vavro, C. Guthy, K. I. Winey, J. E. Fischer, L. M. Ericson, *et al.*, "Single wall carbon nanotube fibers extruded from super-acid suspensions: Preferred orientation, electrical, and thermal transport," *Journal of Applied Physics*, vol. 95, pp. 649-655, Jan 15 2004.

[148] I. Heller, J. Kong, K. A. Williams, C. Dekker, and S. G. Lemay, "Electrochemistry at single-walled carbon nanotubes: The role of band structure and quantum capacitance," *Journal of the American Chemical Society*, vol. 128, pp. 7353-7359, Jun 7 2006.

[149] M. S. Dresselhaus and P. C. Eklund, "Phonons in carbon nanotubes," *Advances in Physics*, vol. 49, pp. 705-814, Sep 2000.

[150] R. Saito, G. Dresselhaus, and M. S. Dresselhaus, "Trigonal warping effect of carbon nanotubes," *Physical Review B*, vol. 61, pp. 2981-2990, Jan 15 2000.

[151] I. Heller, J. Kong, H. A. Heering, K. A. Williams, S. G. Lemay, and C. Dekker, "Individual single-walled carbon nanotubes as nanoelectrodes for electrochemistry," *Nano Letters*, vol. 5, pp. 137-42, Jan 2005.

[152] S. N. Kim, J. F. Rusling, and F. Papadimitrakopoulos, "Carbon nanotubes for electronic and electrochemical detection of biomolecules," *Advanced Materials*, vol. 19, pp. 3214-3228, Oct 19 2007.

[153] H. R. Byon and H. C. Choi, "Network single-walled carbon nanotube-field effect transistors (SWNT-FETs) with increased Schottky contact area for highly sensitive biosensor applications," *Journal of the American Chemical Society*, vol. 128, pp. 2188-2189, Feb 22 2006.

[154] C. Li, M. Curreli, H. Lin, B. Lei, F. N. Ishikawa, R. Datar, *et al.*, "Complementary detection of prostate-specific antigen using ln(2)O(3) nanowires and carbon nanotubes," *Journal of the American Chemical Society*, vol. 127, pp. 12484-12485, Sep 14 2005.

[155] I. Heller, A. M. Janssens, J. Mannik, E. D. Minot, S. G. Lemay, and C. Dekker, "Identifying the mechanism of biosensing with carbon nanotube transistors," *Nano Letters*, vol. 8, pp. 591-595, Feb 2008.

[156] J. Kong, N. R. Franklin, C. W. Zhou, M. G. Chapline, S. Peng, K. J. Cho, *et al.*, "Nanotube molecular wires as chemical sensors," *Science*, vol. 287, pp. 622-625, Jan 28 2000.

[157] I. Heller, J. Kong, H. A. Heering, K. A. Williams, S. G. Lemay, and C. Dekker, "Individual single-walled carbon nanotubes as nanoelectrodes for electrochemistry," *Nano Letters*, vol. 5, pp. 137-142, Jan 2005.

[158] W. H. Yeo, F. L. Chou, K. Oh, J. H. Chung, and K. H. Lee, "Hybrid Nanofibril Assembly Using an Alternating Current Electric Field and Capillary Action," *Journal of Nanoscience and Nanotechnology,* vol. 9, pp. 7288-7292, Dec 2009.

[159] M. Ciszkowska and Z. Stojek, "Voltammetric & amperometric - Detection - Without added electrolyte," *Analytical Chemistry,* vol. 72, pp. 754A-760A, Dec 2000.

VITA

Jong-Hoon Kim was born in Seoul, South Korea. He received a degree of Bachelor of Science in Physics from Hanyang University, South Korea in 2004, and a Master of Science in Electrical and Computer Science Engineering from the University of California, San Diego in 2009. His research of interest is in Nano/biomedicine and point-of-care diagnostics for infectious diseases. He published 8 peer-reviewed journals and received 6 conference papers as main- and co-authors.